

UNCLASSIFIED

AD 274 375

*Reproduced
by the*

**ARMED SERVICES TECHNICAL INFORMATION AGENCY
ARLINGTON HALL STATION
ARLINGTON 12, VIRGINIA**



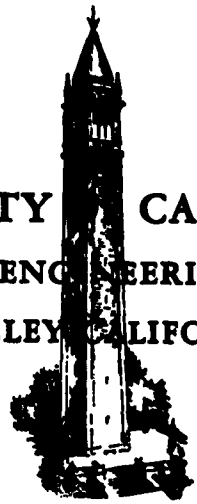
UNCLASSIFIED

NOTICE: When government or other drawings, specifications or other data are used for any purpose other than in connection with a definitely related government procurement operation, the U. S. Government thereby incurs no responsibility, nor any obligation whatsoever; and the fact that the Government may have formulated, furnished, or in any way supplied the said drawings, specifications, or other data is not to be regarded by implication or otherwise as in any manner licensing the holder or any other person or corporation, or conveying any rights or permission to manufacture, use or sell any patented invention that may in any way be related thereto.

CATALOGED BY ASTIA
AS 446500
274377

TECHNICAL REPORT
HE-150-196

UNIVERSITY OF CALIFORNIA
INSTITUTE OF ENGINEERING RESEARCH
BERKELEY, CALIFORNIA



446500

THERMAL STRESS-STRAIN DISTRIBUTION
IN A TRANSVERSELY ANISOTROPIC MATERIAL DURING TRANSIENT HEATING

By

Bob Hiro Suzuki

ASTIA
RECEIVED
APR 24 1962
RECEIVED
TISIA B

SERIES NO.....128.....
ISSUE NO.....8.....
DATE.....March 30, 1962.....

PURCHASE ORDER 1207900
UCX-2266
REPORT NO. HE-150-196
SERIES NO. 128-8
MARCH 30, 1962

SPONSORED BY THE
LAWRENCE RADIATION LABORATORY
UNIVERSITY OF CALIFORNIA
LIVERMORE, CALIFORNIA

THERMAL STRESS-STRAIN DISTRIBUTION
IN A TRANSVERSELY ANISOTROPIC MATERIAL DURING TRANSIENT HEATING

by

Bob Hiro Suzuki

A portion of a Master of Science Thesis
in Mechanical Engineering

Reproduction in whole or in part is permitted
for any purpose of the United States Government

FACULTY INVESTIGATOR:

W. H. Giedt, Professor of Aeronautical Sciences
J. Frisch, Associate Professor of Mechanical Engineering

APPROVED



ABSTRACT

The potential of a recently developed material, pyrolytic graphite, as a skin structure for re-entry vehicles led to an investigation of its thermal and mechanical behavior during transient heating and at elevated temperatures.

The general three-dimensional equations of thermoelasticity are developed for a material whose properties exhibit the same anisotropic behavior as those of pyrolytic graphite. These equations are then solved exactly for a two-dimensional temperature distribution which closely approximates the temperatures measured experimentally in pyrolytic graphite plates.

An oxyacetylene flame apparatus was used to subject 1/8 inch and 1/4 inch thick pyrolytic graphite plates to transient heating. Measurements were made to determine the temperature distribution through the thickness and along the length of the plates. An experimental technique was developed for measuring transient strains up to a temperature of 1500° F using a Tuckerman optical strain gage. The technique was applied to measure the thermal strain variation in the heated pyrolytic graphite plates.

The thermal strains calculated from the analytical solution are compared with the measured strains and generally found to agree within experimental error. Calculations of the stress distributions show that maximum stresses of -1400 psi and -3000 psi were produced in the 1/8 inch and 1/4 inch thick plates, respectively. Finally, the effect of anisotropy on the state of stress is evaluated.

TABLE OF CONTENTS

	ABSTRACT	i
	NOMENCLATURE	iv
	LIST OF FIGURES	v
1.0	INTRODUCTION	1
2.0	THERMAL STRESS-STRAIN DISTRIBUTION IN A TRANSVERSELY ANISOTROPIC PLATE	5
	2.1 General Thermoelastic Equations	5
	2.2 Solution for a Two-Dimensional Temperature Distribution	12
	2.3 Calculated Results	26
3.0	EXPERIMENTAL PROGRAM	28
	3.1 Material Tested	28
	3.2 Heating Apparatus	28
	3.3 Technique and Test Procedure for Temperature Measurements	30
	3.4 Development of Technique for Transient High Temperature Strain Measurements	31
	3.5 Test Procedure for Strain Measurements	35
4.0	EXPERIMENTAL RESULTS	38
	4.1 Temperature Distribution	38
	4.2 Strain Variation	39
5.0	DISCUSSION OF RESULTS	41
	5.1 Comparison of Calculated Results with Experimental Data	41
	5.2 Stress Distributions	42
	5.3 Effect of Anisotropy on Thermal Stresses	45
	5.4 Recommendations	47

6.0	CONCLUSIONS	50
	BIBLIOGRAPHY	51
	FIGURES	54
	APPENDIX I	97
	APPENDIX II	104

NOMENCLATURE

a_{ik}	elastic constants	
E	elastic modulus	psi
G	shearing modulus	psi
h	thickness of plate	in
L	length of plate	in
l, m, n	direction cosines	
T	temperature	$^{\circ}F$
u, v, w	displacements	
x_i	cartesian space coordinates ($i = 1, 2, 3$)	
X_i	body-force components ($i = 1, 2, 3$)	
\bar{X}_i	surface-force components ($i = 1, 2, 3$)	
X	x_1/L , dimensionless length coordinate	
Z	x_3/h , dimensionless thickness coordinate	

Greek Symbols

α	coefficient of thermal expansion	in/in- $^{\circ}F$
$\beta, \gamma, \eta, \zeta$	anisotropic elastic parameters [defined by eqn. (17)]	
ϵ_i	strain components ($i = 1, 2, \dots, 6$)	in/in
ν	Poisson's ratio	
ϕ	Airy stress function [defined by eqn. (11)]	
σ_i	stress components ($i = 1, 2, \dots, 6$)	psi
τ	time	sec

LIST OF FIGURES

1. Coordinate System for a Transversely Anisotropic Plate
2. Oxyacetylene Flame Apparatus
3. Detail of Test Section Assembly
4. Temperature Measurement System
5. Schematic Diagram of Tuckerman Optical Strain Gage
6. Calibration of Tuckerman Extensometer (0.4 Lozenge)
7. Strain Measurement System
- 8.A-8.E Temperature Rise at Various Depths in a 1/8 inch Thick Pyrolytic Graphite Plate at Distances of 1/2, 1-1/8, 1-7/8, 3-3/8, and 5-3/8 inches From the Leading Edge
- 9.A-9.E Temperature Rise at Various Depths in a 1/4 inch Thick Pyrolytic Graphite Plate at Distances of 1/3, 1-1/8, 1-7/8, 3-3/8, and 5-3/8 inches From the Leading Edge
10. Temperature Distribution at Various Times Through 1/8 inch thick Pyrolytic Graphite Plate 5-3/8 inches from Leading Edge
11. Temperature Distribution at Various Times Through 1/4 inch thick Pyrolytic Graphite Plate 5-3/8 inches from Leading Edge
- 12.A-12.E Temperature Distribution Along Length of 1/8 inch Thick Pyrolytic Graphite Plate at Various Depths after 5, 10, 15, 20, and 30 Seconds of Heating
- 13.A-13.G Temperature Distribution Along Length of 1/4 inch Thick Pyrolytic Graphite Plate at Various Depths after 10, 20, 30, 40, 50, 60, and 70 Seconds of Heating
14. Comparison of Experimental Data with Calculated Strains at Unheated Surface of 1/8 inch Thick Pyrolytic Graphite Plate
15. Comparison of Experimental Data with Calculated Strains at Unheated Surface of 1/4 inch Thick Pyrolytic Graphite Plate
16. Distribution of σ_1 through 1/8 inch thick Plate after 20 Seconds of Heating
17. Distribution of σ_1 through 1/4 inch thick Plate after 40 Seconds of Heating

18. Variation of σ_1 at Heated Surface and Midplane of 1/8 inch Thick Plate
19. Variation of σ_1 at Heated Surface and Midplane of 1/4 inch Thick Plate
20. Distribution of σ_3 Through 1/4 inch Thick Plate After 40 Seconds of Heating
21. Distribution of σ_5 Through 1/4 inch Thick Plate After 40 Seconds of Heating
22. Variation of Thermal Stress with Degree of Anisotropy
23. Modulus of Elasticity of Pyrolytic Graphite in the "a"-Direction vs. Temperature
24. Thermal Expansion of Pyrolytic Graphite in the "a"-Direction
25. Thermal Expansion of Pyrolytic Graphite in the "c"-Direction

1.0 INTRODUCTION

One of the more important problems that arise during re-entry of space vehicles at hypersonic speeds is caused by the skin temperatures attained as a result of the aerodynamic heating. Adiabatic wall temperatures under these conditions can exceed temperature limitations of materials commonly used in the manufacture of such vehicles. The difficulty is compounded by the fact that these elevated temperatures are often accompanied by severe temperature gradients. Thermal stresses are produced by these large temperature differences and may be an important factor in determining structural requirements.

Although thermal protection systems for present space vehicles as well as those in the near future can be designed and built with available materials, the performance of these vehicles (e.g., range) will be limited by weight requirements. The possibilities of improving performance have led to the development of several new types of materials possessing promising potentialities. One such material, which has undergone extensive investigation during the past two years, is pyrolytic graphite. This material is one of the strongest structural materials known for use at very high temperatures. Its highly directional thermal properties are such that it is considered to be a thermal insulator in a direction normal to the surface of deposition (basal plane), while being a thermal conductor in a direction parallel to the surface. These unusual properties of pyrolytic graphite may be regarded as a combination which offers the advantages of a composite heat shield and skin structure.

Because of the interest and need for information regarding the behavior of pyrolytic graphite during transient heating and at elevated

temperatures, a research program was undertaken at the University of California, under the sponsorship of the Lawrence Radiation Laboratory, to investigate in particular the thermal and mechanical behavior of a flat plate specimen when one surface was subjected to parallel flow heating from an oxyacetylene flame. The oxyacetylene heating apparatus was developed and used in previous work^{16,17,18*} and found to provide an average heating rate of approximately 40 Btu/ft²-sec. Pyrolytic graphite specimens selected for the tests were 6" x 4" x 1/8" plates and 6" x 4" x 1/4" plates.

The experimental phase of the investigation included measurements of the temperature distribution in the plates and the thermal strain at the unheated surface of the plates during transient heating. An earlier report¹ describes the technique employed in measuring the temperature distributions. That report also presents an analytical solution for predicting the two-dimensional transient temperature variation in a thermally orthotropic plate and compares this solution with the experimental data for a pyrolytic graphite plate. In the present report a technique is described for measuring transient strains up to a temperature of 1500° F using a Tuckerman optical strain gage. The technique was developed and used to measure the thermal strain variation of the heated pyrolytic graphite plates. The stresses corresponding to the measured strains were found to reach maximum values of -1400 psi and -3000 psi in the 1/8 inch and 1/4 inch thick plates, respectively.

There are a number of theoretical analyses dealing with the problem of thermal stresses in isotropic plates.^{2,3,4} A rather general solution

*Note: Numbers in superscript denote references listed in Bibliography.

to this problem, which extends the analysis of Reference 5, was recently presented by Gatewood.⁶ He considered the three-dimensional thermal stresses in a moderately thick elastic plate in which the temperature is taken as a polynomial in the thickness variable but with relatively large, although restricted, gradients with respect to the coordinates of the plane of the plate. However, the properties of pyrolytic graphite are not isotropic, but are highly directional so that the available isotropic solutions cannot, in general, be applied. A thermoelastic analysis of such a material must proceed from the generalized Hooke's law for anisotropic solids.

In contrast to the isotropic case, there appears to be little literature available which deals with thermal stresses in anisotropic plates. Pell⁷ has considered the thermoelastic behavior of an anisotropic plate, having a plane of elastic symmetry parallel to the plane of the plate, using thin plate theory. However, he was unable to obtain a general solution of the problem. More recently Nowacki⁸ presented a method of solution utilizing Galerkin's functions²⁴ for the case of plane stress in an orthotropic plate. Although the method reduces the problem to that of determining three functions, the mathematical difficulties appear to remain formidable. Nowacki also obtained a solution in closed form for the thermal stresses in an infinite orthotropic plate with a constant temperature prescribed in a rectangular region in the infinite plane and zero temperature prescribed outside this region. The applicability of this solution is, of course, limited by the imposed idealization.

In the present analysis, thermal stresses are considered in a transversely anisotropic plate which not only exhibits orthotropic symmetry but also exhibits symmetry about an axis normal to one of the orthogonal

planes. Such symmetry is exhibited by pyrolytic graphite. As usually done in thermoelastic analyses, the effects of thermoelastic dissipation and inertia are ignored so that uncoupled quasi-static thermoelastic theory⁹ can be applied. The analysis then proceeds from the general three-dimensional equations of thermoelasticity without the use of plane stress or thin plate theory. The formulation of the solution is similar to that of Boley and Tolin's⁴ for isotropic free beams. Although the solution presented is for a particular two-dimensional temperature distribution, the general method of analysis appears applicable to plates having a more general temperature distribution and a higher degree of anisotropy.

2.0 THERMAL STRESS-STRAIN DISTRIBUTION IN A TRANSVERSELY ANISOTROPIC PLATE

In this section the general equations of thermoelasticity are developed for a material whose properties exhibit the same anisotropic behavior as those of pyrolytic graphite. These equations are then solved in three-dimensions for a temperature distribution which closely approximates the temperatures measured experimentally in a pyrolytic graphite plate.

2.1 General Thermoelastic Equations

Solutions to general three-dimensional problems of thermoelasticity must satisfy the familiar equations of equilibrium and the conditions of compatibility. Additionally, they must satisfy the prescribed boundary conditions at the surface of the particular body considered. These equations in rectangular cartesian coordinates x_1 , x_2 , and x_3 are given in Reference 10:

Equilibrium equations

$$\begin{aligned} \frac{\partial \sigma_1}{\partial x_1} + \frac{\partial \sigma_6}{\partial x_2} + \frac{\partial \sigma_5}{\partial x_3} &= X_1 \\ \frac{\partial \sigma_2}{\partial x_2} + \frac{\partial \sigma_6}{\partial x_1} + \frac{\partial \sigma_4}{\partial x_3} &= X_2 \\ \frac{\partial \sigma_3}{\partial x_3} + \frac{\partial \sigma_5}{\partial x_1} + \frac{\partial \sigma_4}{\partial x_2} &= X_3 \end{aligned} \tag{1}$$

where X_1 , X_2 , X_3 are the body-force components in the x_1 , x_2 , x_3 directions, respectively.

Compatibility conditions

$$\frac{\partial^2 \epsilon_1}{\partial x_2^2} + \frac{\partial^2 \epsilon_2}{\partial x_1^2} = \frac{\partial^2 \epsilon_6}{\partial x_1 \partial x_2}$$

$$\frac{\partial^2 \epsilon_2}{\partial x_3^2} + \frac{\partial^2 \epsilon_3}{\partial x_2^2} = \frac{\partial^2 \epsilon_4}{\partial x_2 \partial x_3}$$

$$\frac{\partial^2 \epsilon_3}{\partial x_1^2} + \frac{\partial^2 \epsilon_1}{\partial x_3^2} = \frac{\partial^2 \epsilon_5}{\partial x_1 \partial x_3}$$

(2)

$$2 \frac{\partial^2 \epsilon_1}{\partial x_2 \partial x_3} = \frac{\partial}{\partial x_1} \left(-\frac{\partial \epsilon_4}{\partial x_1} + \frac{\partial \epsilon_5}{\partial x_2} + \frac{\partial \epsilon_6}{\partial x_3} \right)$$

$$2 \frac{\partial^2 \epsilon_2}{\partial x_1 \partial x_3} = \frac{\partial}{\partial x_2} \left(\frac{\partial \epsilon_4}{\partial x_1} - \frac{\partial \epsilon_5}{\partial x_2} + \frac{\partial \epsilon_6}{\partial x_3} \right)$$

$$2 \frac{\partial^2 \epsilon_3}{\partial x_1 \partial x_2} = \frac{\partial}{\partial x_3} \left(\frac{\partial \epsilon_4}{\partial x_1} + \frac{\partial \epsilon_5}{\partial x_2} - \frac{\partial \epsilon_6}{\partial x_3} \right)$$

Boundary conditions

$$\sigma_1^s + \sigma_6^m + \sigma_5^n = \bar{X}_1$$

$$\sigma_2^m + \sigma_4^n + \sigma_6^s = \bar{X}_2$$

(3)

$$\sigma_3^n + \sigma_5^s + \sigma_4^m = \bar{X}_3$$

where \bar{X}_1 , \bar{X}_2 , \bar{X}_3 are the components of the prescribed surface tractions in the x_1 , x_2 , x_3 directions respectively, and where $\delta_{m,n}$ are the direction cosines of the outward-drawn surface normal.

The equations presented above are based on purely mechanical and geometrical considerations and therefore apply generally to any elastic solid, whether isotropic or anisotropic, isothermal or nonisothermal. Furthermore, a uniqueness theorem¹⁰ assures that a solution which satisfies (1), (2), and (3) constitutes an exact and unique solution.

For the most general case of an anisotropic elastic solid, the generalized Hooke's law relation contains 36 elastic constants.¹¹ However, it can be shown by arguments based on thermodynamics¹² that not all of these are independent, and it is now generally accepted that there are 21 independent elastic constants for the most general case of anisotropy.¹³ When thermal effects are taken into account, the Hooke's law relations contain 6 additional independent coefficients of thermal expansion. The number of independent elastic and thermal constants reduce considerably when a solid exhibits structural symmetry with respect to a plane or about an axis.

In particular, pyrolytic graphite is a material which exhibits symmetry with respect to three orthogonal planes and also about an axis which is normal to one of the orthogonal planes. Love¹¹ refers to a material exhibiting such symmetry as "transversely isotropic." However, the slightly more descriptive phrase, "transversely anisotropic," will be used here in referring to the material. It is shown in Appendix I that for this case of symmetry the reduced generalized Hooke's law relation, written in rectangular cartesian coordinates, contains 5

independent elastic constants and 2 independent thermal expansion coefficients.

Consider the transversely anisotropic plate of Figure 1. The rectangular cartesian coordinates are oriented such that the isometric planes are parallel with the orthogonal planes of symmetry. The x_1x_2 -plane is chosen to lie parallel to the basal plane (referred to as the "a"-direction in pyrolytic graphite). Then the x_3 -axis is an axis of symmetry, parallel with a normal to the basal plane ("c"-direction). In this case the generalized Hooke's law is written as (cf. Appendix I)

$$\epsilon_1 = a_{11}\sigma_1 + a_{12}\sigma_2 + a_{13}\sigma_3 + \alpha_1 T$$

$$\epsilon_2 = a_{12}\sigma_1 + a_{11}\sigma_2 + a_{13}\sigma_3 + \alpha_1 T$$

$$\epsilon_3 = a_{13}\sigma_1 + a_{13}\sigma_2 + a_{33}\sigma_3 + \alpha_3 T$$

$$\epsilon_4 = a_{44}\sigma_4$$

$$\epsilon_5 = a_{44}\sigma_5$$

$$\epsilon_6 = a_{66}\sigma_6$$

where $a_{66} = 2(a_{11} - a_{12})$.

These equations may be rewritten in terms of normally measured physical constants as follows:*

* e.g., see Reference 13 for this procedure.

$$\begin{aligned}
\epsilon_1 &= \frac{1}{E_{11}} \sigma_1 - \frac{\nu_{12}}{E_{11}} \sigma_2 - \frac{\nu_{13}}{E_{33}} \sigma_3 + \alpha_1 T \\
\epsilon_2 &= -\frac{\nu_{12}}{E_{11}} \sigma_1 + \frac{1}{E_{11}} \sigma_2 - \frac{\nu_{13}}{E_{33}} \sigma_3 + \alpha_1 T \\
\epsilon_3 &= -\frac{\nu_{13}}{E_{33}} \sigma_1 - \frac{\nu_{13}}{E_{33}} \sigma_2 + \frac{1}{E_{33}} \sigma_3 + \alpha_3 T \\
\epsilon_4 &= \frac{1}{G_{44}} \sigma_4 \\
\epsilon_5 &= \frac{1}{G_{44}} \sigma_5 \\
\epsilon_6 &= \frac{2}{E_{11}} (1 + \nu_{12}) \sigma_6
\end{aligned} \tag{4}$$

It is often convenient to express the conditions of compatibility (2) in terms of the stresses. The Hooke's law relation given by equations (4) permits this transformation. For example, taking the first of equations (2):

$$\frac{\partial^2 \epsilon_1}{\partial x_2^2} + \frac{\partial^2 \epsilon_2}{\partial x_1^2} = \frac{\partial^2 \epsilon_6}{\partial x_1 \partial x_2}$$

Appropriate substitutions from equations (4) yield:

$$\begin{aligned}
&\frac{1}{E_{11}} \left(\frac{\partial^2}{\partial x_2^2} - \nu_{12} \frac{\partial^2}{\partial x_1^2} \right) \sigma_1 + \frac{1}{E_{11}} \left(\frac{\partial^2}{\partial x_1^2} - \nu_{12} \frac{\partial^2}{\partial x_2^2} \right) \sigma_2 \\
&- \frac{\nu_{13}}{E_{33}} \left(\frac{\partial^2}{\partial x_1^2} + \frac{\partial^2}{\partial x_2^2} \right) \sigma_3 + \alpha_1 \left(\frac{\partial^2}{\partial x_1^2} + \frac{\partial^2}{\partial x_2^2} \right) T = \frac{2}{E_{11}} (1 + \nu_{12}) \frac{\partial^2 \sigma_6}{\partial x_1 \partial x_2}
\end{aligned} \tag{5}$$

Differentiating the first and second of the equilibrium equations (1), taking the body-force components to be zero, gives

$$\frac{\partial^2 \sigma_6}{\partial x_1 \partial x_2} = - \frac{\partial^2 \sigma_1}{\partial x_1^2} - \frac{\partial^2 \sigma_5}{\partial x_1 \partial x_3} \quad , \quad \frac{\partial^2 \sigma_6}{\partial x_1 \partial x_2} = - \frac{\partial^2 \sigma_2}{\partial x_2^2} - \frac{\partial^2 \sigma_4}{\partial x_2 \partial x_3}$$

Adding and using the third of equations (1) results in

$$2 \frac{\partial^2 \sigma_6}{\partial x_1 \partial x_2} = - \frac{\partial^2 \sigma_1}{\partial x_1^2} - \frac{\partial^2 \sigma_2}{\partial x_1^2} - \frac{\partial}{\partial x_3} \left(\frac{\partial \sigma_4}{\partial x_2} + \frac{\partial \sigma_5}{\partial x_1} \right) = - \frac{\partial^2 \sigma_1}{\partial x_1^2} - \frac{\partial^2 \sigma_2}{\partial x_2^2} + \frac{\partial^2 \sigma_3}{\partial x_3^2}$$

Finally, substitution of this result into (5) leads to

$$\begin{aligned} \frac{1}{E_{11}} \left[\frac{\partial^2}{\partial x_1^2} + \frac{\partial^2}{\partial x_2^2} \right] (\sigma_1 + \sigma_2) - \left[\frac{\nu_{13}}{E_{33}} \left(\frac{\partial^2}{\partial x_1^2} + \frac{\partial^2}{\partial x_2^2} \right) + \frac{(1+\nu_{12})}{E_{11}} \frac{\partial^2}{\partial x_3^2} \right] \sigma_3 \\ + \alpha_1 \left(\frac{\partial^2}{\partial x_1^2} + \frac{\partial^2}{\partial x_2^2} \right) T = 0 \end{aligned} \quad (6a)$$

By following similar procedures on the remaining compatibility conditions (2), the following relations are obtained:

$$\begin{aligned} - \left[\frac{1}{2G_{44}} \frac{\partial^2}{\partial x_1^2} + \frac{\nu_{13}}{E_{33}} \frac{\partial^2}{\partial x_2^2} + \frac{\nu_{12}}{E_{11}} \frac{\partial^2}{\partial x_3^2} \right] \sigma_1 + \left[\left(\frac{1}{2G_{44}} - \frac{\nu_{13}}{E_{33}} \right) \frac{\partial^2}{\partial x_2^2} + \frac{1}{E_{11}} \frac{\partial^2}{\partial x_3^2} \right] \sigma_2 \\ + \left[\frac{1}{E_{33}} \frac{\partial^2}{\partial x_2^2} + \left(\frac{1}{2G_{44}} - \frac{\nu_{13}}{E_{33}} \right) \frac{\partial^2}{\partial x_3^2} \right] \sigma_3 + \left(\alpha_1 \frac{\partial^2}{\partial x_3^2} + \alpha_3 \frac{\partial^2}{\partial x_2^2} \right) T = 0 \end{aligned} \quad (6b)$$

$$\left[\left(\frac{1}{2G_{44}} - \frac{\nu_{13}}{E_{33}} \right) \frac{\partial^2}{\partial x_1^2} + \frac{1}{E_{11}} \frac{\partial^2}{\partial x_3^2} \right] \sigma_1 - \left[\frac{\nu_{13}}{E_{33}} \frac{\partial^2}{\partial x_1^2} + \frac{1}{2G_{44}} \frac{\partial^2}{\partial x_2^2} + \frac{\nu_{12}}{E_{11}} \frac{\partial^2}{\partial x_3^2} \right] \sigma_2$$

$$+ \left[\frac{1}{E_{33}} \frac{\partial^2}{\partial x_1^2} + \left(\frac{1}{2G_{44}} - \frac{\nu_{13}}{E_{33}} \right) \frac{\partial^2}{\partial x_3^2} \right] \sigma_3 + \left(\alpha_3 \frac{\partial^2}{\partial x_1^2} + \alpha_1 \frac{\partial^2}{\partial x_3^2} \right) T = 0 \quad (6c)$$

$$\frac{2}{E_{11}} \frac{\partial^2}{\partial x_2 \partial x_3} (\sigma_1 + \sigma_2) + \left[\frac{1}{G_{44}} - \frac{2\nu_{13}}{E_{33}} \right] \frac{\partial^2 \sigma_3}{\partial x_2 \partial x_3}$$

$$+ \left[\frac{1}{G_{44}} \left(\frac{\partial^2}{\partial x_1^2} + \frac{\partial^2}{\partial x_2^2} \right) + \frac{2}{E_{11}} (1+\nu_{12}) \frac{\partial^2}{\partial x_3^2} \right] \sigma_4 + 2\alpha_1 \frac{\partial^2 T}{\partial x_2 \partial x_3} = 0 \quad (6d)$$

$$\frac{2}{E_{11}} \frac{\partial^2}{\partial x_1 \partial x_3} (\sigma_1 + \sigma_2) + \left[\frac{1}{G_{44}} - \frac{2\nu_{13}}{E_{33}} \right] \frac{\partial^2 \sigma_3}{\partial x_1 \partial x_3}$$

$$+ \left[\frac{1}{G_{44}} \left(\frac{\partial^2}{\partial x_1^2} + \frac{\partial^2}{\partial x_2^2} \right) + \frac{2}{E_{11}} (1+\nu_{12}) \frac{\partial^2}{\partial x_3^2} \right] \sigma_5 + 2\alpha_1 \frac{\partial^2 T}{\partial x_1 \partial x_3} = 0 \quad (6e)$$

$$\left[\frac{1}{G_{44}} - \frac{2\nu_{13}}{E_{33}} \right] \frac{\partial^2}{\partial x_1 \partial x_2} (\sigma_1 + \sigma_2) + \frac{2}{E_{33}} \frac{\partial^2 \sigma_3}{\partial x_1 \partial x_2}$$

$$+ \left[\frac{1}{G_{44}} \left(\frac{\partial^2}{\partial x_1^2} + \frac{\partial^2}{\partial x_2^2} \right) + \frac{2}{E_{11}} (1+\nu_{12}) \frac{\partial^2}{\partial x_3^2} \right] \sigma_6 + 2\alpha_3 \frac{\partial^2 T}{\partial x_1 \partial x_2} = 0 \quad (6f)$$

The six relations given by equations (6) represent the general stress formulation of the compatibility conditions for a transversely anisotropic material with constant properties.

2.2 Solution for a Two-Dimensional Temperature Distribution

Consider again the transversely anisotropic plate of Figure 1. Let the plate be subjected in its interior to a temperature distribution given by

$$T(x_1, x_3) = ax_1 + bx_1^2 + cx_1^2 x_3^2 + T_H(x_3) \quad (7)$$

where a , b , and c are constants and $T_H(x_3)$ is an arbitrary function of x_3 . The particular form of (7) was chosen because the experimentally measured temperature distributions were found to be closely approximated by such an expression (cf. Section 4.1). The plate is supposed free of external loads and body forces.

The stress distribution due to $T_H(x_3)$ in a transversely anisotropic plate is identical to that in an isotropic plate with the same temperature distribution. This is attributed to the isotropic behavior of the transversely anisotropic plate in directions parallel to its plane. The solution for this case is given by Timoshenko¹⁰ who arrived at the solution by physical arguments involving the application and removal of boundary forces. The same solution is derived by Boley and Weiner⁹, who used a more rigorous semi-inverse approach. The solution leads to the following expressions for the stresses in the plate:¹⁰

$$\sigma_3 = \sigma_4 = \sigma_5 = \sigma_6 = 0$$

$$\sigma_1 = \sigma_2 = \frac{1}{1-\nu_{12}} \left[-\alpha_1 E_{11} T + \frac{1}{h} N_T + \frac{12(x_3 - \frac{1}{2}h)}{h^3} M_T \right] \quad (8)$$

where h is the plate thickness and

$$N_T = \int_0^h \alpha_1 E_{11} T dx_3 \quad ; \quad M_T = \int_0^h \alpha_1 E_{11} T (x_3 - \frac{1}{2}h) dx_3$$

Obviously, the solution is not correct at the edges of the plate since the stresses do not vanish there. However, by Saint Venant's principle the stresses at distances away from the edges which are larger than the thickness of the plate will be correct to a high order of magnitude. Note that the stresses given by equations (8) take into account the variation of properties with temperature.

The strain components corresponding to the stresses are obtained by substitution of equations (8) into the Hooke's law relations given by equations (4). The results are

$$\epsilon_1 = \epsilon_2 = \frac{1}{E_{11}} \left[\frac{1}{h} N_T + \frac{12(x_3 - \frac{1}{2}h)}{h^3} M_T \right]$$

$$\epsilon_3 = \frac{\nu_{13}}{E_{33}(1-\nu_{12})} \left[\alpha_1 E_{11} T - \frac{1}{h} N_T - \frac{12(x_3 - \frac{1}{2}h)}{h^3} M_T \right] + \alpha_3 T \quad (9)$$

$$\epsilon_4 = \epsilon_5 = \epsilon_6 = 0$$

Because of the linearity of the thermoelastic equations, the solution given by equations (8) and (9) can be simply added to the solution which follows.

The formulation of the stresses due to the remaining terms in (7) remains to be developed. The analysis to follow is an extension of the exact theory of Boley and Tolins¹⁴ for isotropic free beams.

The solution will be obtained by the semi-inverse method in which the posteriori assumptions are made that

$$\frac{\partial \sigma_1}{\partial x_2} = \frac{\partial \sigma_2}{\partial x_2} = \frac{\partial \sigma_3}{\partial x_2} = \frac{\partial \sigma_4}{\partial x_2} = \frac{\partial \sigma_5}{\partial x_2} = \frac{\partial \sigma_6}{\partial x_2} = 0 \quad (10)$$

As the analysis proceeds, it will be shown that all the general equations of thermoelasticity developed in Section 2.1 can be satisfied on this basis.

An Airy stress function, assumed independent of x_2 , is now introduced such that

$$\sigma_1 = \frac{\partial^2 \phi}{\partial x_3^2}, \quad \sigma_5 = -\frac{\partial^2 \phi}{\partial x_1 \partial x_3}, \quad \sigma_3 = \frac{\partial^2 \phi}{\partial x_1^2} \quad (11)$$

Then the first and third of the equilibrium equations (1) are satisfied.

Substitution of (11) into the compatibility condition (6e) gives

$$\frac{\partial^2 \sigma_2}{\partial x_1 \partial x_3} = \nu_{13} \frac{E_{11}}{E_{33}} \frac{\partial^2}{\partial x_1 \partial x_3} \left(\frac{\partial^2 \phi}{\partial x_1^2} \right) + \nu_{12} \frac{\partial^2}{\partial x_1 \partial x_3} \left(\frac{\partial^2 \phi}{\partial x_3^2} \right) - \alpha_1 E_{11} \frac{\partial^2 T}{\partial x_1 \partial x_3}$$

where $T = T(x_1, x_3)$.

Integration with respect to x_1 and x_3 yields

$$\sigma_2 = \nu_{13} \frac{E_{11}}{E_{33}} \frac{\partial^2 \phi}{\partial x_1^2} + \nu_{12} \frac{\partial^2 \phi}{\partial x_3^2} - \alpha_1 E_{11} T + g_1(x_1) + g_2(x_3) \quad (12)$$

Substitution of (12) into compatibility conditions (6a), (6b), and (6c)

leads to the following results:

$$\left. \begin{aligned} \frac{d^2 g_1}{dx_1^2} &= 0 \\ \frac{d^2 g_2}{dx_3^2} &= 0 \end{aligned} \right\} \quad (13)$$

$$\begin{aligned} & \frac{\partial^4 \phi}{\partial x_3^4} + \frac{2}{1-\nu_{12}^2} \cdot \frac{E_{11}}{E_{33}} \left(\frac{E_{33}}{2G_{44}} - \nu_{13} - \nu_{12}\nu_{13} \right) \frac{\partial^4 \phi}{\partial x_1^2 \partial x_3^2} \\ & + \frac{1}{1-\nu_{12}^2} \frac{E_{11}}{E_{33}} \left(1 - \nu_{13}^2 \frac{E_{11}}{E_{33}} \right) \frac{\partial^4 \phi}{\partial x_1^4} \\ & = - \frac{\alpha_1 E_{11}}{1-\nu_{12}^2} (1+\nu_{12}) \frac{\partial^2 T}{\partial x_3^2} - \frac{\alpha_1 E_{11}}{1-\nu_{12}^2} \left(\nu_{13} \frac{E_{11}}{E_{33}} + \frac{\alpha_3}{\alpha_1} \right) \frac{\partial^2 T}{\partial x_1^2} \end{aligned} \quad (14)$$

Equations (13) give

$$g_1 = c_1 x_1 + c_3'$$

$$g_2 = c_2 x_3 + c_3''$$

Or

$$\varepsilon_1 + \varepsilon_2 = c_1 x_1 + c_2 x_3 + c_3$$

Thus (12) may be written as

$$\sigma_2 = \nu_{13} \frac{E_{11}}{E_{33}} \cdot \frac{\partial^2 \phi}{\partial x_1^2} + \nu_{12} \frac{\partial^2 \phi}{\partial x_3^2} - \alpha_1 E_{11} T + c_1 x_1 + c_2 x_3 + c_3 \quad (15)$$

The expression given by (14) will be abbreviated in the following form:

$$\frac{\partial^4 \phi}{\partial x_3^4} + \beta \frac{\partial^4 \phi}{\partial x_1^2 \partial x_3^2} + \gamma \frac{\partial^4 \phi}{\partial x_1^4} = -\eta \frac{\partial^2 T}{\partial x_3^2} - \zeta \frac{\partial^2 T}{\partial x_1^2} \quad (16)$$

where:

$$\left. \begin{aligned} \beta &= \frac{2}{1-\nu_{12}} \cdot \frac{E_{11}}{E_{33}} \left(\frac{E_{33}}{2G_{44}} - \nu_{13} - \nu_{12}\nu_{13} \right) \\ \gamma &= \frac{1}{1-\nu_{12}} \cdot \frac{E_{11}}{E_{33}} \left(1 - \nu_{13}^2 \frac{E_{11}}{E_{33}} \right) \\ \eta &= \frac{\alpha_1 E_{11}}{1 - \nu_{12}} \\ \zeta &= \frac{\alpha_1 E_{11}}{1-\nu_{12}} \left(\nu_{13} \frac{E_{11}}{E_{33}} + \frac{\alpha_3}{\alpha_1} \right) \end{aligned} \right\} \quad (17)$$

To solve (16), it is assumed that

$$\phi = \phi_1 + \phi_2 + \dots = \sum_{i=1}^{\infty} \phi_i \quad (18)$$

where the φ_i 's are chosen as follows:

$$\frac{\partial^4 \varphi_1}{\partial x_3^4} = -\eta \frac{\partial^2 T}{\partial x_3^2} \quad (19a)$$

$$\frac{\partial^4 \varphi_2}{\partial x_3^4} = -\zeta \frac{\partial^2 T}{\partial x_1^2} - \beta \frac{\partial^4 \varphi_1}{\partial x_1^2 \partial x_3^2} \quad (19b)$$

$$\frac{\partial^4 \varphi_3}{\partial x_3^4} = -\beta \frac{\partial^4 \varphi_2}{\partial x_1^2 \partial x_3^2} - \gamma \frac{\partial^4 \varphi_1}{\partial x_1^4} \quad (19c)$$

$$\frac{\partial^4 \varphi_i}{\partial x_3^4} = -\beta \frac{\partial^4 \varphi_{i-1}}{\partial x_1^2 \partial x_3^2} - \gamma \frac{\partial^4 \varphi_{i-2}}{\partial x_1^4} \quad (i = 4, 5, 6, \dots) \quad (19d)$$

By substitution, it is easily shown that equations (19) satisfy the differential equation (16). It follows from (11) and (18) that the stresses will be given by

$$\begin{aligned} \sigma_1 &= \frac{\partial^2 \varphi}{\partial x_3^2} = \frac{\partial^2 \varphi_1}{\partial x_3^2} + \frac{\partial^2 \varphi_2}{\partial x_3^2} + \dots \\ \sigma_5 &= -\frac{\partial^2 \varphi}{\partial x_1 \partial x_3} = -\frac{\partial^2 \varphi_1}{\partial x_1 \partial x_3} - \frac{\partial^2 \varphi_2}{\partial x_1 \partial x_3} - \dots \\ \sigma_3 &= \frac{\partial^2 \varphi}{\partial x_1^2} = \frac{\partial^2 \varphi_1}{\partial x_1^2} + \frac{\partial^2 \varphi_2}{\partial x_1^2} + \dots \end{aligned} \quad (20)$$

The following boundary conditions hold for a free plate:

$$\sigma_1 = \frac{\partial^2 \phi}{\partial x_3^2} = 0 \quad \text{at } x_1 = 0, \quad x_1 = L \quad (21a)$$

$$\sigma_5 = \frac{\partial^2 \phi}{\partial x_1 \partial x_3} = 0 \quad \text{at } x_3 = 0, \quad x_3 = h \quad (21b)$$

$$\sigma_3 = \frac{\partial^2 \phi}{\partial x_1^2} = 0 \quad \text{at } x_3 = 0, \quad x_3 = h \quad (21c)$$

However, it is often not possible to satisfy exactly condition (21a). In such cases the following integral boundary conditions will be substituted:

$$\int_0^h \sigma_1 dx_3 = \int_0^h \frac{\partial^2 \phi}{\partial x_3^2} dx_3 = 0 \quad (21a')$$

$$\int_0^h x_3 \sigma_1 dx_3 = \int_0^h x_3 \frac{\partial^2 \phi}{\partial x_3^2} dx_3 = 0 \quad (21a'')$$

These boundary conditions will lead to the correct solution within the approximation of Saint Venant's principle. Each of the ϕ_i 's will be required to satisfy the conditions given by equations (21).

The particular temperature distributions to be considered here are the terms in (7) other than $T_H(x_3)$ so that

$$T(x_1, x_3) = ax_1 + bx_1^2 + cx_1^2 x_3^2$$

Substitution into (19a) gives

$$\frac{\partial^4 \phi_1}{\partial x_3^4} = -2c\eta x_1^2$$

Integration yields

$$\frac{\partial^2 \phi_1}{\partial x_3^2} = -c\eta x_1^2 x_3^2 + x_3 S_1(x_1) + S_2(x_3)$$

where S_1 and S_2 are undetermined functions of x_1 . It is apparent from inspection of this result that the exact boundary conditions (21a) cannot be satisfied. Therefore (21a') and (21a'') are applied

$$\begin{aligned} \int_0^h \frac{\partial^2 \phi_1}{\partial x_3^2} dx_3 &= \int_0^h \left[-c\eta x_1^2 x_3^2 + x_3 S_1(x_1) + S_2(x_3) \right] dx_3 \\ &= -\frac{h^3}{3} c\eta x_1^2 + \frac{h^2}{2} S_1 + h S_2 = 0 \end{aligned}$$

$$\begin{aligned} \int_0^h x_3 \frac{\partial^2 \phi_1}{\partial x_3^2} dx_3 &= \int_0^h \left[-c\eta x_1^2 x_3^2 + x_3^2 S_1(x_1) + x_3 S_2(x_3) \right] dx_3 \\ &= -\frac{h^4}{4} c\eta x_1^2 + \frac{h^3}{3} S_1 + \frac{h^2}{2} S_2 = 0 \end{aligned}$$

Upon solving simultaneously

$$S_1 = c\eta h x_1^2$$

$$S_2 = -\frac{1}{6} c\eta h^2 x_1^2$$

Thus

$$\frac{\partial^2 \phi_1}{\partial x_3^2} = c\eta h^2 x_1^2 \left[-\frac{1}{6} + \frac{x_3}{h} - \left(\frac{x_3}{h}\right)^2 \right] \quad (22)$$

Now integration of (22) leads to

$$\varphi_1 = c\eta h^2 x_1^2 \left[-\frac{1}{12} x_3^2 + \frac{1}{6} \frac{x_3^2}{h} - \frac{1}{12} \frac{x_3^4}{h^2} \right] + x_3 s_3(x_1) + s_4(x_1)$$

Applying (21c) results in

$$\frac{d^2 s_4}{dx_1^2} = 0 \quad , \quad \frac{d^2 s_3}{dx_1^2} = 0$$

Hence

$$s_3 = c_4 x_1 + c_5 \quad , \quad s_4 = c_6 x_1 + c_7$$

Then

$$\begin{aligned} \varphi_1 = c\eta h^2 x_1^2 \left[-\frac{1}{12} x_3^2 + \frac{1}{6} \frac{x_3^3}{h} - \frac{1}{12} \frac{x_3^4}{h^2} \right] \\ + c_4 x_3 x_1 + c_5 x_3 + c_6 x_1 + c_7 \end{aligned}$$

So that

$$\frac{\partial^2 \varphi_1}{\partial x_1^2} = 2c\eta h^4 \left[-\frac{1}{12} \left(\frac{x_3}{h} \right)^2 + \frac{1}{6} \left(\frac{x_3}{h} \right)^3 - \frac{1}{12} \left(\frac{x_3}{h} \right)^4 \right] \quad (23)$$

and

$$\frac{\partial^2 \varphi_1}{\partial x_1 \partial x_3} = 2c\eta h^2 x_1 \left[-\frac{1}{6} x_3 + \frac{1}{2} \frac{x_3^2}{h} - \frac{1}{3} \frac{x_3^3}{h^2} \right] + c_4$$

Conditions (21b) demands that

$$c_4 = 0$$

Thus

$$\frac{\partial^2 \varphi_1}{\partial x_1 \partial x_3} = -2c\eta h^3 x_1 \left[-\frac{1}{6} x_3 + \frac{1}{2} \left(\frac{x_3}{h} \right)^2 - \frac{1}{3} \left(\frac{x_3}{h} \right)^3 \right] \quad (24)$$

From (19b) and (23)

$$\frac{\partial^4 \phi_2}{\partial x_3^4} = -2b\zeta - 2c\zeta x_3^2 - 2c\beta\eta h^2 \left[-\frac{1}{6} + \frac{x_3}{h} - \left(\frac{x_3}{h}\right)^2 \right]$$

Upon integrating

$$\frac{\partial^2 \phi_2}{\partial x_3^2} = -b\zeta x_3^2 - \frac{1}{6}c\zeta x_3^4 - 2c\beta\eta h^2 \left[-\frac{1}{12} x_3^2 + \frac{1}{6} \frac{x_3^3}{h} - \frac{1}{12} \frac{x_3^4}{h^2} \right]$$

$$+ x_3 T_1(x_1) + T_2(x_1)$$

Applying boundary conditions (21a') and (21a'') to this result and solving for T_1 and T_2 gives

$$T_1 = b\zeta h + \frac{2}{15} c\zeta h^3$$

$$T_2 = -\frac{1}{6} b\zeta h^2 - \frac{1}{180} c\beta\eta h^4 - \frac{1}{30} c\zeta h^4$$

Thus

$$\begin{aligned} \frac{\partial^2 \phi_2}{\partial x_3^2} = & b\zeta h^2 \left[-\frac{1}{6} + \frac{x_3}{h} - \left(\frac{x_3}{h}\right)^2 \right] + c\zeta h^4 \left[-\frac{1}{30} + \frac{2}{15} \frac{x_3}{h} - \frac{1}{6} \left(\frac{x_3}{h}\right)^4 \right] \\ & + c\beta\eta h^4 \left[-\frac{1}{180} + \frac{1}{6} \left(\frac{x_3}{h}\right)^2 - \frac{1}{3} \left(\frac{x_3}{h}\right)^3 + \frac{1}{6} \left(\frac{x_3}{h}\right)^4 \right] \end{aligned} \quad (25)$$

Integration of (25) yields

$$\begin{aligned} \varphi_2 = & b\zeta h^4 \left[-\frac{1}{12} \left(\frac{x_3}{h} \right)^2 + \frac{1}{6} \left(\frac{x_3}{h} \right)^3 - \frac{1}{12} \left(\frac{x_3}{h} \right)^4 \right] + c\zeta h^6 \left[-\frac{1}{60} \left(\frac{x_3}{h} \right)^2 + \frac{1}{45} \left(\frac{x_3}{h} \right)^3 - \frac{1}{180} \left(\frac{x_3}{h} \right)^6 \right] \\ & + c\beta\eta h^6 \left[-\frac{1}{360} \left(\frac{x_3}{h} \right)^2 + \frac{1}{72} \left(\frac{x_3}{h} \right)^4 - \frac{1}{60} \left(\frac{x_3}{h} \right)^5 + \frac{1}{180} \left(\frac{x_3}{h} \right)^6 \right] \\ & + x_3 T_3(x_1) + T_4(x_1) \end{aligned}$$

Then

$$\frac{\partial^2 \varphi_2}{\partial x_1^2} = x_3 \frac{d^2 T_3}{dx_1^2} + \frac{d^2 T_4}{dx_1^2}$$

Boundary condition (21c) leads to the conclusion that

$$\frac{d^2 T_3}{dx_1^2} = 0 \quad , \quad \frac{d^2 T_4}{dx_1^2} = 0$$

It follows that

$$T_3 = D_1 x_1 + D_2$$

$$T_4 = D_3 x_1 + D_4$$

Thus

$$\frac{\partial^2 \varphi_2}{\partial x_1^2} = 0$$

(26)

and

$$\varphi_2 = f(x_3) + D_1 x_1 x_3 + D_2 x_3 + D_3 x_1 + D_4$$

Hence

$$\frac{\partial^2 \varphi_2}{\partial x_1 \partial x_3} = D_1$$

Condition (21b) demands that $D_1 = 0$. Therefore

$$\frac{\partial^2 \phi_2}{\partial x_1 \partial x_3} = 0 \quad (27)$$

Now from (20c) and differentiation of equations (23) and (25)

$$\frac{\partial^4 \phi_3}{\partial x_3^4} = 0$$

Integrating,

$$\frac{\partial^2 \phi_3}{\partial x_3^2} = x_3 U_1(x_1) + U_2(x_1)$$

In this case the exact boundary conditions (21a) can be satisfied.

Then

$$U_1 = U_2 = 0$$

So

$$\frac{\partial^2 \phi_3}{\partial x_3^2} = 0 \quad (28)$$

It follows that

$$\frac{\partial^2 \phi_3}{\partial x_3^2} = \frac{\partial^2 \phi_3}{\partial x_1 \partial x_3} = 0 \quad (29)$$

Thus the series in the ϕ_1 's may be truncated after two terms since the second derivatives of the remaining terms are identically zero. The

expressions for φ_1 and φ_2 constitute the solution since they satisfy the differential equation (16) and the boundary conditions (21). Now recall that σ_2 is given by (15) as

$$\sigma_2 = \nu_{13} \frac{E_{11}}{E_{33}} \frac{\partial^2 \varphi}{\partial x_1^2} + \nu_{12} \frac{\partial^2 \varphi}{\partial x_3^2} - \alpha_1 E_{11} T + c_1 x_1 + c_2 x_3 + c_3$$

To determine c_1 , c_2 , and c_3 the following boundary conditions are imposed on σ_2 :

$$\int_0^L \int_0^h \sigma_2 dx_3 dx_1 = 0$$

$$\int_0^L \int_0^h x_1 \sigma_2 dx_3 dx_1 = 0$$

$$\int_0^L \int_0^h x_3 \sigma_2 dx_3 dx_1 = 0$$

The following result is then obtained:

$$\begin{aligned} \sigma_2 = \nu_{13} \frac{E_{11}}{E_{33}} \left(\sigma_3 + \frac{1}{180} c \eta h^4 \right) + \nu_{12} \sigma_1 + \alpha_1 E_{11} b L^2 \left[-\frac{1}{6} + \frac{x_1}{L} - \left(\frac{x_1}{L} \right)^2 \right] \\ + \alpha_1 E_{11} c h^2 L^2 \left[-\frac{2}{9} + \frac{1}{3} \frac{x_1}{L} + \frac{1}{3} \frac{x_3}{h} - \left(\frac{x_1}{L} \right)^2 \left(\frac{x_3}{h} \right)^2 \right] \end{aligned} \quad (30)$$

Complete expressions for σ_1 , σ_2 , σ_3 , and σ_5 are now available by appropriate substitutions in equations (20) and (30). Note that these stresses were found independent of σ_4 and σ_6 .

Now σ_4 and σ_6 will be required to satisfy the stress-free boundary conditions exactly. Then it necessarily follows from assumptions (10) that

$$\sigma_4 = \sigma_6 = 0$$

The remaining compatibility equations (6d) and (6f) and the second of the equilibrium equations (1) are identically satisfied by this choice.

For convenience the expressions for the stresses are summarized below:

$$\begin{aligned} \sigma_1 &= c\eta h^2 L^2 X^2 \left[-\frac{1}{6} + z - z^2 \right] + b\xi h^2 \left[-\frac{1}{6} + z - z^2 \right] \\ &\quad + c\xi h^4 \left[-\frac{1}{30} + \frac{2}{15} z - \frac{1}{6} z^4 \right] + c\beta\eta h^4 \left[-\frac{1}{180} + \frac{1}{6} z^2 - \frac{1}{3} z^3 + \frac{1}{6} z^4 \right] \\ \sigma_2 &= \nu_{13} \frac{E_{11}}{E_{33}} \left[\sigma_3 + \frac{1}{180} c\eta h^4 \right] + \nu_{12} \sigma_1 + \alpha_1 E_{11} b L^2 \left[-\frac{1}{6} + x - x^2 \right] \\ &\quad + \alpha_1 E_{11} c h^2 L^2 \left[-\frac{2}{9} + \frac{1}{3} x + \frac{1}{3} z - x^2 z^2 \right] \quad (31) \\ \sigma_3 &= c\eta h^4 \left[-\frac{1}{6} z^2 + \frac{1}{3} z^3 - \frac{1}{6} z^4 \right] \\ \sigma_5 &= -c\eta h^3 L X \left[-\frac{1}{3} z + z^2 - \frac{2}{3} z^3 \right] \\ \sigma_4 &= \sigma_6 = 0 \end{aligned}$$

where:

$$x = \frac{x_1}{L}, \quad z = \frac{x_3}{h}$$

The strains corresponding to these stresses are easily obtained by substitution of equations (31) into the Hooke's law relations (4). In particular, the strain, ϵ_1 , at the unheated surface ($Z = 0$), which will be of interest in comparing with experimental data, is given by

$$\begin{aligned} \epsilon_1(X,0) = & \frac{1-\nu_{12}}{E_{11}} \left[\frac{1}{6} c\eta h^2 L^2 X^2 + \frac{1}{6} b\zeta h^2 + \frac{1}{30} c\zeta h^4 + \frac{1}{180} c\beta\eta h^4 \right] \\ & - \frac{1}{180} \frac{\nu_{12}\nu_{13}}{E_{33}} c\eta h^4 + \nu_{12}\alpha_1 bL^2 \left[\frac{1}{6} - X \right] \\ & + \nu_{12}\alpha_1 c h^2 L^2 \left[\frac{2}{9} - \frac{1}{3} X \right] + \alpha_1 aLX \\ & + \alpha_1 bL^2 X^2 (1+\nu_{12}) \end{aligned} \quad (32)$$

2.3 Calculated Results

The solution presented in the previous section for a transversely anisotropic plate was used to calculate the thermal stresses and strains in the pyrolytic graphite plates of the two sizes used in the experimental program (cf. Section 3.2). The strain at the unheated surface was calculated from equations (9) and (32), and the stresses from equations (8) and (31).

It should be recalled that equations (31) and (32) were based on constant properties, while equations (8) and (9) accounted for variable properties. Stresses calculated from equation (8) were found to be significantly affected by the temperature variation of the thermal expansion coefficient, α_1 , in the "a"-direction of pyrolytic graphite (see Figure 24). When a constant average value of α_1 was used in equation (8),

the resulting stresses were found to differ by as much as 50 percent from the calculated stresses based on a variable α_1 . A similar influence was found on the strains calculated from equation (9). These calculations emphasized the importance of accounting for property variations with temperature. However, although equations (31) and (32) did not account for variations in α_1 , they added only minor contributions to the stresses and strains so that the errors induced by the use of a constant average value of α_1 in these equations were felt to be relatively unimportant.

Details of the calculation procedures are presented in Appendix II. The results will be presented and discussed in Section 4.0.

3.0 EXPERIMENTAL PROGRAM

The objectives of the experimental program were to determine the temperature and thermal strain distributions in pyrolytic graphite plates subjected to transient heating from a high-temperature oxyacetylene flame. Descriptions of the material tested, the heating apparatus, the experimental techniques, and the test procedures will be presented in the following sections.

3.1 Material Tested

Pyrolytic graphite is produced by the deposition of a gaseous hydrocarbon onto a mandrel of commercial graphite which is maintained at a temperature above 3600° F. The properties of the resulting material can be varied considerably by variations in the processing parameters. There is also some evidence that property variations may occur within an individual sample depending on the amount of residual stress present in the material. Recent reports¹⁵ indicate that it may be possible to classify pyrolytic graphite into as many as 16 different types based on the micro-structure.

The pyrolytic graphite specimens selected for the tests were 6" x 4" x 1/8" plates and 6" x 4" x 1/4" plates. Four flat plate specimens of each thickness were used in the experiment.

3.2 Heating Apparatus

The heating apparatus used for the experimental phase of this investigation was developed and used previously for the determination of the behavior of ablating materials at low heat rates. A detailed description of this apparatus and its heating characteristics are

given in References 16, 17, and 18. Only the important features will be discussed here.

The primary elements of the heating apparatus are the oxygen and acetylene fuel sources, the fuel lines and regulators, and multiple-nozzle flame head, the test section, and the water-cooled exhaust duct. The general arrangement in the test area can be seen in Figure 2. The apparatus provided an average heating rate of approximately $40 \text{ Btu/ft}^2\text{-sec}$ to one surface of a flat plate specimen mounted parallel to the flame. The velocity was 300 ft/sec , and the gas temperature approximately 5000° F at atmospheric pressure. Heating rates were reproduced to within about $\pm 2 \text{ Btu/ft}^2\text{-sec}$ from test to test.

For the purposes of the present investigation, it was necessary to modify the test section in such a way that a flat plate specimen could be mounted at the top of the section. This was accomplished by surrounding the sides and bottom of the test section with refractory bricks which were lined with thin plates of ordinary commercial graphite to alleviate the flame damage. The plate was then placed on the bricks which formed the sides of the section. The open sections in front of the leading edge and behind the trailing edge of the plate were covered with refractory bricks so that the oxyacetylene flame was completely enclosed. Details of the test section assembly are shown in Figure 3. With the plate in position, the leading edge was about $1/8''$ above and $1/2''$ downstream of the top row of nozzles and a $3 \text{ inch} \times 6 \text{ inch}$ area of one surface of the plate was exposed to heating by the flame. Flame leakage was prevented by filling openings with Sauereisen No. 7 and by maintaining a smooth fit between the plate and the bricks.

3.3 Technique and Test Procedure for Temperature Measurements

Since the technique and test procedure for measuring the transient temperature distribution in a pyrolytic graphite plate have already been described in Reference 1, only a brief description will be presented here.

The basic technique was to insert thermocouples into small ($1/8$ " diameter) flat-bottomed holes milled in the plate. Starting near the unheated surface, these holes were made progressively deeper so that the temperature variation through the thickness of the plate could be measured. The effect of the holes on the temperature distribution was believed to be small because of the high thermal conductivity of pyrolytic graphite in its basal planes. The thermocouples were threaded into 0.10 inch diameter ceramic tubes and spring-loaded into the holes with the device shown in Figure 4. Number 32 gauge chromel-alumel thermocouples were used and a continuous record of their output obtained on a twelve-channel Minneapolis-Honeywell recording oscillograph.

Temperature distributions were measured in both the $1/8$ inch and $1/4$ inch thick plates. Temperatures at the unheated surface of a plate were measured first. In successive tests temperatures were measured in holes located along the center-line of the plate parallel to the flow at distances of $1/2$, $1-1/8$, $1-7/8$, $3-3/8$, and $5-3/8$ inches from the leading edge by the technique described above. The $1/8$ inch thick plate was heated for a period of approximately 30 seconds in each test; while the $1/4$ inch thick plate was heated for approximately 70 seconds in each test.

3.4 Development of Technique for Transient High Temperature Strain Measurements

During the early phases of this investigation, a study was made of the available experimental techniques for measuring transient strains at high temperatures. Of the various techniques studied, the electric-resistance foil gage and the Tuckerman optical strain gage appeared the most promising. Therefore, preliminary tests were conducted using both types of strain gage.

Foil gages were bonded to pyrolytic graphite using both Trans-Sonics, Inc. Type 64-C and Allen PB-X (Baldwin-Lima-Hamilton) cements. Although both cements appeared to have sufficient bonding strength to pyrolytic graphite at room temperature, they failed when tested at high temperatures up to 1000° F. Since this bonding problem did not appear resolvable within a reasonable time period, efforts in this direction were discontinued. Other difficulties were also anticipated, such as the determination of the corrections necessary for the thermal expansion of the gage itself and for the heating of the lead wires.

Because it offered certain potential advantages over the electric-resistance foil gages, the Tuckerman optical strain gage system was finally selected for the experimental measurements.

The two basic units of the system are the extensometer and the autocollimator. The extensometer consists of one fixed knife edge and one rotating knife edge, or lozenge, on which there is a mirrored surface. The two knife edges are placed against the sample under test. Deformation of the sample causes the lozenge to rock.

The autocollimator is a precision telescope consisting of a highly corrected objective lens system, a scale, a light source which projects a fiducial spot on the scale, and an eyepiece.

The principle by which the two units work is illustrated in the schematic diagram of Figure 5. Light emanating from the autocollimator strikes the mirrored surface of the lozenge, then the fixed mirror, and is reflected back to the objective lens which focuses the fiducial spot on the scale. The position of this spot on the scale is a function of the lozenge rotation caused by the specimen deformation. Readings obtained are readily converted to strain values by a simple formula.

The extensometer used in the tests was a standard model with a 1-inch gage length and a 0.4-inch lozenge. With this extensometer the least count of the vernier scale readings was about 8 microinches per inch.

The Tuckerman optical strain gage is designed primarily for static strain measurements at steady state temperatures and is recommended for use up to a temperature of 500° F.¹⁹ The limiting condition is excessive heating of the mirrored surface of the extensometer. Because of the highly transient conditions of the tests, it was felt that the gage might be usable up to surface temperatures of approximately 1000° F without damaging the mirrored surface. In adapting the gage for measuring the transient strains in a pyrolytic graphite plate, several innovations in instrumentation and in technique were necessary.

A specially designed stand was built for supporting and aligning the autocollimator above the test section. (See Figure 2) Alignment of the autocollimator with the extensometer presented no difficulties. The

extensometer was placed on the unheated surface of the plate and held in place by a spring-tensioned wire which exerted a downward force of about one pound. The wire was easily displaced to permit immediate removal of the extensometer. The unheated surface was obviously the most practical location for the strain measurements since the lowest temperatures occurred there and it was readily accessible for the instrumentation.

A preliminary test on a 1/8 inch thick plate was conducted to see if the response of the Tuckerman gage could be followed visually. The results were favorable, suggesting that a sufficient number of values to define a curve could be obtained without special recording equipment.

Further tests were conducted to measure the thermal strains in both a 1/8 inch and a 1/4 inch thick plate. A push-button switch which transmitted an electrical signal to a recording oscillograph was devised for synchronizing the visual strain readings with a time scale. Temperatures at the unheated surface were measured near the leading edge by a thermocouple held down with a two pound spring force. The length of time of heating was gradually increased with each test to a maximum of 45 seconds for the 1/8 inch thick plate and to a maximum of 85 seconds for the 1/4 inch thick plates. Generally, 10 to 15 strain readings could be taken in these time intervals. A maximum temperature of 1500° F was reached on the unheated surface with no apparent damage to the mirrored surface of the extensometer. Excellent reproduction of temperatures from test to test indicated that heating rates were being reproduced quite well.

Considerable scatter in the strain data was observed in the first few tests of each plate. Differences were also noted between the strain curves of the "mandrel" side of a plate and the "deposition" side.

However, after four or five tests on each side of the plates, consistent data could be obtained. This behavior was attributed to the presence of residual stresses in the plates which apparently were eliminated by the annealing effect of the heating and cooling.

During the course of these preliminary tests, it became evident that the extensometer was being subjected to considerable heating. It was then realized that the resulting thermal expansion of the extensometer was registering as an apparent compressive strain and seriously influencing the strain data.

In order to determine the correction for this effect, the thermal expansion of the extensometer was calibrated. The calibration was performed by first heating the extensometer with an electric blower-type heater. It was then placed on an unheated pyrolytic graphite plate; and as it cooled, strain readings were observed through the autocollimator and the body temperature measured by a thermocouple. The thermal expansion of the pyrolytic graphite plate was believed negligible due to its low thermal expansion coefficient in the plane. The calibration points obtained are shown in Figure 6. The average thermal expansion coefficient of the extensometer was found to be 7.30 microinches per inch per degree Fahrenheit.

Of course, the next step was to determine the amount of the temperature rise of the extensometer during a test. Measurements showed that this temperature rise was about 100° F. However, this temperature rise was not uniform. Temperature differences as large as 20° F were measured between locations on the extensometer. Since there was no way of determining the "effective" temperature with which the extensometer

expanded, accurate corrections to the observed strain readings were not possible.

A solution to this problem was seen when it was established that about 80% of the heat transfer to the extensometer was by radiation. The advantages of a heat shield placed between the extensometer body and the plate surface were then immediately obvious. A heat shield was made from thin sheets of nichrome separated by thin insulating sheets of mica. Holes were cut in the shield to accommodate the knife edge and lozenge. Wires were stretched across the plate to hold the shield in position. Figure 7 shows the final arrangement of the instrumentation in the test section.

The use of the heat shield was quite effective in reducing the radiation heat transfer. The temperature rise of the extensometer was reduced to less than 30° F and the maximum temperature difference was reduced to about 3° F, corresponding to a maximum uncertainty in the correction of about 20 microinches per inch.

3.5 Test Procedure for Strain Measurements

The uncertainties in the observed strain readings and in the corrections to these readings were expected to cause considerable scatter in the data points for a particular test. With this in mind, a number of tests were conducted on both the 1/8 inch and the 1/4 inch thick plates so that the mean trend of the strains for each plate could be determined. The strains were measured along the center line of each plate parallel to the flow with the center of the extensometer located approximately 3-1/2 inches from the trailing edge. A few additional measurements were

made on the $1/8$ inch thick plate with the center of the extensometer located approximately 1 inch from the trailing edge. However, these latter measurements were not entirely successful and will be discussed below. Each of the plates tested had been subjected to a number of previous tests so that any residual stresses present were probably eliminated.

The procedure followed during each test was the same. The plate was placed in its usual position ($1/8$ " above and $1/2$ " downstream of the nozzles) in the test section. The extensometer, instrumented with two thermocouples, was placed on the plate together with the heat shield and held in place by the spring-tensioned wire. It was necessary to press the extensometer against the plate to form grooves for the knife edges. A thermocouple was lowered on the plate to measure the temperature near the leading edge. The outputs of the three thermocouples were recorded on the Minneapolis-Honeywell recording oscillograph. Each test began with the ignition of the oxyacetylene flame. Care had to be exercised in this operation because an explosive ignition would usually knock the extensometer off scale so that readings could not be taken. The $1/8$ inch thick plates were heated for about 35 seconds in each test and the $1/4$ inch thick plates for about 70 seconds. The visual strain readings observed during a test were synchronized with a time scale by means of the push-button switch. At the termination of a test, the extensometer was immediately removed to minimize its exposure to heating.

During the early part of a test the strain variation was so rapid that it was not possible to read the vernier scale. However, by interpolating between the lines of the primary scale, readings could be

taken to within an accuracy of about ± 20 microinches per inch. The strain variation decreased considerably during the latter part of the test so that it became possible to read the vernier. This increase in accuracy was, however, offset by the increase in the uncertainty of the correction for the extensometer expansion due to larger temperature differences in the extensometer.

Considerable difficulties were encountered in the strain measurements near the trailing edge of the $1/8$ inch thick plate. The main difficulty was due to flame leakage from the trailing edge of the plate which considerably increased the heat transfer to the extensometer. This resulted in large temperature differences in the extensometer and invalidated much of the data obtained. Contact between the heat shield and the exhaust duct also proved to be troublesome. The vibrations of the duct caused by the flowing gases were transmitted through the heat shield to the extensometer, making it impossible to take readings. In spite of these difficulties, some fairly reasonable data were obtained in two of the tests.

4.0 EXPERIMENTAL RESULTS

A large amount of data was obtained during the numerous experimental runs. All of the data were analyzed and only those considered to be reasonably valid were retained. The following two sections present the experimental results representing the best data obtained from the temperature and strain measurements.

4.1 Temperature Distribution

The continuous temperature records obtained from the oscillograph for both the 1/8 inch and the 1/4 inch thick plates are shown in Figures 8A through 9E. The temperatures are plotted as functions of time at various depths from the unheated surface and each figure is for a particular distance from the leading edge. These temperature records were cross-plotted in two ways. First, the temperature distributions through the thickness were plotted at various times. Figures 10 and 11 show these distributions for both plates at only the one location near the trailing edge since these were typical and were the only ones of this type required for the calculation of the thermal stresses and strains. The second type of cross-plots are shown in Figures 12A through 13G from which the temperature distributions along the length of the plates can be seen at various depths. Each figure is for a particular time after heating. Also shown in these figures are the approximate temperature curves with their corresponding equations which were fitted to the experimental data. It can be seen that these fitted curves represent a fairly good approximation of the actual temperature distributions. Notice that the temperatures given by the term $T_H(X_3)$ are just the

temperatures through the thickness near the trailing edge which were shown in Figures 10 and 11.

Temperature measurements across the width of a 1/4 inch thick plate showed that the maximum variation was only about 25° F.¹ There was no reason for believing that this variation was very much larger in the 1/8 inch thick plate. Thus, these measurements indicated that the temperature distributions in the plates were very nearly two-dimensional.

4.2 Strain Variation

The results of the strain measurements taken in a number of tests are presented in Figures 14 and 15 where the strain variation with time is shown for both the 1/8 inch and 1/4 inch thick plates. The data points which are plotted have been corrected for the thermal expansion of the extensometer. The scatter in the data points for both plates is approximately ± 20 microinches per inch, except for the data points of tests 5 and 6, and corresponds to the experimental error (cf., Section 3.5) expected in the measurements. Although the uncertainty in the strain measurements was relatively large, it is seen from the figures that the mean trend of the strain variation at $X_1 = 3.5''$ is well defined.

The strains measured near the trailing edge ($x_1 = 1.0''$) of the 1/8 inch thick plate are represented by the data points of tests 5 and 6. Because of the experimental difficulties previously mentioned (cf., Section 3.5), these strain measurements are of questionable accuracy. However, they were included in Figure 14 for the purpose of showing the general trend of strains near the trailing edge.

The variation of the strains in both plates is seen to follow the same pattern. In each case the initially compressive strains reverse into almost linearly increasing tensile strains. This behavior is compared to the strain variation predicted from the analytical solution in the next section.

5.0 DISCUSSION OF RESULTS

It is axiomatic in experimental stress analysis that the experimenter must rely directly on theoretical analysis for his knowledge of the state of stress in a body. Stresses are rarely measured directly; whereas strains are almost always measured. Therefore, the usual test of the validity of a theoretical analysis is to compare the experimentally measured strains with the strains calculated from the analytical solution. Then if agreement is found, there is some justification for believing that the calculated stress distribution represents the actual state of stress.

In Section 5.1 the experimentally measured strains are compared with the strains calculated from the analytical solution. Then in Section 5.2 the calculated stress distributions are discussed. The effect of anisotropy on the thermal stresses is examined in Section 5.3. Finally, Section 5.4 concludes with a discussion on further developments suggested by the results of this investigation.

5.1 Comparison of Calculated Results with Experimental Data

In Figure 14 the calculated strain variations at two locations on the unheated surface of the 1/8 inch thick pyrolytic graphite plate are compared with the experimental data. Reasonably good agreement (within ± 20 microinches per inch) is found at $x_1 = 3.5''$, but the comparison is inconclusive at $x_1 = 1''$ due to the limited experimental data available at this location. However, the predicted strain curve does follow the general trend of this data. Discrepancies which exist are probably due to the uncertainty in the strain measurements.

The comparison of the strain variation at the unheated surface

of the 1/4 inch thick pyrolytic graphite plate with the experimental data is shown in Figure 15. The agreement is within experimental error (± 20 microinches per inch) up to about 50 seconds; after this time the predicted strain curve gradually diverges from the data to a maximum difference of 80 microinches per inch at 75 seconds. No definite explanation was found for this deviation, although the influence of the constant properties solution (cf., Section 2.2) on the calculated strains is suspected.

In regard to the calculations, it should be mentioned that the calculated strains were quite sensitive to small changes in the assumed thermal expansion curve in the "a"-direction for pyrolytic graphite. The thermal expansion curve assumed in the final calculations is shown in Figure 24. The use of this curve in the strain calculations was found to yield the best fit to the experimental data of both plates.

5.2 Stress Distributions

The behavior of the strain curves presented in the previous section is better understood by first examining the calculated stress distributions in the plates. The stress distribution of σ_2 will not be presented here since it is not very different from the distribution of σ_1 .

Figures 16 and 17 show typical distributions of the normal stress, σ_1 , through the thickness of both a 1/8 inch and 1/4 inch thick plate at various locations along the length. The stresses at both surfaces of a plate are compressive, the larger stress occurring at the heated surface. The compressive stresses near the surfaces are exactly balanced by the tensile stresses deeper in the plate. The

stress distribution near the trailing edge ($x_1/L = 1/6$) is almost solely due to the temperature distribution $T_H(x_3)$. Other temperature variations contribute to the stress distribution at distances farther along the length. These are seen to increase the stresses.

Since the maximum compressive stresses occur at the heated surface and the maximum tensile stresses occur near the midplane ($x_3/h = 0.5$), the stresses at both of these locations were plotted as functions of time for both plates in Figures 18 and 19. The stresses increase during the initial heating period, but gradually approach constant values as the temperature gradients in the plates cease changing. This behavior is in marked contrast to the strain variations in the plates which appear to increase without limit.

Figures 18 and 19 also show how the calculated stresses increase with increasing distances from the trailing edge. As mentioned above, temperature variations other than $T_H(x_3)$ are responsible for this variation. The proportional increase in the stresses is much greater in the 1/8 inch thick plate than in the 1/4 inch thick plate. This is due to the larger lengthwise temperature gradients which occurred in the 1/8 inch thick plates.

Distributions of the normal stress, σ_3 , perpendicular to the plane of the plate and the shearing stress, σ_5 , are shown in Figures 20 and 21. These are typical for both the 1/8 inch and 1/4 inch thick plates. The stresses are seen to be of negligible magnitude. Therefore, one might be led to apply the usual plane stress approximation for the two cases considered here. Upon closer examination, however, it becomes clear that the plane stress solution would lead to completely erroneous

results since the temperature distribution given by equation (7) does not satisfy simultaneously both the assumptions of plane stress and the compatibility conditions. This is more easily shown by inspection of either equations (8) or equations (31) from which the important stresses are seen to be strong functions of the thickness coordinate, x_3 (also see Figures 16 and 17). On the other hand, the stresses calculated from plane stress are assumed independent of x_3^* , and so they would be totally inconsistent with the exact results. The solution may be slightly simplified by assuming at the outset that σ_3 , σ_4 , and σ_5 are zero, but the full three-dimensional equations would still have to be retained in formulating the solution.

The strain variation in the plates can now be explained on the basis of the information presented on the stress distributions. The strain, ϵ_1 , at the unheated surface is given by the Hooke's law relation (4)

$$\epsilon_1 = \frac{1}{E_{11}} \sigma_1 - \frac{\nu_{12}}{E_{11}} \sigma_2 - \frac{\nu_{13}}{E_{33}} \sigma_3 + \alpha_1 T$$

where the stresses and the thermal expansion are evaluated at the unheated surface. Since σ_3 is negligible and σ_2 is of the same order as σ_1 , the strain is approximately

$$\epsilon_1 \approx \frac{(1 - \nu_{12})}{E_{11}} \sigma_1 + \alpha_1 T$$

* Note: This is true, at least, for the first-order plane stress approximation. Higher-order plane stress approximations may approach the exact solution for certain temperature distributions⁹, but the use of these higher-order approximations probably would not simplify the solution.

Now σ_1 at the unheated surface is always compressive (See Figures 16 and 17), and at low temperatures the thermal expansion, $\alpha_1 T$, is negative. Thus, it is seen from the above relation that the strain will be compressive during the early heating period (See Figures 14 and 15). At later times σ_1 becomes nearly constant (Figures 18 and 19), while $\alpha_1 T$ becomes positive and increases almost linearly with the temperature rise. The thermal expansion eventually overtakes the compressive strains produced by σ_1 and then dominates the strain variation. The tensile strain variation is due to this effect.

The stress levels produced in the pyrolytic graphite plates are relatively low compared to the ultimate tensile strength of about 20,000 psi²⁰ measured for pyrolytic graphite. Figures 18 and 19 show that maximum stresses of -1400 psi and -3000 psi were produced in the 1/8 inch and 1/4 inch thick plates, respectively. However, one should bear in mind that the plates were subjected to a relatively low heating rate of about 40 Btu/sec-ft², and that higher heating rates would lead to more severe temperature gradients, which in turn would increase the thermal stresses. When one considers the fact that a heating rate of 1000 Btu/sec-ft² is not uncommon during the re-entry of space vehicles, the increased significance of thermal stresses is appreciated.

5.3 Effect of Anisotropy

The effect of the degree of anisotropy on the thermal stresses in a transversely anisotropic plate can be conveniently examined by considering the particular temperature distribution given by

$$T = bx_1^2$$

From equation (31) the normal stress σ_1 arising from this temperature distribution is

$$\sigma_1 = \frac{\alpha_1 E_{11} b h^2}{1 - \nu_{12}^2} \left(\nu_{13} \frac{E_{11}}{E_{33}} + \frac{\alpha_3}{\alpha_1} \right) \left[-\frac{1}{6} + z - z^2 \right]$$

The maximum value of the terms in the brackets is - 0.1667. The maximum stress can therefore be written in the following form:

$$-\frac{(1 - \nu_{12}^2)}{\alpha_1 E_{11} b h^2} \sigma_1 = 0.1667 \left(\nu_{13} \frac{E_{11}}{E_{33}} + \frac{\alpha_3}{\alpha_1} \right)$$

This equation shows that the effect of elastic anisotropy is contained in the ratios E_{11}/E_{33} and α_3/α_1 . In order to examine this effect by itself, it is convenient to specify that the ratio $(1 - \nu_{12}^2)/\alpha_1 E_{11}$, the temperature distribution $T = bx_1^2$, and the plate thickness h all remain constant. Then the maximum stress will simply increase linearly with the anisotropic parameter $\left[\nu_{13} \frac{E_{11}}{E_{33}} + \frac{\alpha_3}{\alpha_1} \right]$ as shown in Figure 22. Values of this parameter corresponding to a pyrolytic graphite plate and to an isotropic plate are indicated on the figure. The larger value for the pyrolytic graphite plate is due to the large value of α_3 compared to α_1 . It is interesting to note that the maximum stress in the pyrolytic graphite plate is more than 10 times the maximum stress in an isotropic plate.

The foregoing analysis may seem somewhat superficial since, in general, the thermal properties would vary with changes in the elastic properties, resulting in different temperature distributions for a given heating rate. For example, instead of comparing the pyrolytic graphite

plate to the isotropic plate with identical thermal properties, it might have been compared to an isotropic plate of ordinary graphite. In this case, the temperature gradients of the type $T = bx_1^2$ would be much smaller in the pyrolytic graphite plate than in the ordinary graphite plate due to its much higher thermal conductivity in the plane. The higher stresses in the pyrolytic graphite plate caused by elastic anisotropy might then be just compensated by the smaller temperature gradients, so that the maximum stress in the pyrolytic graphite plate may be about the same as that in the ordinary graphite plate. Thus, if one were using the comparison of thermal stresses as the criterion for selecting a material for application, it would be important to account for the difference in temperature distributions. However, in practice, the heat shielding capability of a material is usually the governing criterion, in which case there would be no question about the superiority of pyrolytic graphite over ordinary graphite. Moreover, the purpose of the above analysis was simply to provide basic insight into the mechanism of elastic anisotropy. Although it may be more realistic physically to do so, the inclusion of temperature effects would merely tend to obscure the analysis because a general relationship does not appear likely to exist between the elastic properties of materials and their thermal properties.

5.4 Recommendations

In this section a few suggestions are made for extending the theoretical analysis, and some recommendations are forwarded for improving the experimental technique.

The generalization of the solution presented in Section 2.3 to any two-dimensional temperature distribution, $T = T(x_1, x_2)$, does not

appear to present any basic difficulties. It should be noted that the derivation of equation (16), the basic governing differential equation, was not based on the assumption of a particular two-dimensional temperature distribution. In principle, a solution of (16) could be derived for any two-dimensional temperature distribution by repeated integration of equations (19). However, solutions of the compatibility equations, (6d) and (6f), for the stresses, σ_4 and σ_6 , may present additional difficulties.

There also appears to be a good possibility of extending the solution to an orthotropic plate. Basically, this would simply involve some changes in the property coefficients of the transformed compatibility conditions (6). Such changes probably would not introduce any serious difficulties, but the problem has not been investigated.

Although the 500° F extensometer (cf., Section 3.4) proved to be adequate for the purposes of this investigation, it may leave much to be desired for strain measurements at higher temperatures and under highly transient conditions. Considerable improvement in this technique could probably be achieved by the development of an extensometer designed specifically for such conditions. This extensometer should incorporate the following features:

1. Knife edges constructed from a material of low thermal conductivity which can withstand very high temperatures.
2. Body constructed from a material of high thermal conductivity and low thermal expansion.
3. A radiation heat shield integral with the body of the extensometer.

These features would reduce the heat transfer to the body of the extensometer and also reduce the uncertainties involved in the correction for the thermal expansion of the gage itself. Although an extensometer designed for use at temperatures up to 1000° F has been described in Reference 23, it is evidently not yet available commercially.

In addition to these modifications of the extensometer, a means of recording the strain readings by other than visual observations would be desirable.

6.0 CONCLUSIONS

The results of this investigation lead to the following conclusions:

1. The general equations of thermoelasticity were developed for a transversely anisotropic material such as pyrolytic graphite. The equations were solved exactly for a particular two-dimensional temperature distribution in a flat plate to yield a solution for the stress-strain distribution.
2. A technique was described for measuring transient strains up to a temperature of 1500° F using a Tuckerman optical strain gage.
3. The strains measured in heated pyrolytic graphite plates by this technique were generally in agreement within experimental error (± 20 microinches per inch) with the strains calculated from the analytical solution.
4. The calculated stress distributions showed that only the stresses (σ_1 and σ_2) in a direction parallel to the plane of a plate were of significant magnitude. Although the shearing stresses (σ_4 , σ_5 , and σ_6) and the stress normal to the plane (σ_3) were negligible, the plane stress approximation was found to be inapplicable.
5. The thermal stresses in a transversely anisotropic plate were shown to increase linearly with the anisotropic parameter, $\left[\nu_{13} \frac{E_{11}}{E_{33}} + \frac{\alpha_3}{\alpha_1} \right]$, for the temperature distribution $T = bx_1^2$. For this case, the maximum stress in a pyrolytic graphite plate was found to be more than 10 times that in an isotropic plate.

BIBLIOGRAPHY

1. D.R. Hornbaker "Transient Temperature Distributions in a Thermally Orthotropic Plate with Non-uniform Surface Heating," Univ. of Calif. Eng. Proj. Rept. HE-150-189, June 1961.
2. G.Z. Zizicas "Transient Thermal Stresses in Thin Isotropic Elastic Plates," UCLA Eng. Rept. 52.7, April 1952.
3. J.S. Przemieniecki "Transient Temperatures and Stresses in Plates Attained at High-Speed Flight," J. Aero. Sci., 22, 5, 345-8, May 1955.
4. P.J. Schneider "Variation of Maximum Thermal Stresses in Free Plates," J. Aero. Sci., 22, 892, 1955.
5. I.S. Sokolnikoff
E.S. Sokolnikoff "Thermal Stresses in Elastic Plates," Trans. Am. Math. Soc., 45, 235-255, 1939.
6. B.E. Gatewood "Thermal Stresses in Moderately Thick Elastic Plates," J. Appl. Mech., 432-436, Sept. 1959.
7. W.H. Pell "Thermal Deflections of Anisotropic Thin Plates," Quart. Appl. Math., 4, 1, 27-44, April 1946.
8. W. Nowacki "Thermal Stresses in Orthotropic Plates," Bulletin, Polish Academy of Sciences, Vol. VII, No. 1, 1959.
9. B. A. Boley
J. H. Weiner Theory of Thermal Stresses, John Wiley & Sons, Inc., New York, 1960.
10. S. Timoshenko
J.N. Goodier Theory of Elasticity, 2nd Ed., McGraw-Hill Book Co., New York, 1951.
11. A.E.H. Love A Treatise on the Mathematical Theory of Elasticity, 4th Ed., Dover Publications, New York, 1944.

12. H.B. Callen Thermodynamics, John Wiley & Sons, Inc., New York, 1960.
13. I.S. Sokolnikoff Mathematical Theory of Elasticity, 2nd Ed., McGraw-Hill Book Co., New York, 1956.
14. B.A. Boley
 I.S. Tolins "Thermoelastic Stresses and Deflections in Thin-Walled Beams," WADC Tech. Rept. 54-426, Dec. 1954.
15. P. Paine Private communication.
16. D. Wizansky
 E.J. Russ "An Oxyacetylene Flame Apparatus for Surface Ablation Studies," Univ. of Calif. Eng. Proj. Rept. HE-150-167, January 1959.
17. E.J. Russ "Heating Rate Characteristics of an Oxyacetylene Flame Apparatus for Surface Ablation Studies," Univ. of Calif. Eng. Proj. Rept. HE-150-176, December 1959.
18. L.L. Cobb, Jr. "The Influence of Hydrogen Recombination on Turbulent Flow Heat Transfer to a Flat Plate," Univ. of Calif. Eng. Proj. Rept. HE-150-183, June 1960.
19. "Optical Strain Gage," American Instrument Co., Inc., Bulletin 2294, July 1959.
20. W.V. Kotlensky
 H.E. Martens "Tensile Properties of Pyrolytic Graphite to 5000° F," Jet Propulsion Lab. Tech. Rept. No. 32-71, March 10, 1961.
21. "Pyrolytic Graphite Data Book," Lockheed Aircraft Corp., Missiles & Space Div., LMSD-28816, March 1960.
22. "Data Sheet --- Pyrolytic Graphite," High Temperature Materials, Inc., Sept. 1960.

23. H.D. Howerton "Optical Strain Gages for Use at Elevated Temperatures," ASTM, Spec. Tech. Pub. No. 230, 1958.
24. B.G.Galerkin "Determination of Stresses and Strains in an Isotropic Elastic Body Body with the Help of Three Functions," (in Russian) Jzv. Naucz. --- Issl. Inst. Gidrotechn., Vol. 1, Leningrad (1931).

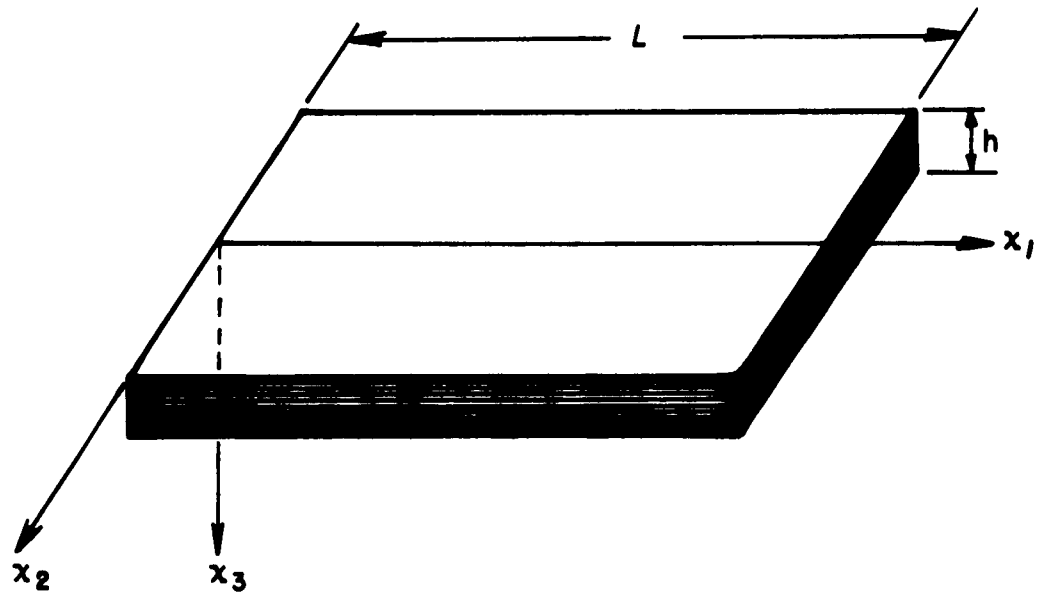


FIG.1 COORDINATE SYSTEM FOR A TRANSVERSELY ANISOTROPIC PLATE

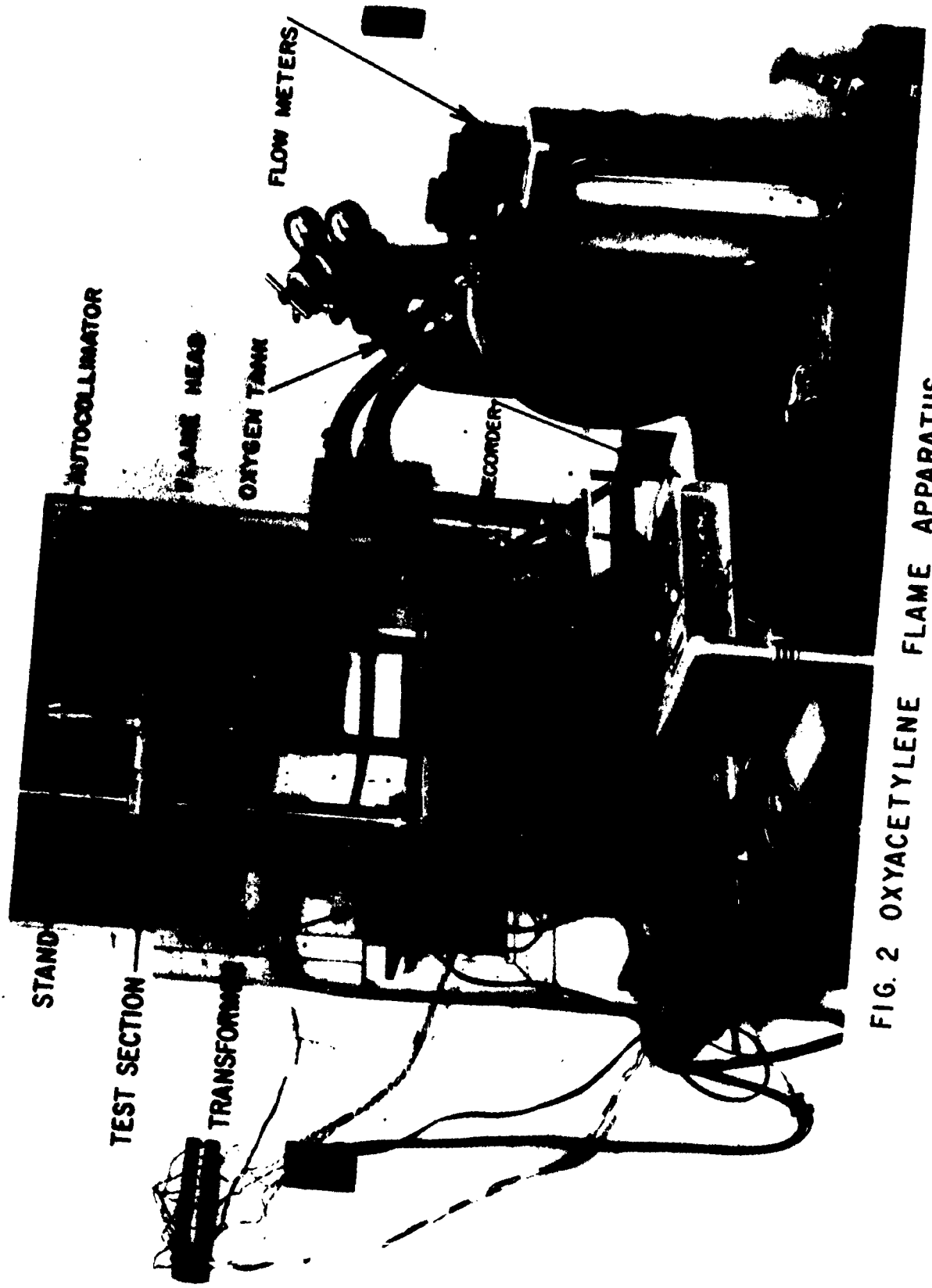


FIG. 2 OXYACETYLENE FLAME APPARATUS

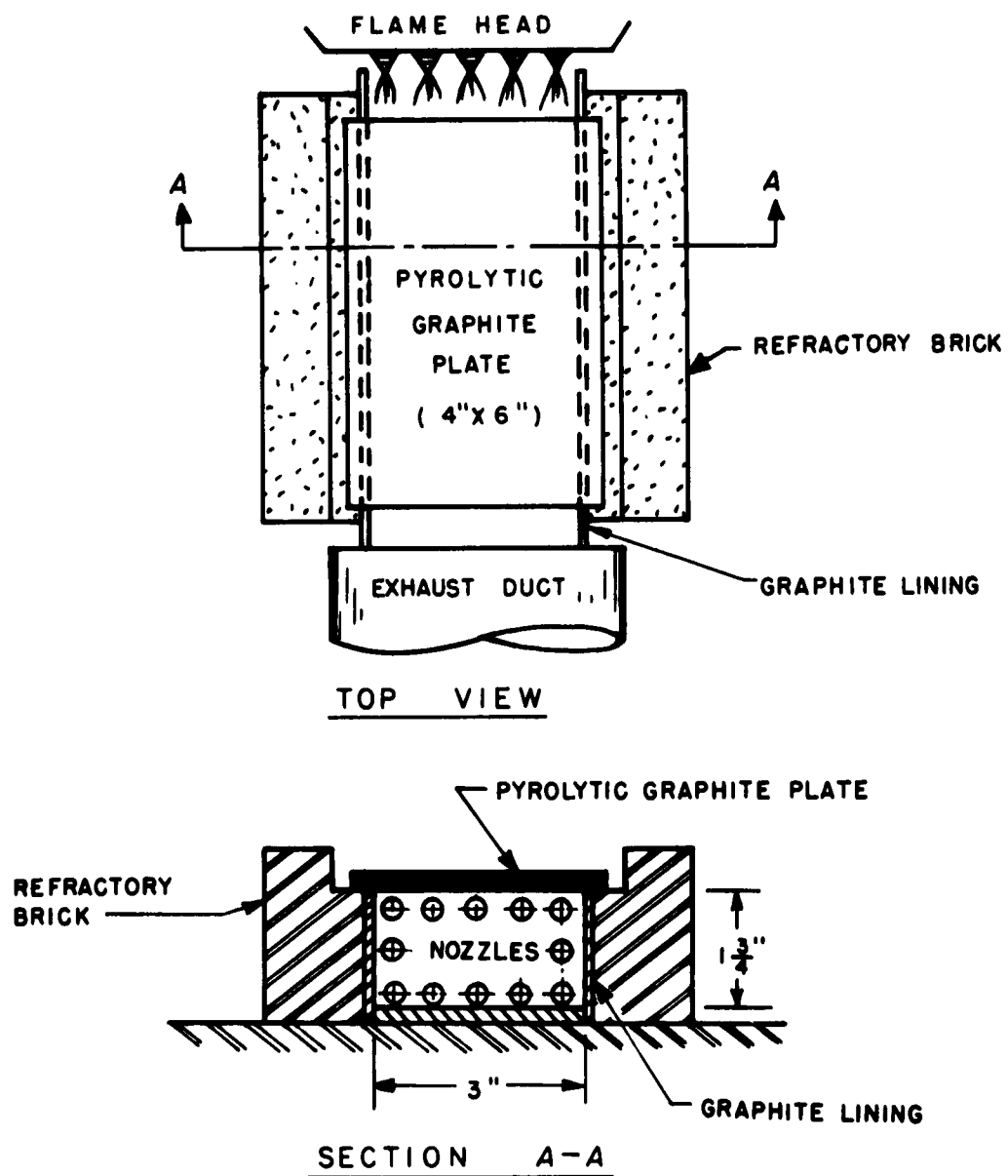


FIG. 3 DETAIL OF TEST SECTION ASSEMBLY

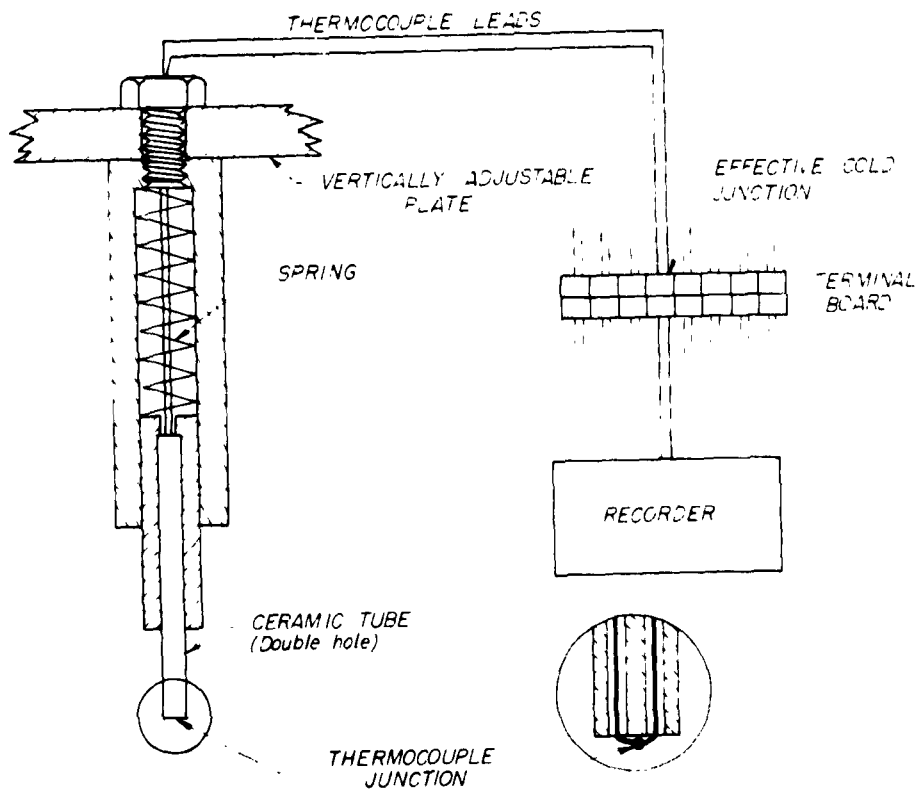


FIGURE 4 A - SCHEMATIC OF THERMOCOUPLE HOLDING DEVICE AND CIRCUIT

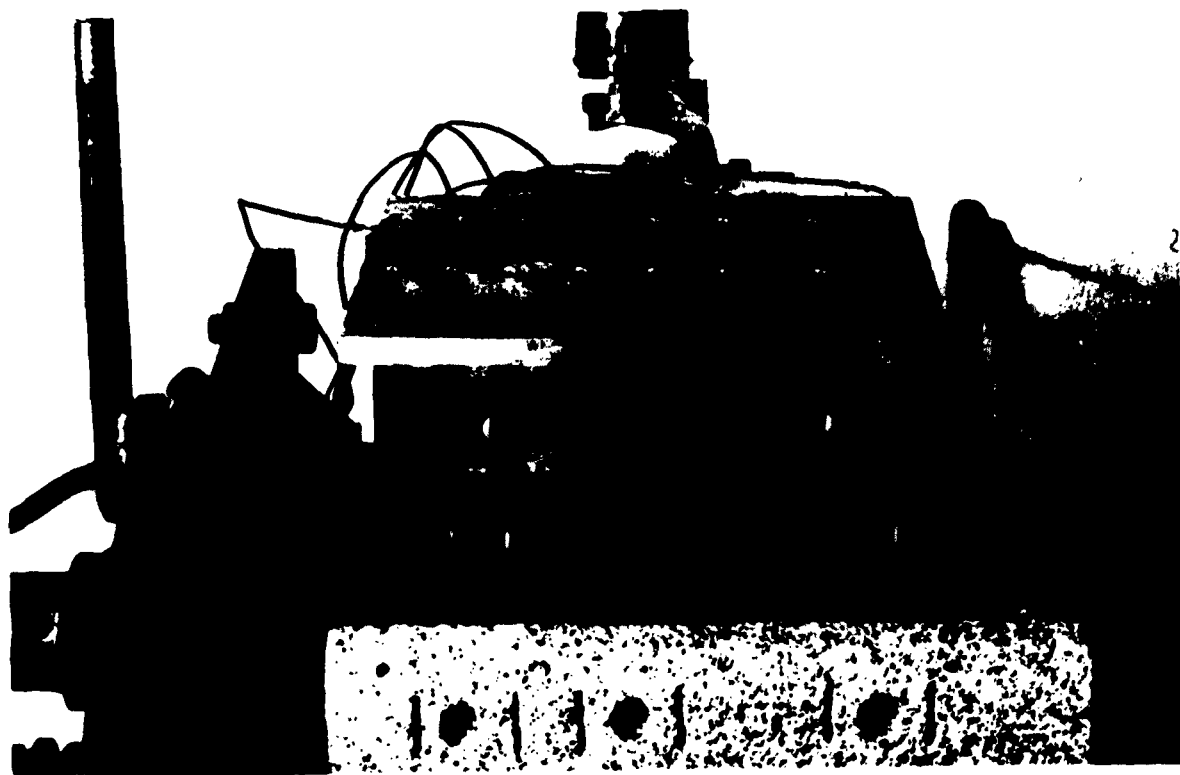


FIGURE 4 B - TEMPERATURE MEASUREMENT SYSTEM

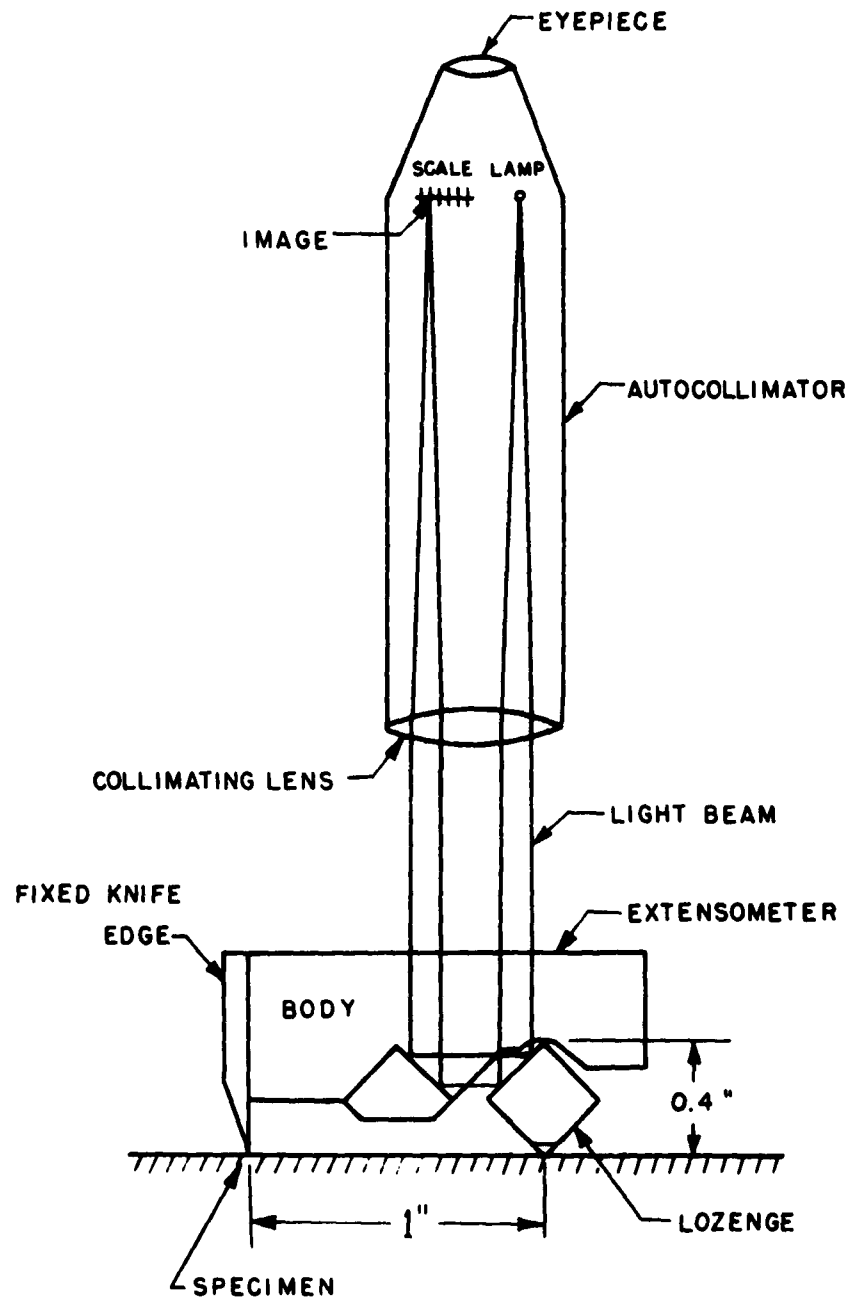


FIG. 5 SCHEMATIC DIAGRAM OF TUCKERMAN
OPTICAL STRAIN GAGE

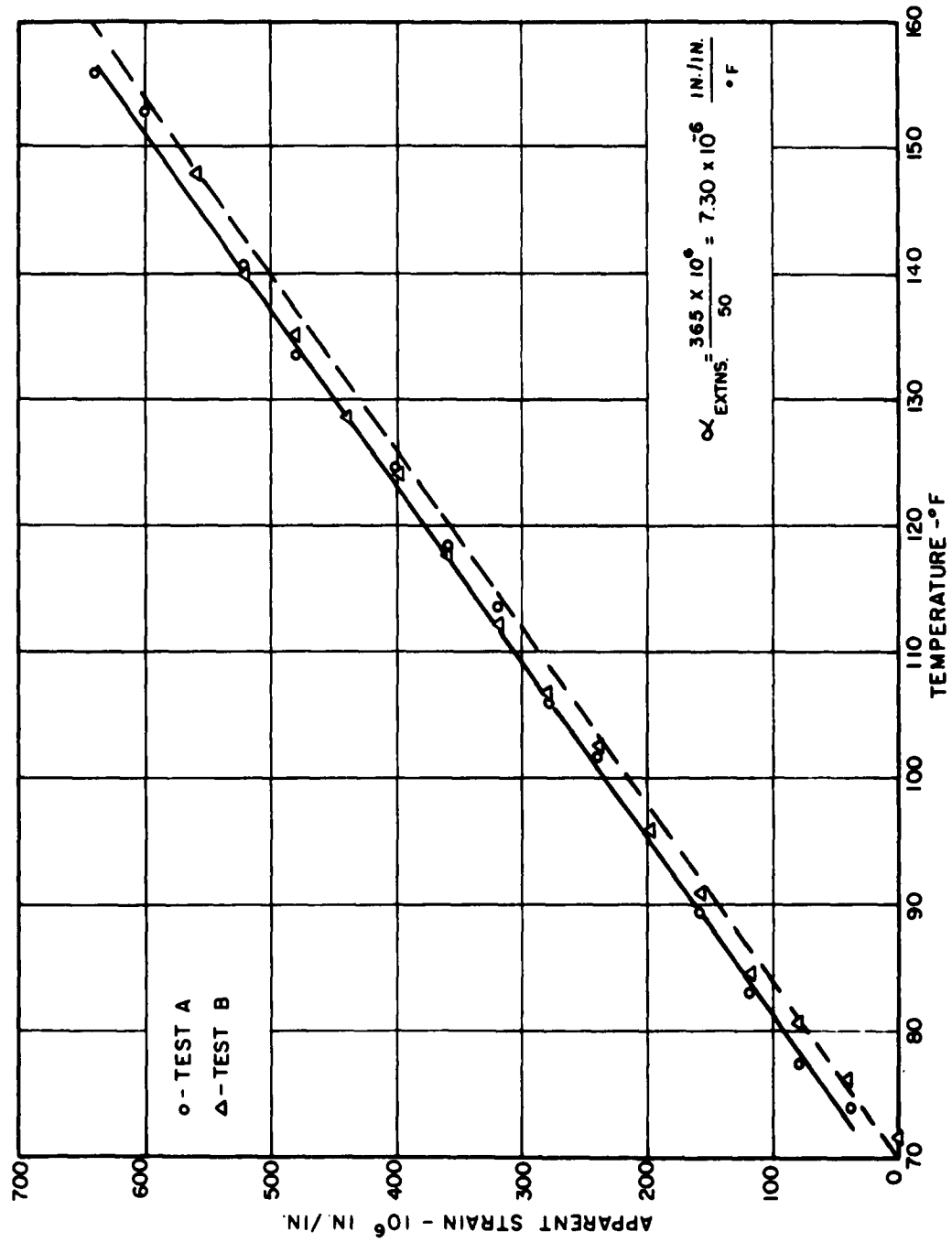


FIG. 6 CALIBRATION OF TUCKERMAN EXTENSOMETER (0.4 IN. LOZENGE)

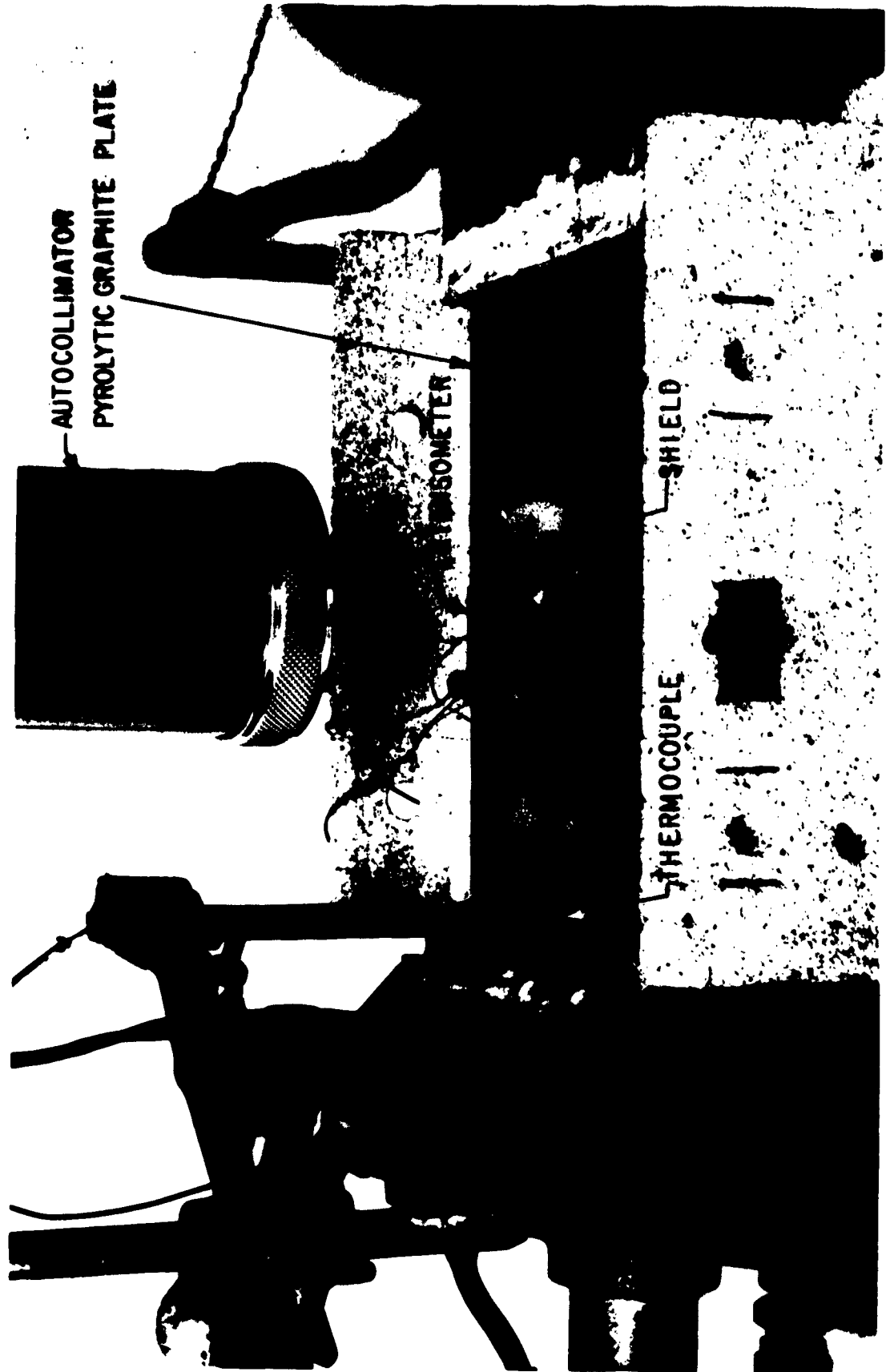
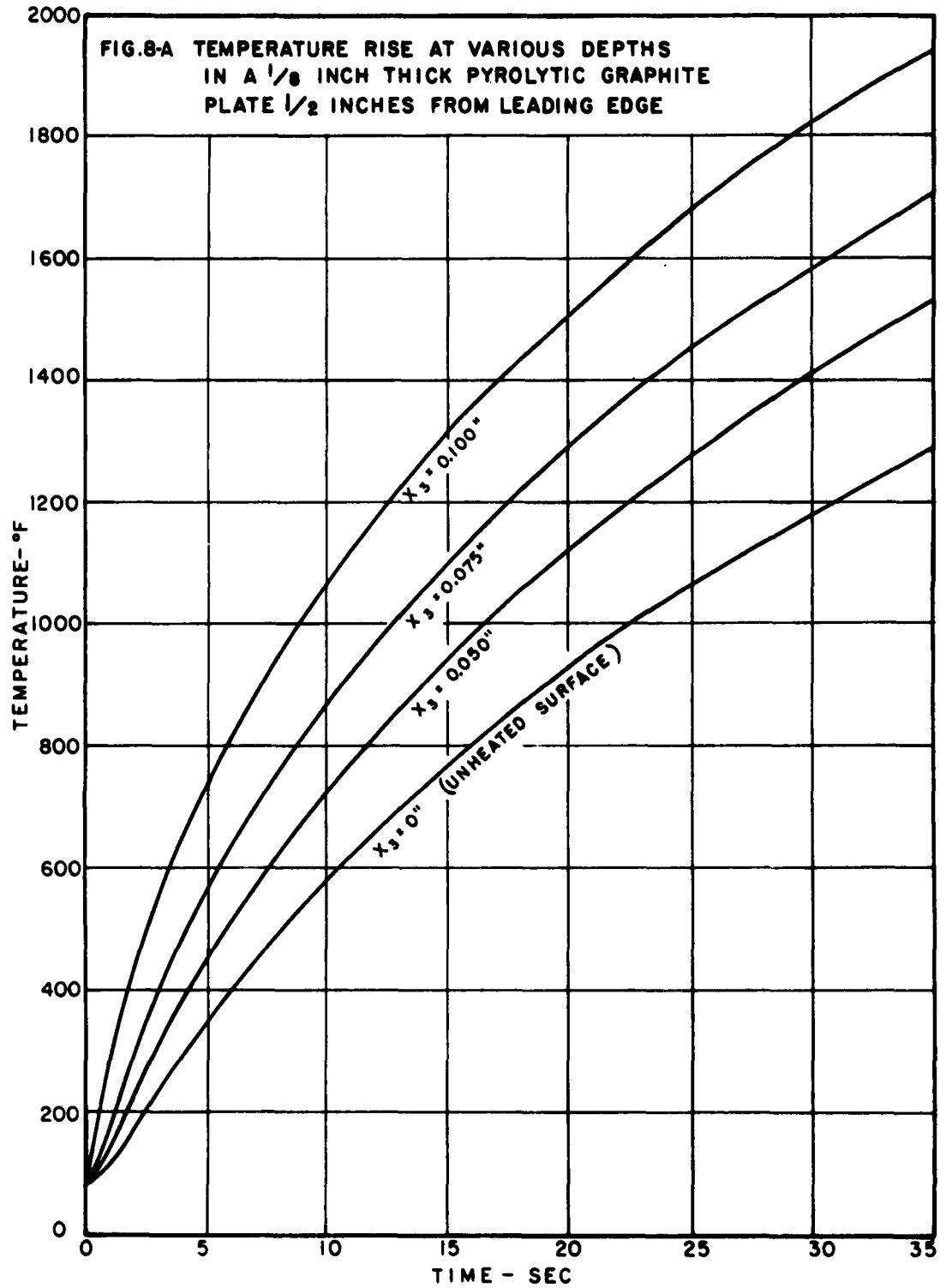
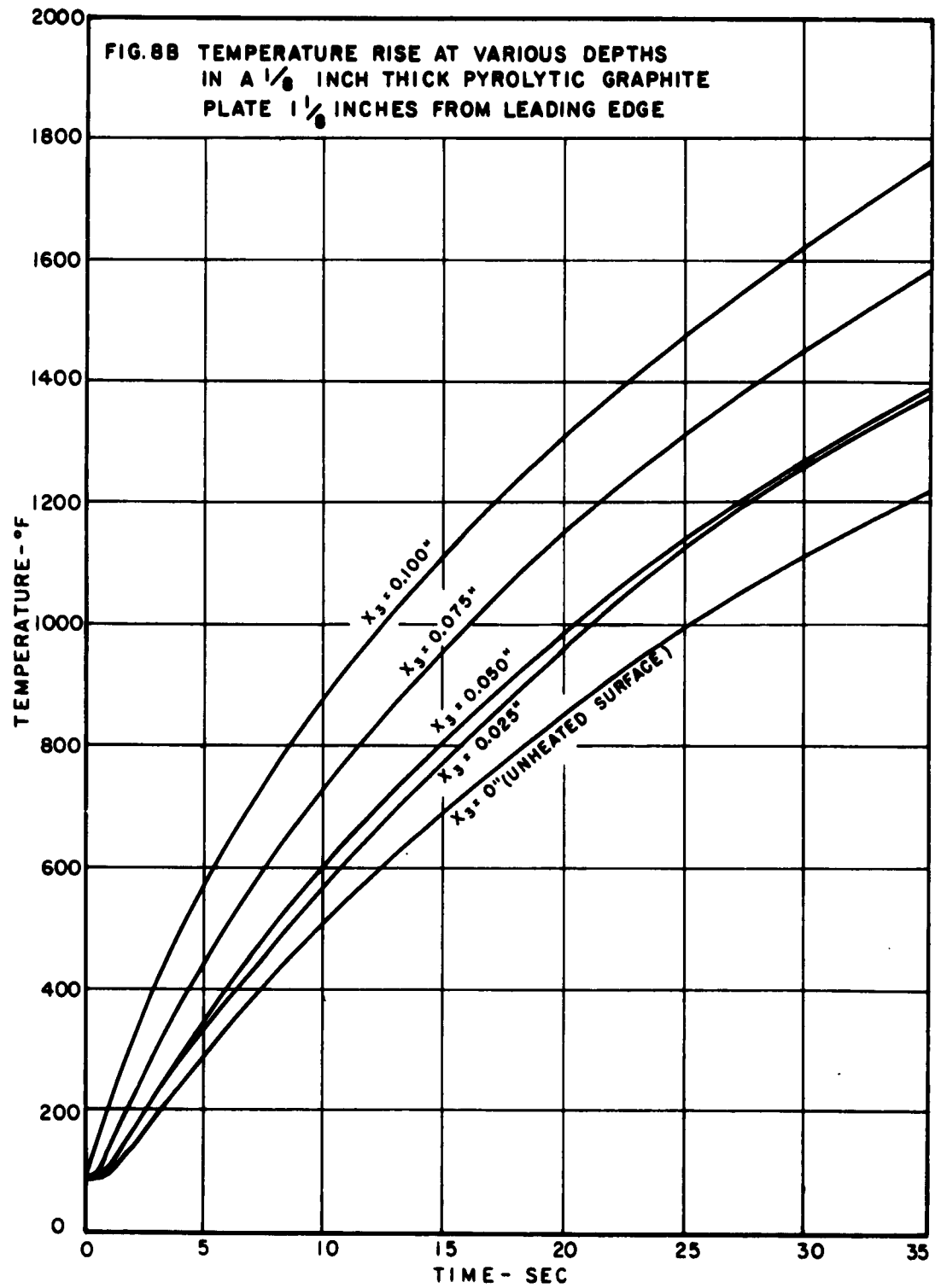
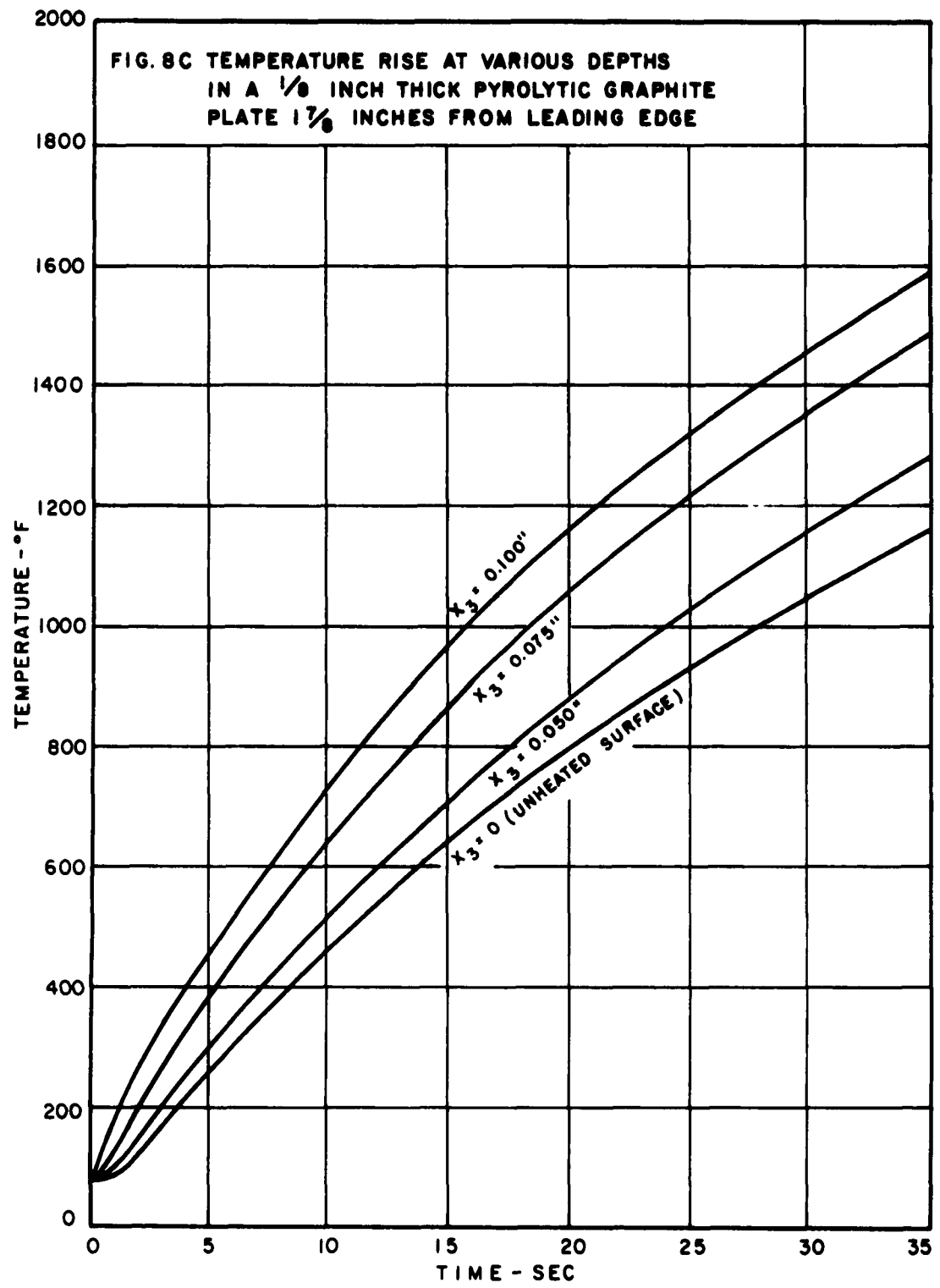
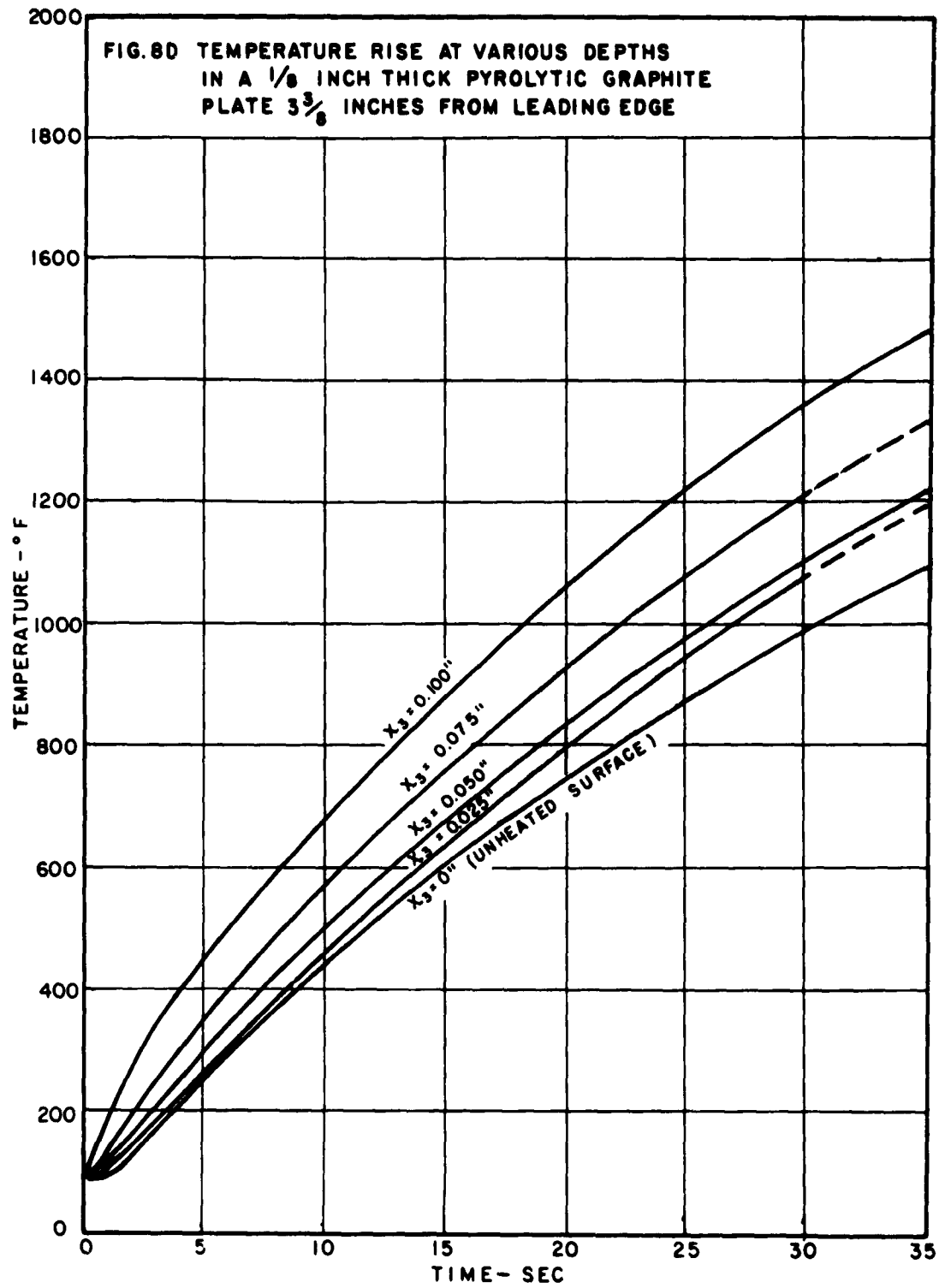


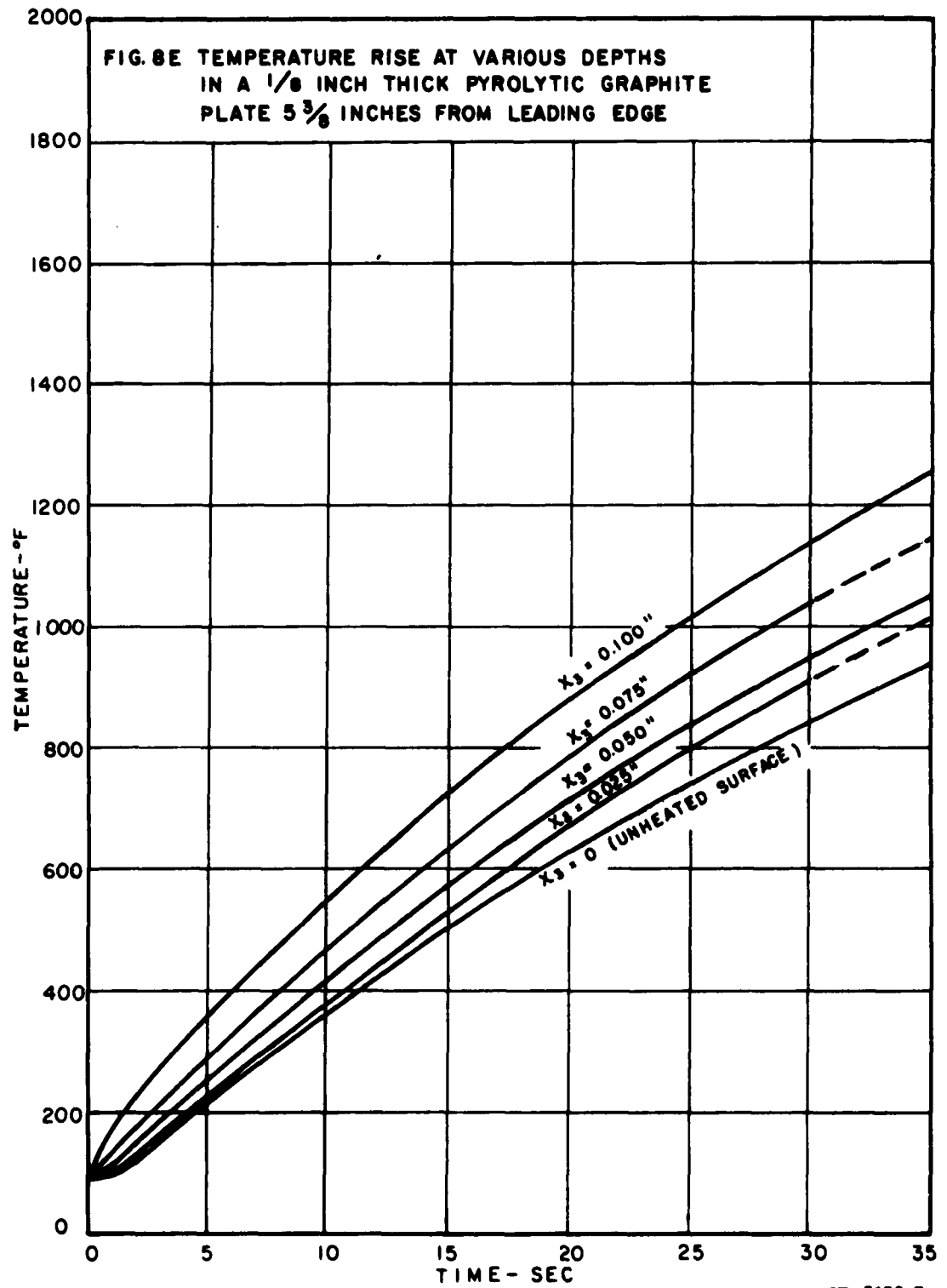
FIG. 7 STRAIN MEASUREMENT SYSTEM

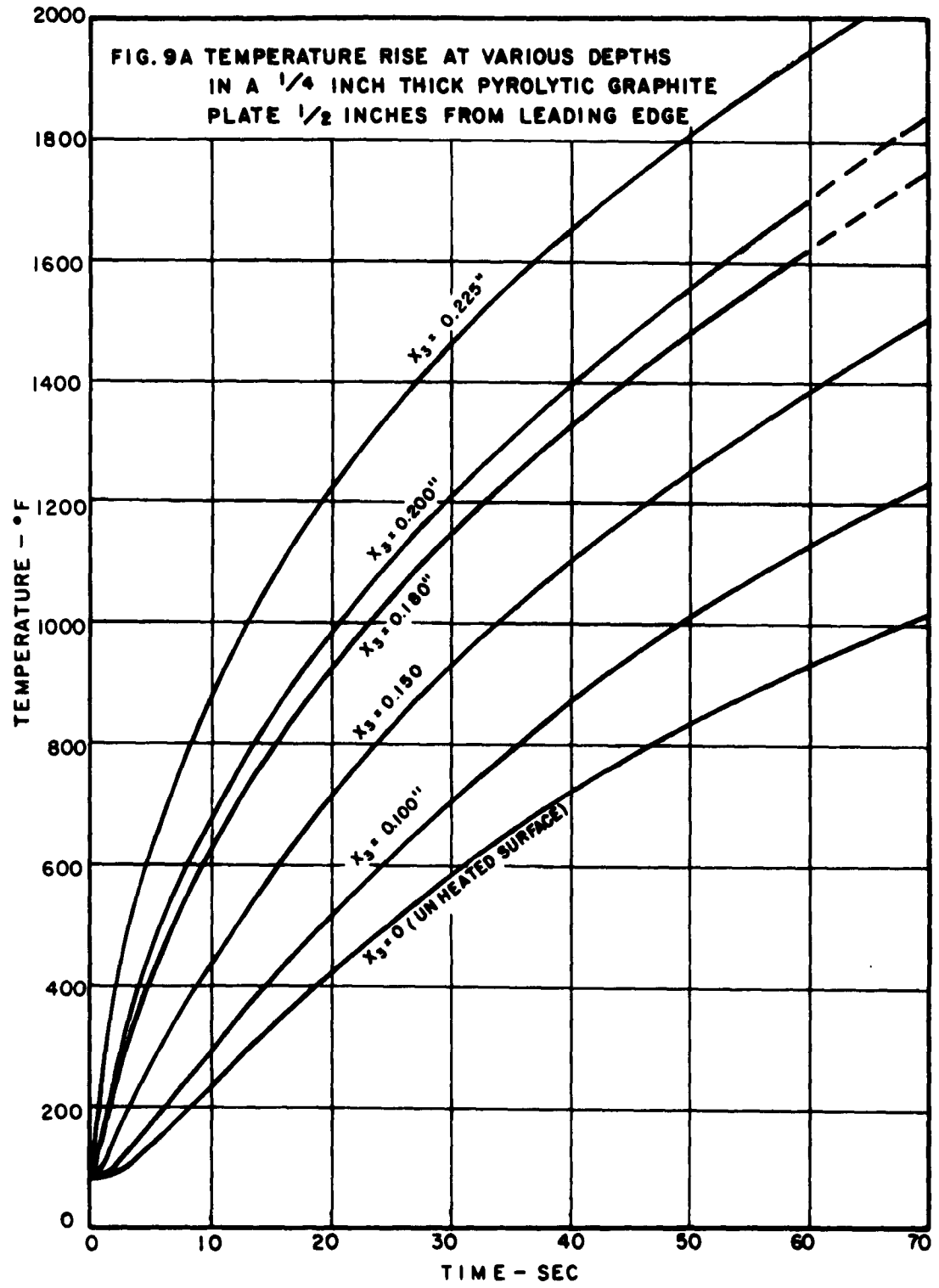




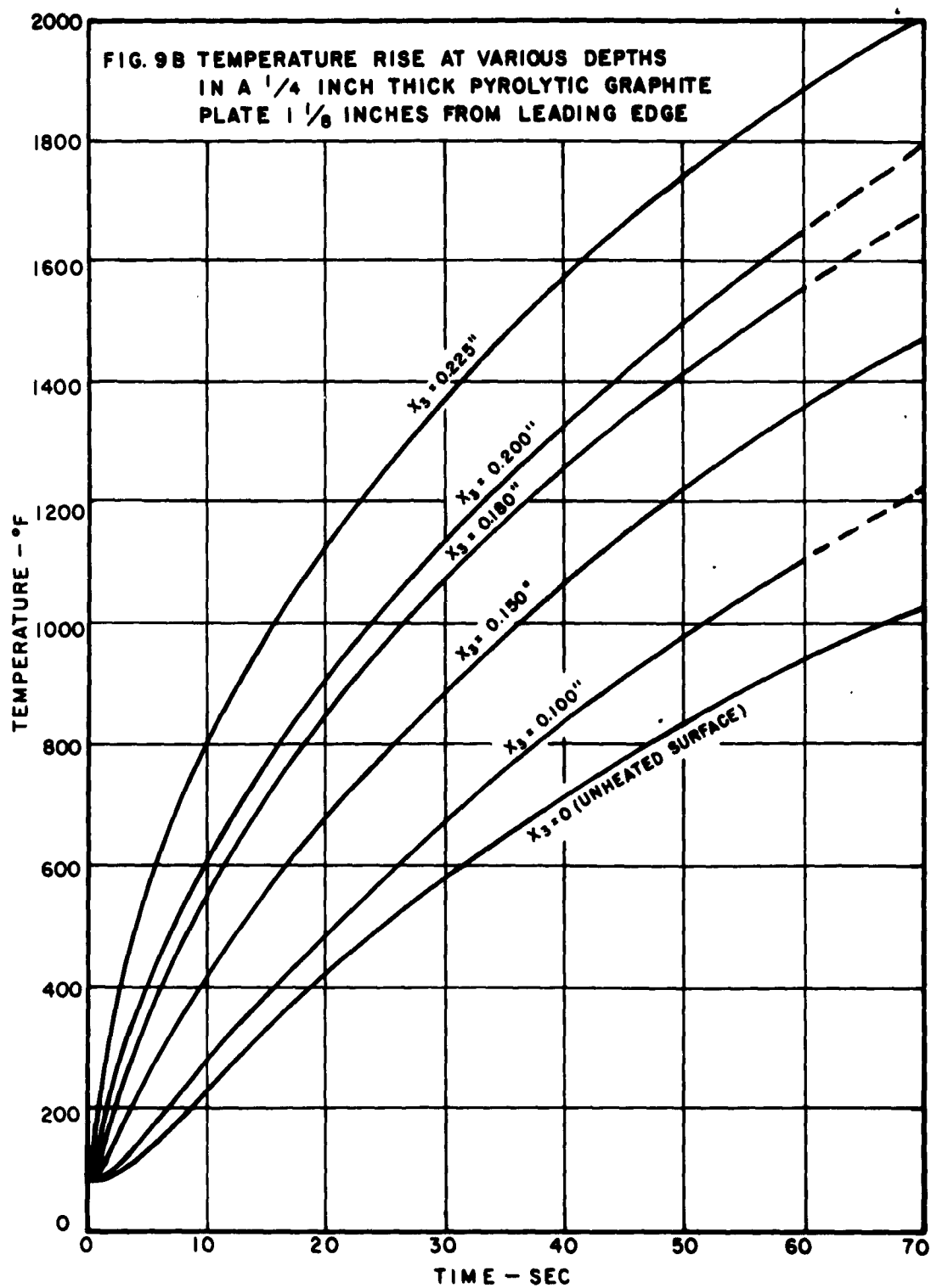


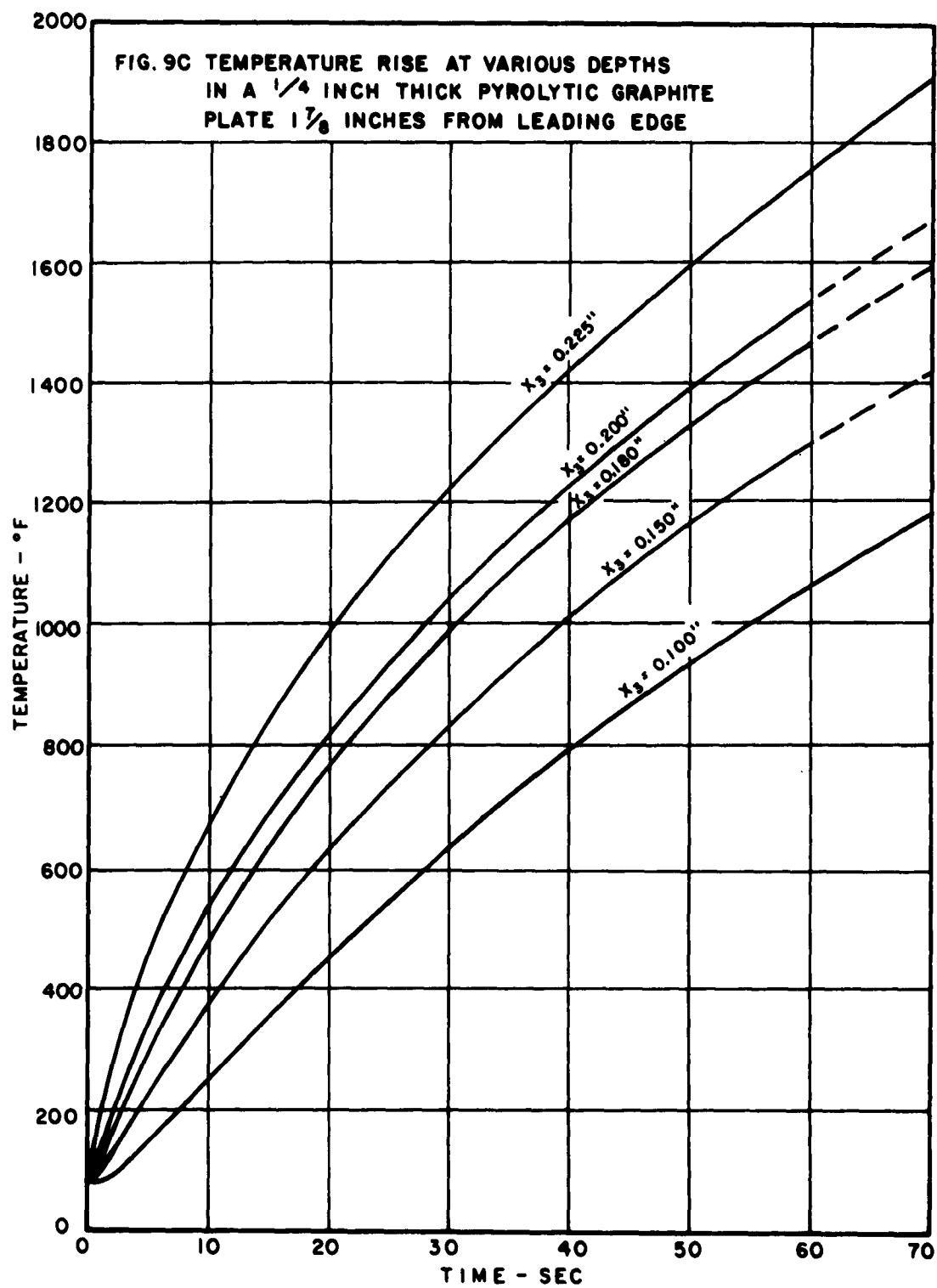




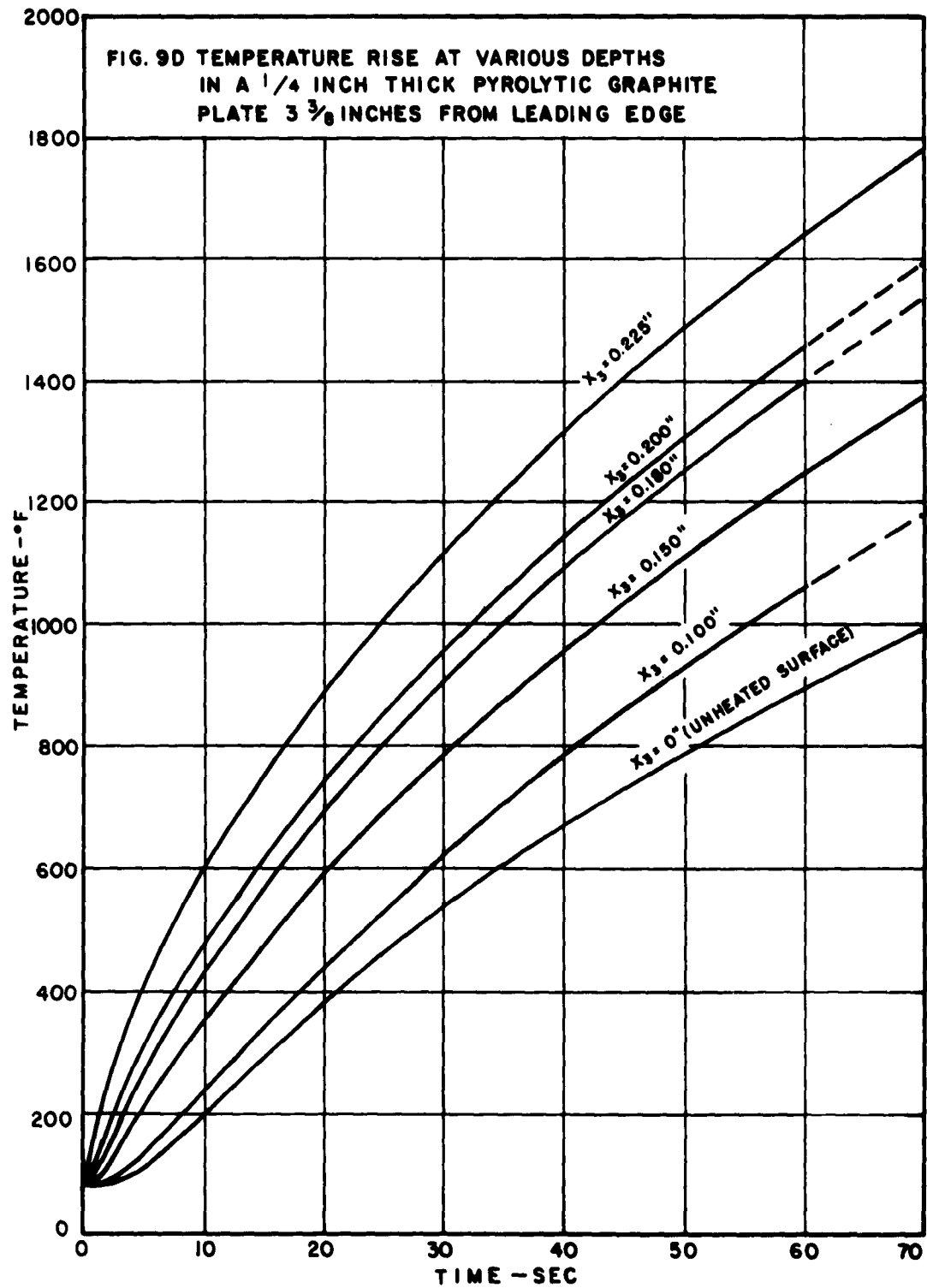


NYD 7674-A

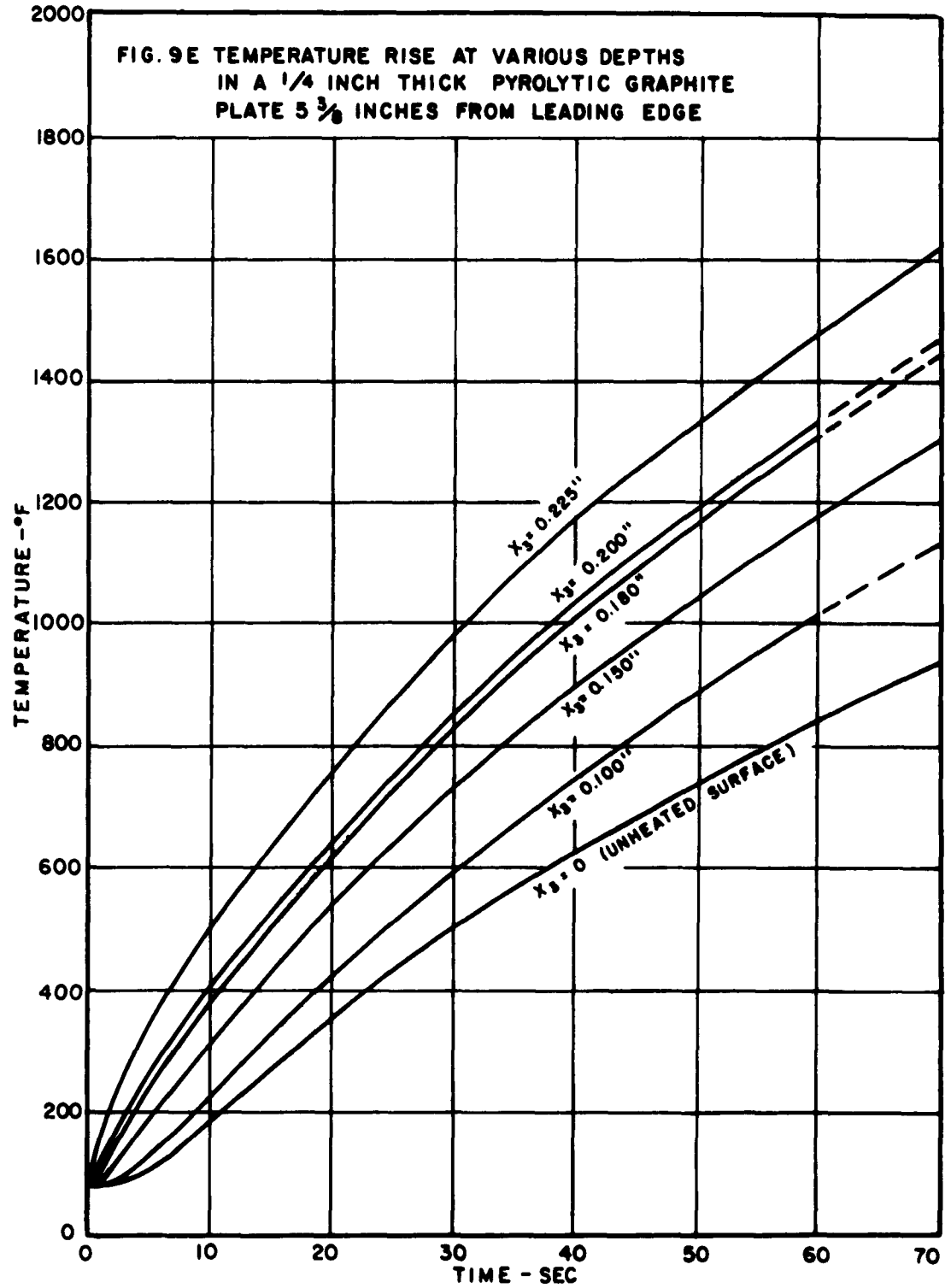




WD 7674-C



NYD 7674-D



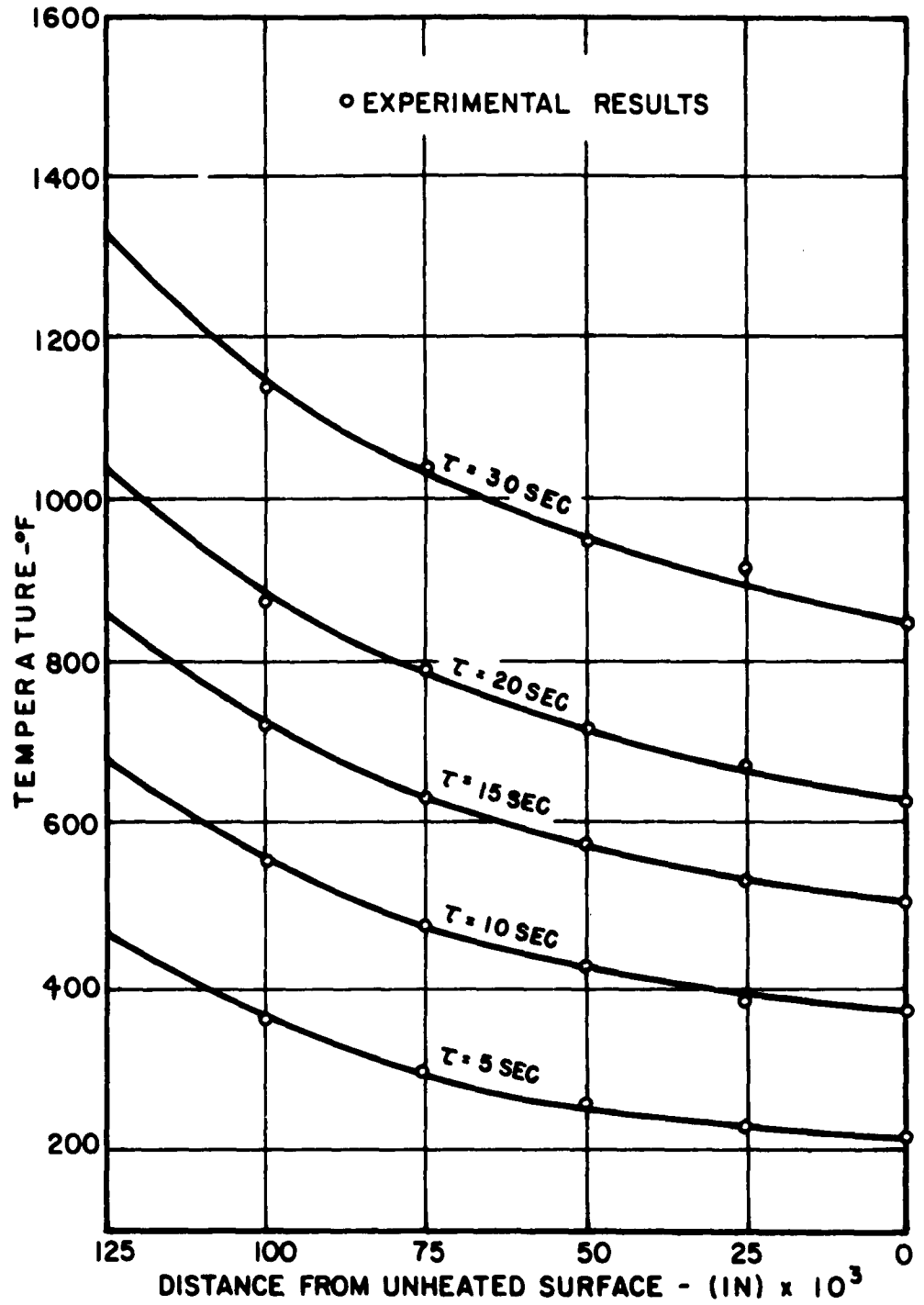
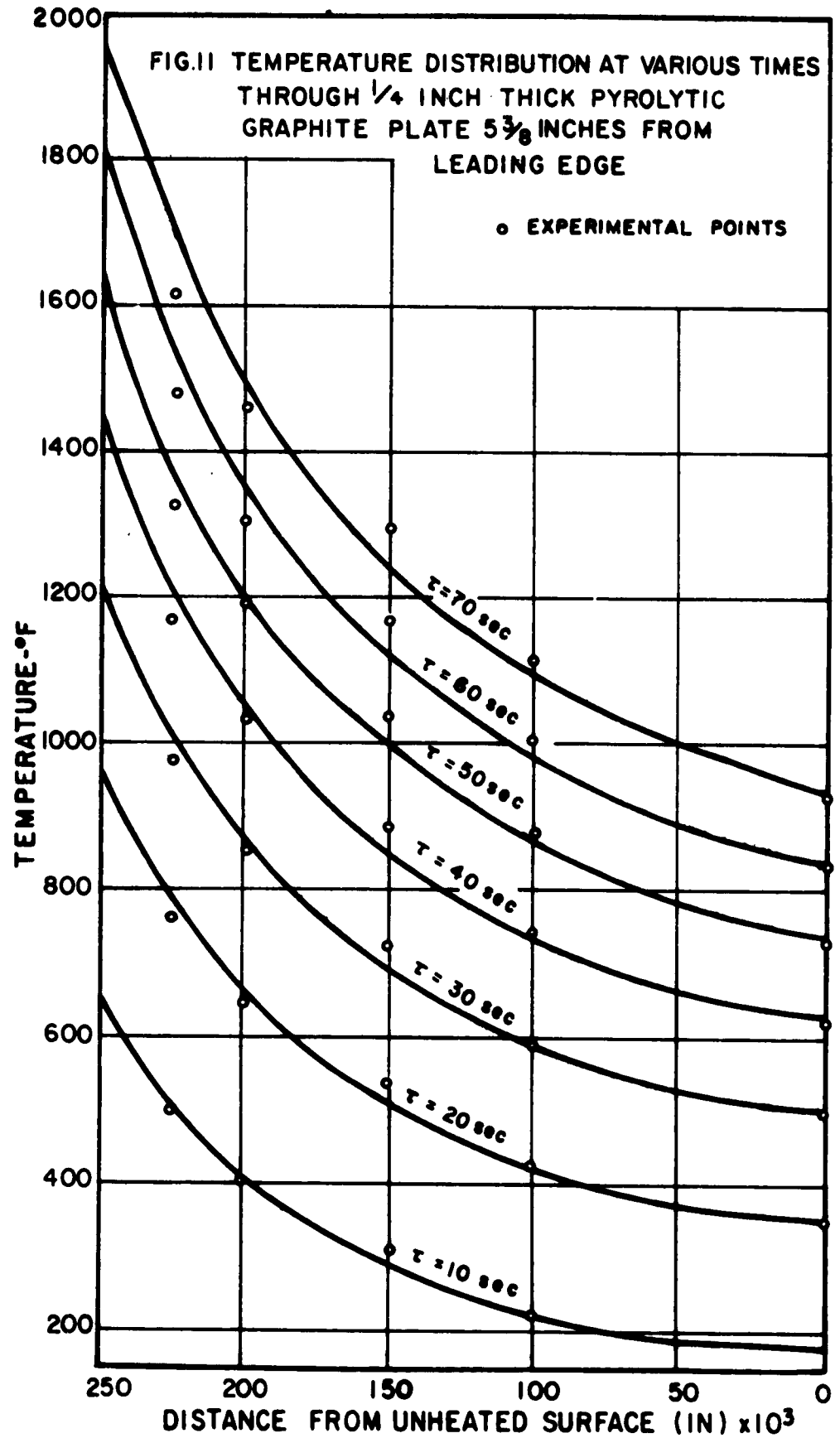


FIG. 10 TEMPERATURE DISTRIBUTION AT VARIOUS TIMES THROUGH $1/8$ INCH THICK PYROLYTIC GRAPHITE PLATE. $5 \frac{3}{8}$ INCHES FROM LEADING EDGE



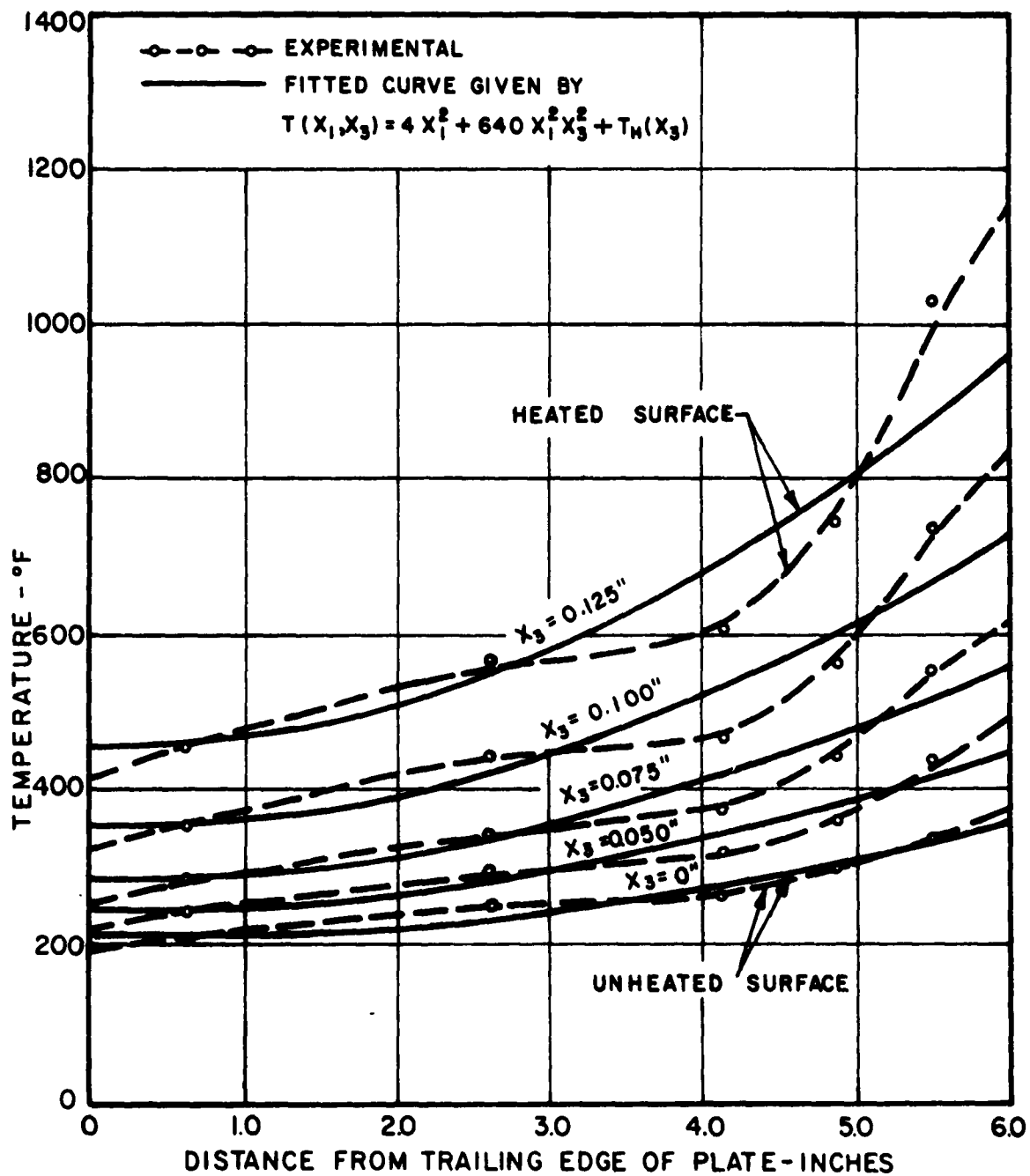


FIG. 12 A TEMPERATURE DISTRIBUTION ALONG LENGTH OF
 1/8 INCH THICK PYROLYTIC GRAPHITE PLATE AT
 VARIOUS DEPTHS AFTER 5 SECONDS OF HEATING

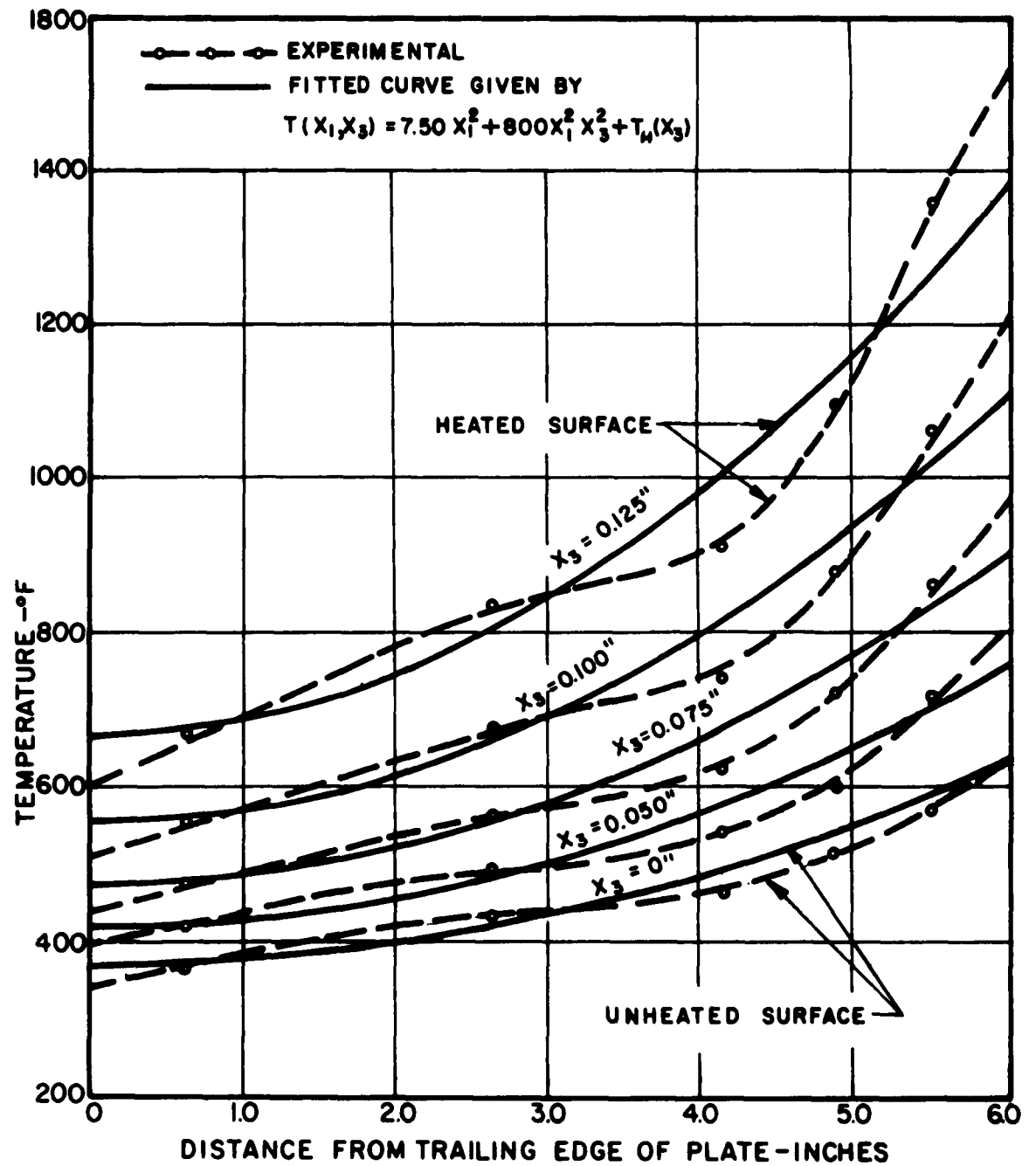


FIG. 12B TEMPERATURE DISTRIBUTION ALONG LENGTH OF
 1/8 INCH THICK PYROLYTIC GRAPHITE PLATE AT
 VARIOUS DEPTHS AFTER 10 SECONDS OF HEATING

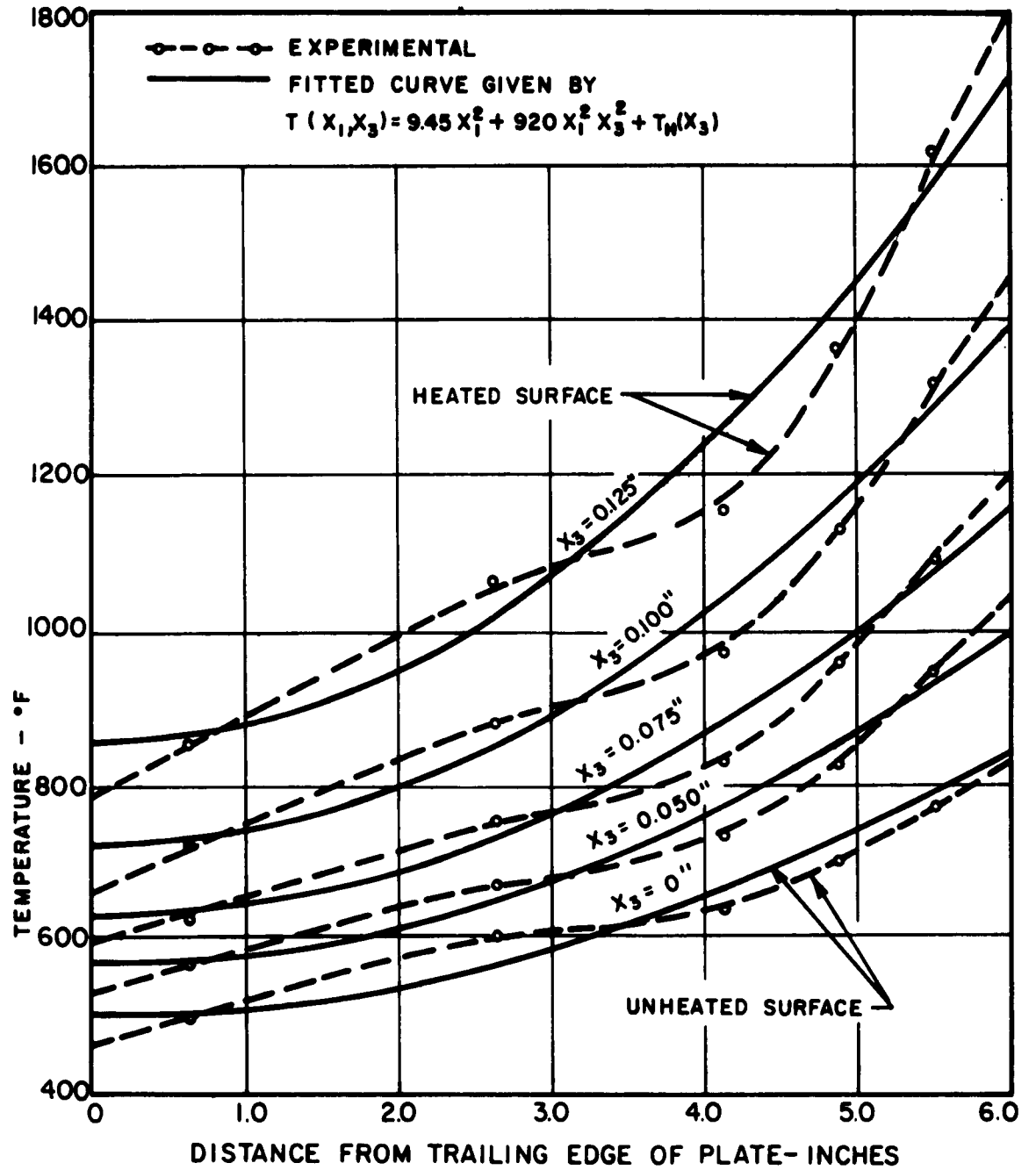


FIG. 12C TEMPERATURE DISTRIBUTION ALONG LENGTH OF
 1/8 INCH THICK PYROLYTIC GRAPHITE PLATE AT
 VARIOUS DEPTHS AFTER 15 SECONDS OF HEATING

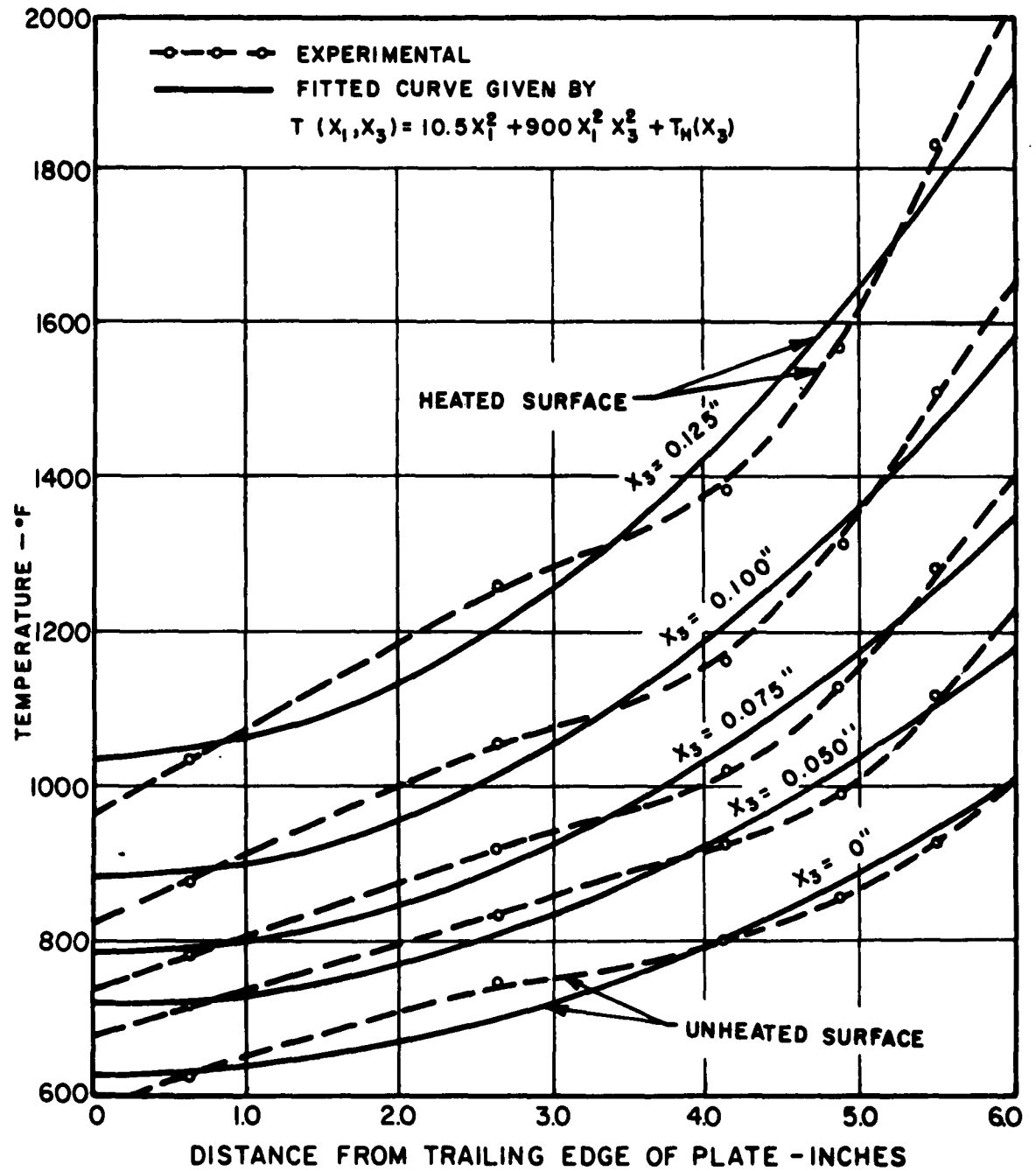


FIG. 12 D TEMPERATURE DISTRIBUTION ALONG LENGTH OF
 1/8 INCH THICK PYROLYTIC GRAPHITE PLATE AT
 VARIOUS DEPTHS AFTER 20 SECONDS OF HEATING

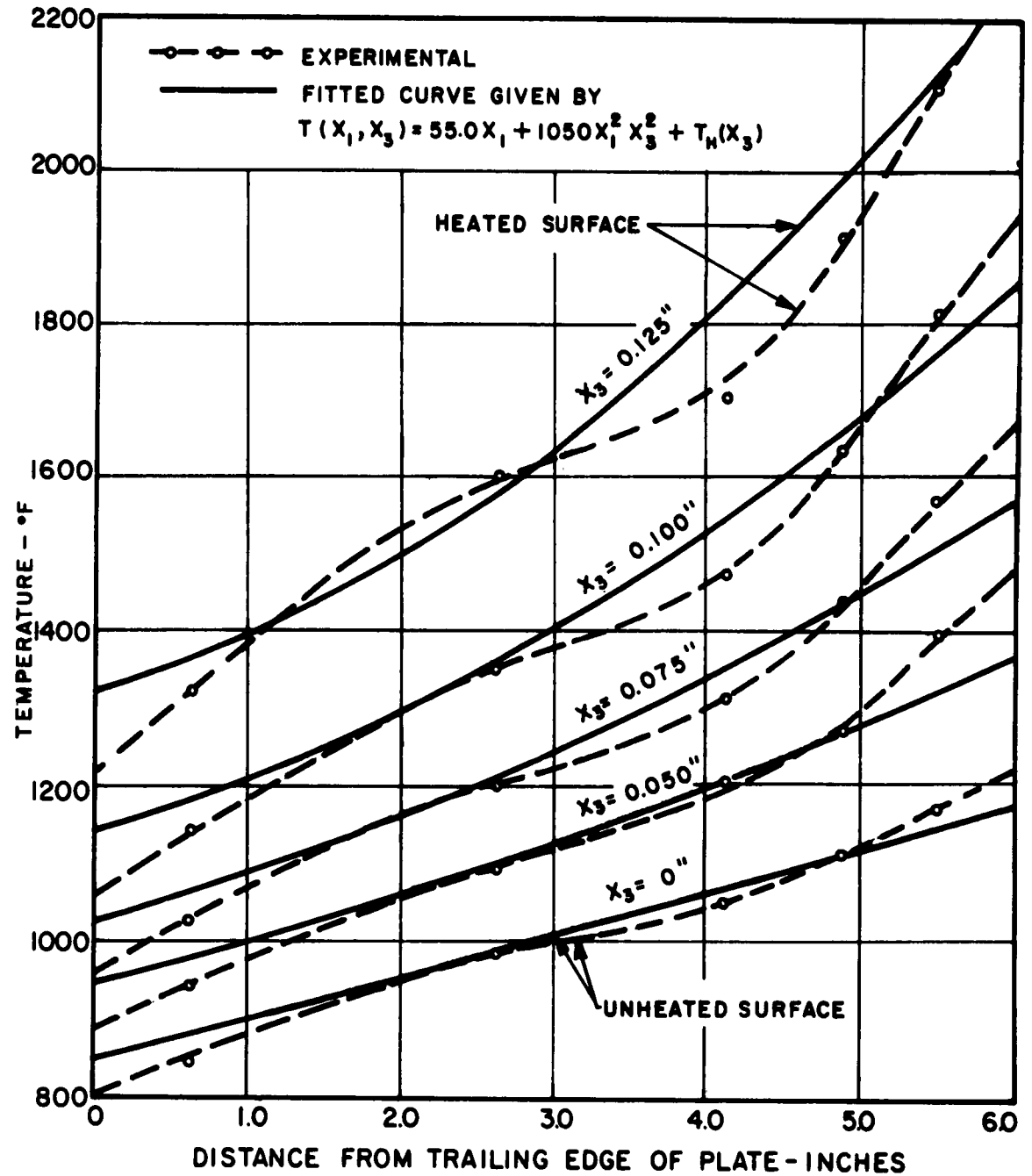


FIG. 12E TEMPERATURE DISTRIBUTION ALONG LENGTH OF
 1/8 INCH THICK PYROLYTIC GRAPHITE PLATE AT
 VARIOUS DEPTHS AFTER 30 SECONDS OF HEATING

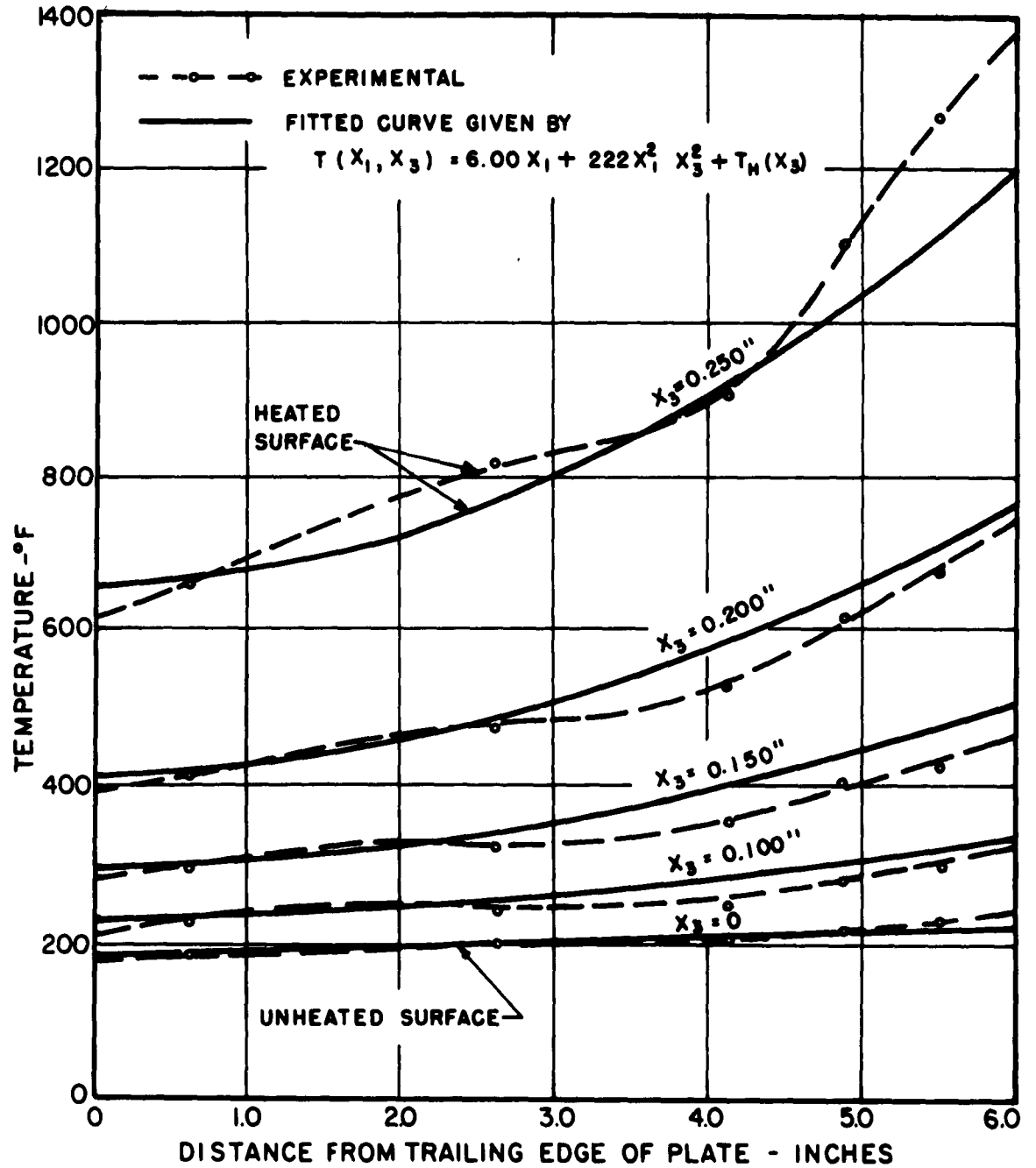


FIG. 13A TEMPERATURE DISTRIBUTION ALONG LENGTH OF 1/4 INCH THICK PYROLYTIC GRAPHITE PLATE AT VARIOUS DEPTHS AFTER 10 SECONDS OF HEATING

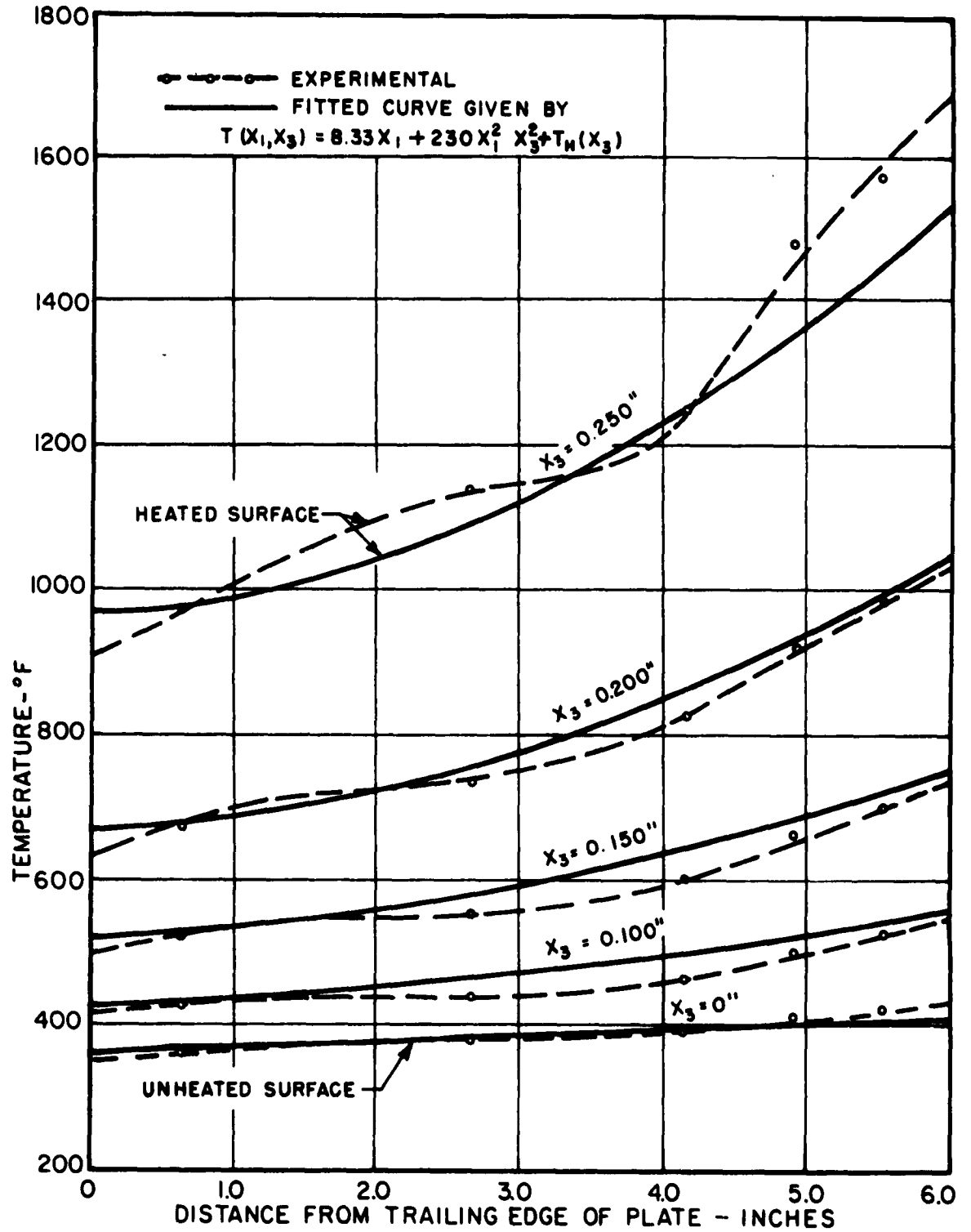


FIG. 13 B TEMPERATURE DISTRIBUTION ALONG LENGTH OF 1/4 INCH THICK PYROLYTIC GRAPHITE PLATE AT VARIOUS DEPTHS AFTER 20 SECONDS OF HEATING

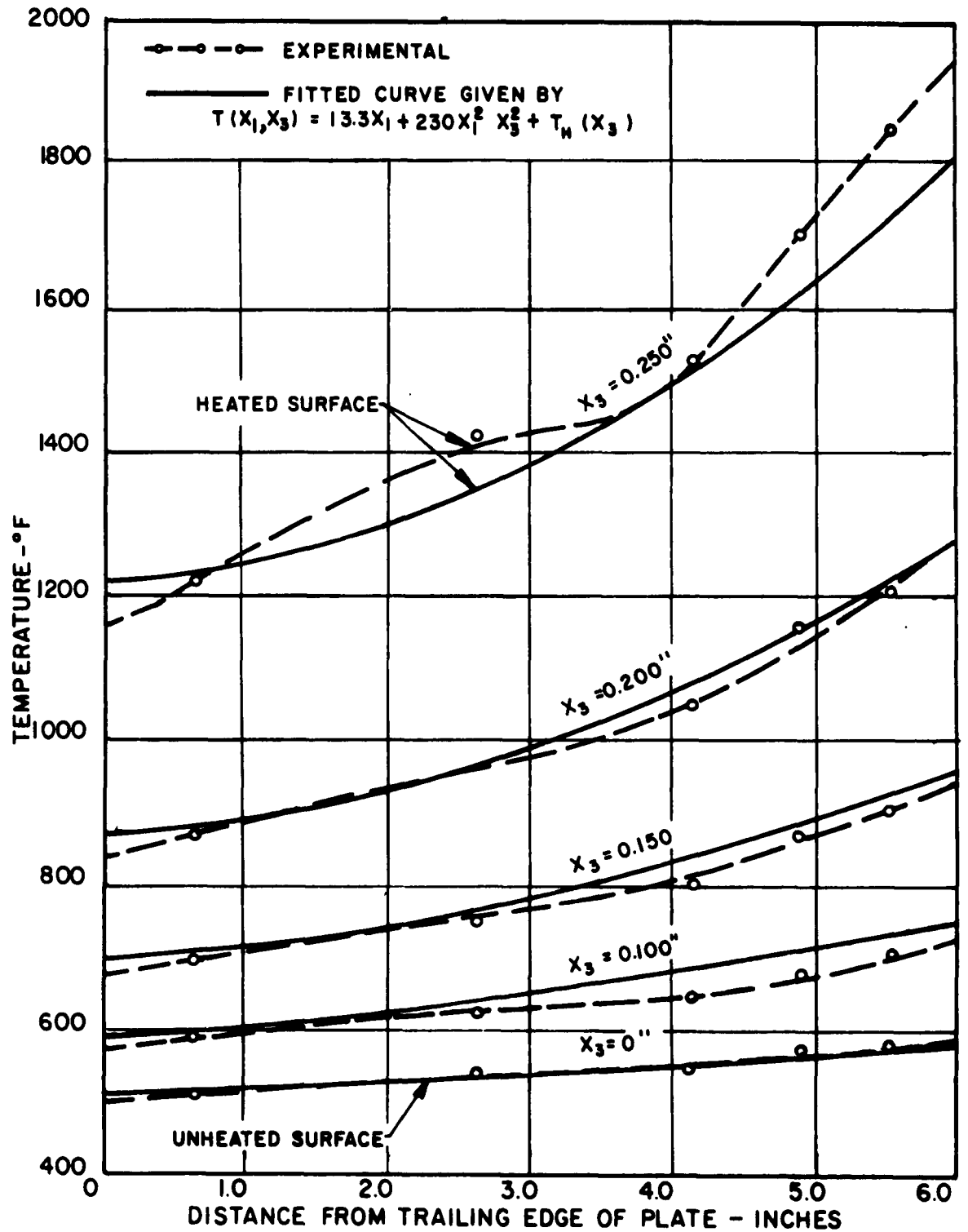


FIG.13C TEMPERATURE DISTRIBUTION ALONG LENGTH OF
 1/4 INCH THICK PYROLYTIC GRAPHITE PLATE AT
 VARIOUS DEPTHS AFTER 30 SECONDS OF HEATING

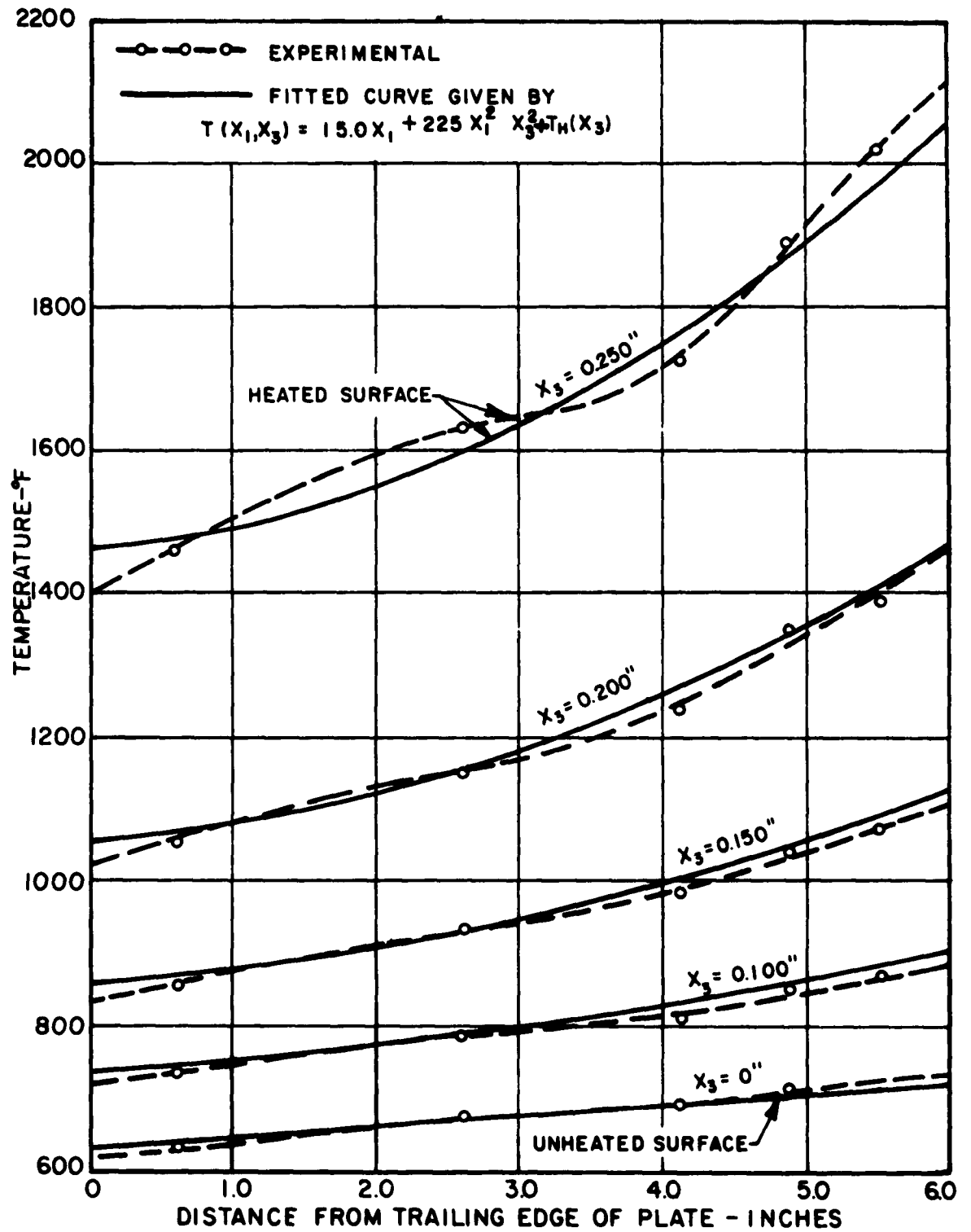


FIG. 13D TEMPERATURE DISTRIBUTION ALONG LENGTH OF 1/4 INCH THICK PYROLYTIC GRAPHITE PLATE AT VARIOUS DEPTHS AFTER 40 SECONDS OF HEATING

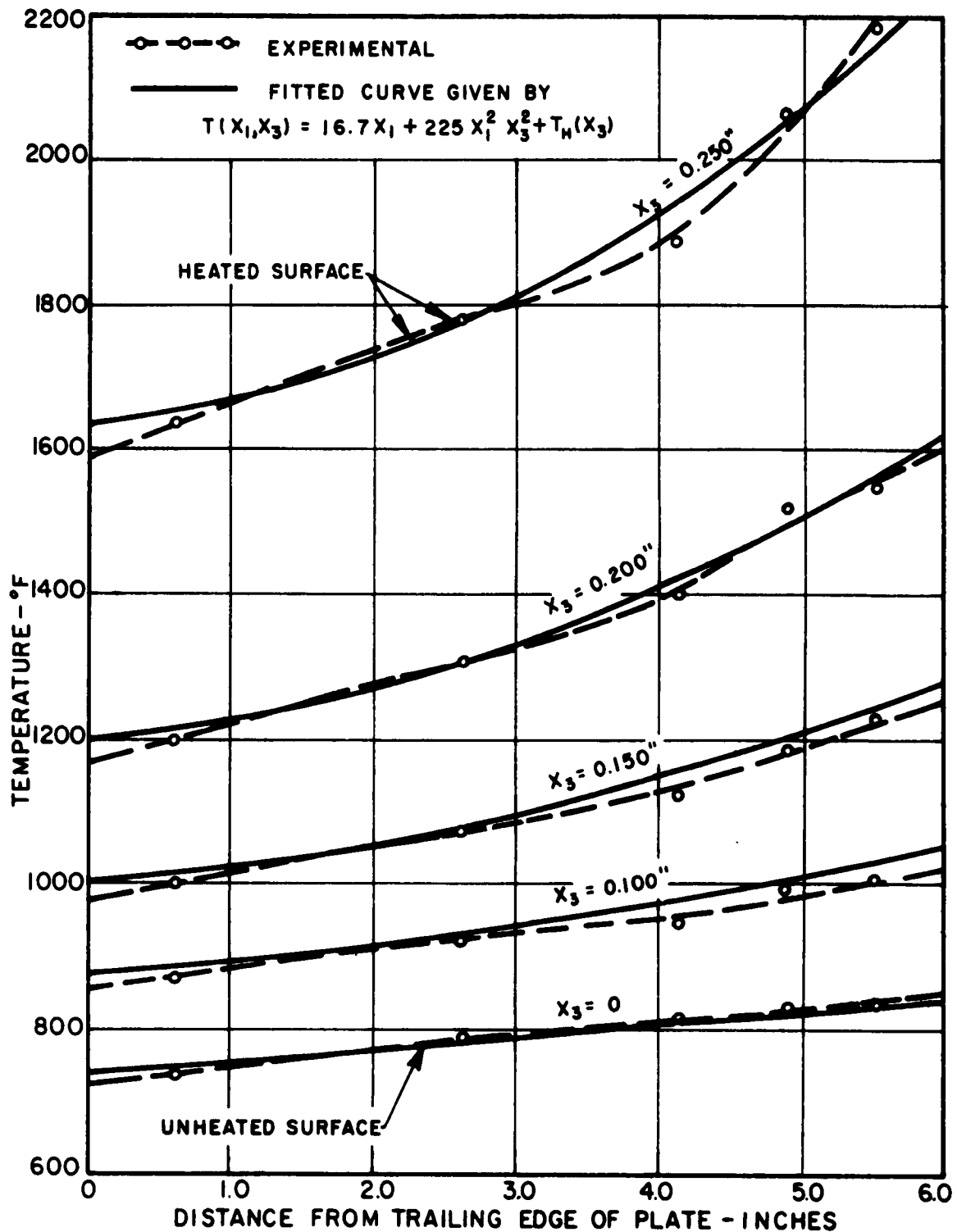


FIG. 13 E TEMPERATURE DISTRIBUTION ALONG LENGTH OF $\frac{1}{4}$ INCH THICK PYROLYTIC GRAPHITE PLATE AT VARIOUS DEPTHS AFTER 50 SECONDS OF HEATING

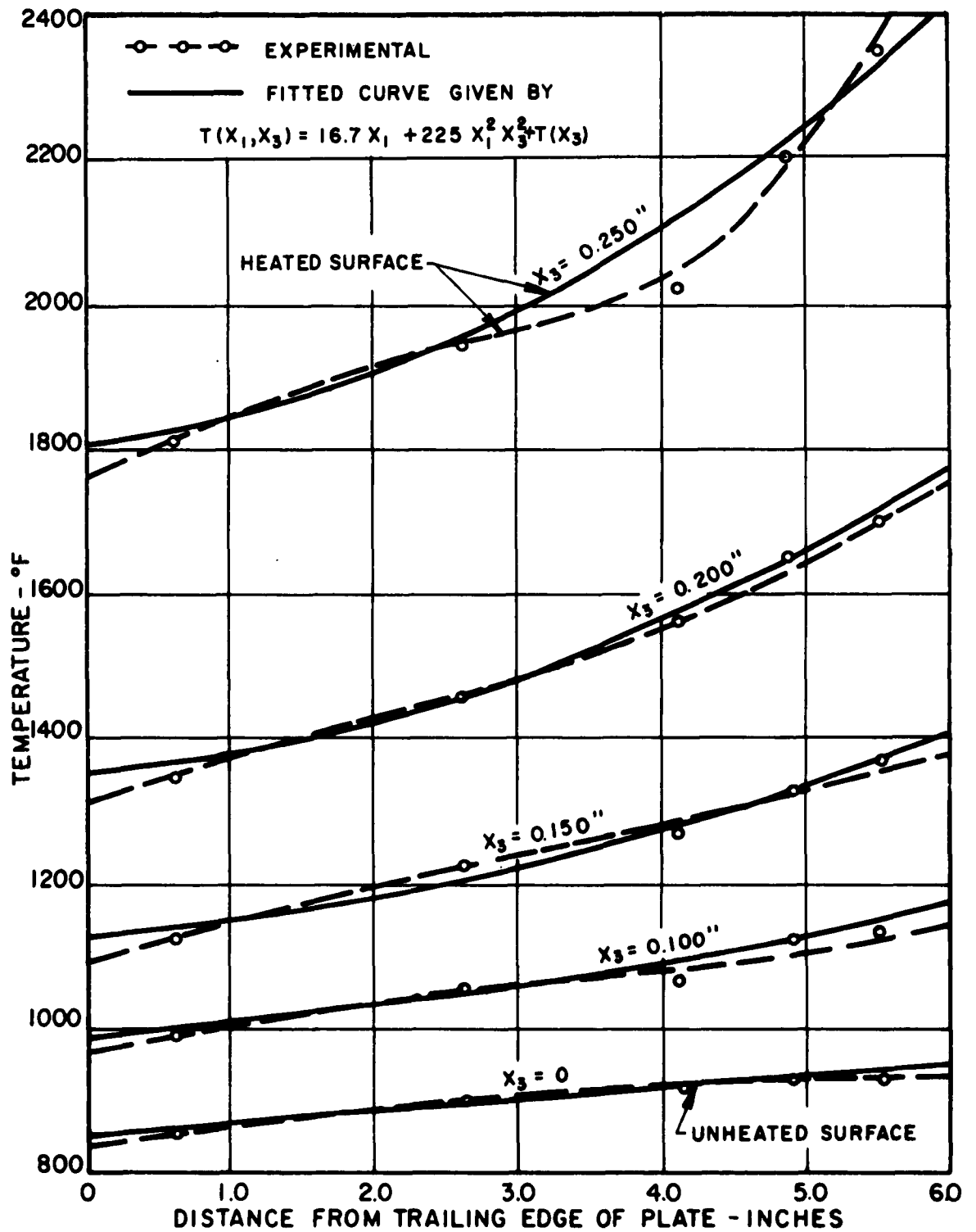


FIG. 13F TEMPERATURE DISTRIBUTION ALONG LENGTH OF
 1/4 INCH THICK PYROLYTIC GRAPHITE PLATE AT
 VARIOUS DEPTHS AFTER 60 SECONDS OF HEATING

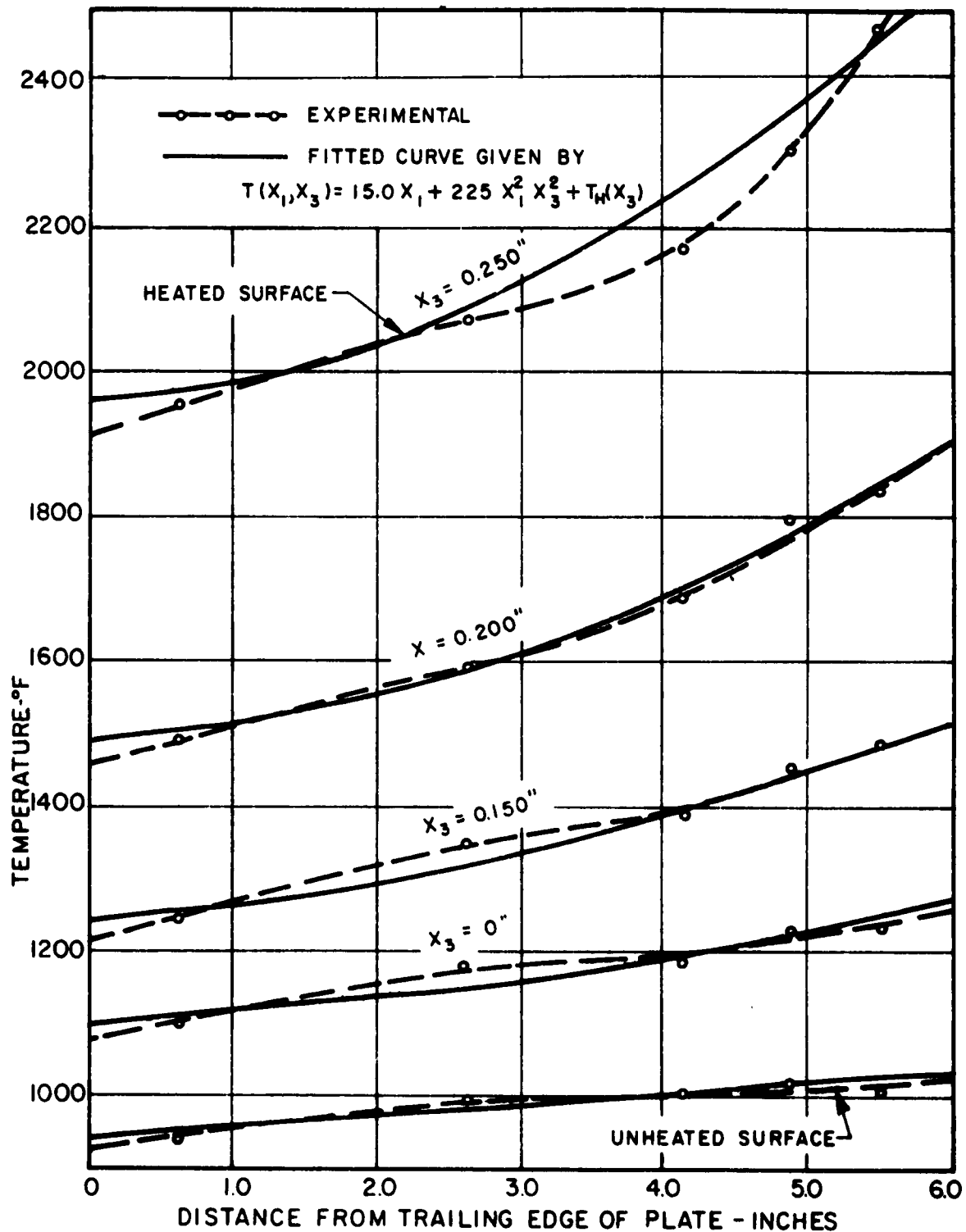


FIG. 13 G TEMPERATURE DISTRIBUTION ALONG LENGTH OF $\frac{1}{4}$ INCH THICK PYROLYTIC GRAPHITE PLATE AT VARIOUS DEPTHS AFTER 70 SECONDS OF HEATING

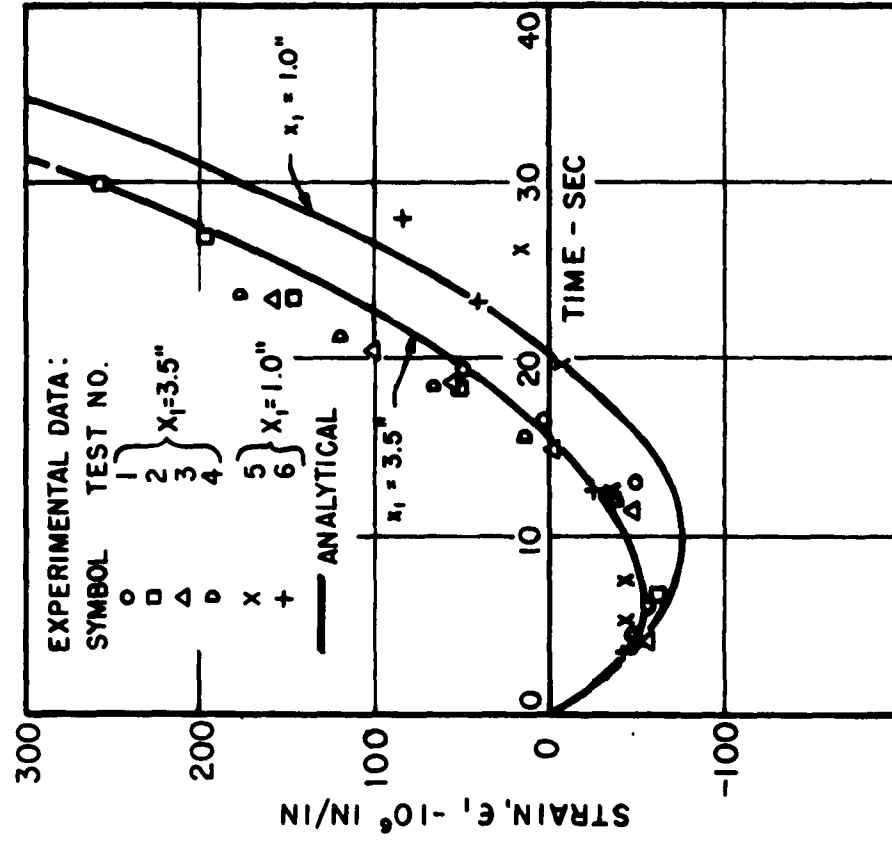


FIG.14 COMPARISON OF EXPERIMENTAL DATA WITH CALCULATED STRAINS AT UNHEATED SURFACE OF 1/8 INCH THICK PYROLYTIC GRAPHITE PLATE

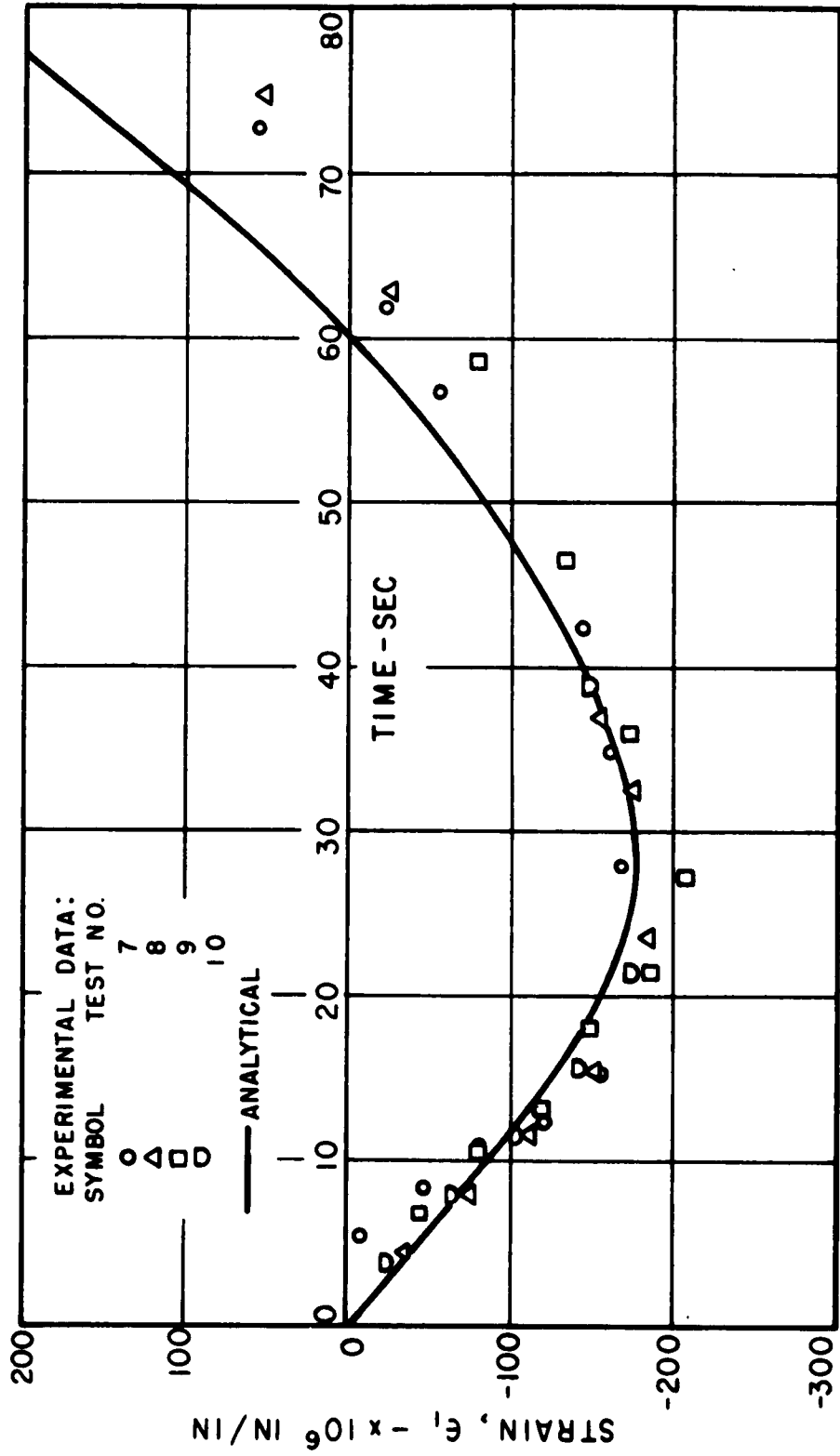


FIG. 15 COMPARISON OF EXPERIMENTAL DATA WITH CALCULATED STRAINS AT UNHEATED SURFACE OF 1/4 INCH THICK PYROLYTIC GRAPHITE PLATE

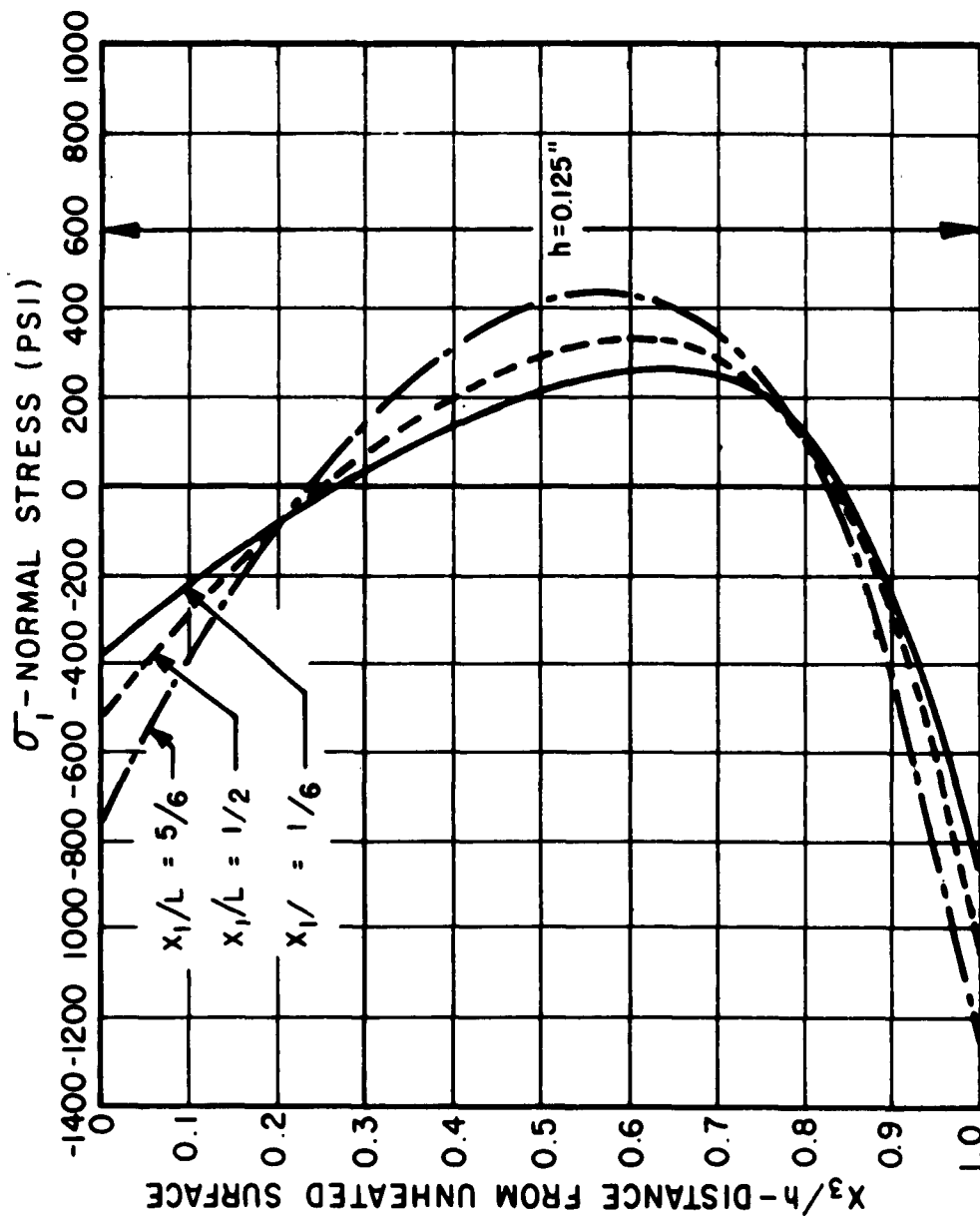


FIG. 16 DISTRIBUTION OF σ_1 THROUGH $1/8$ INCH THICK PLATE AFTER 20 SECONDS OF HEATING

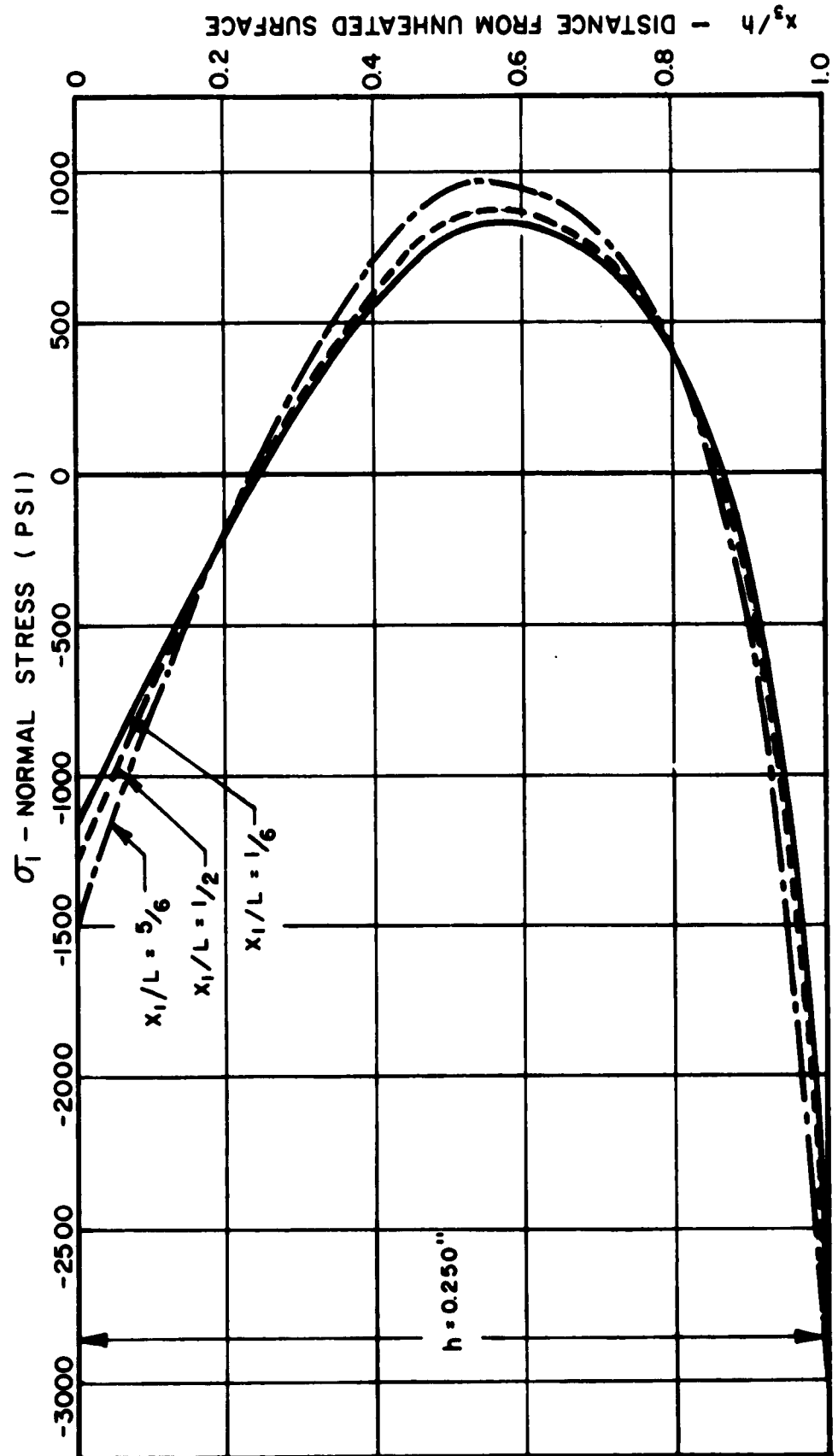


FIG. 17 DISTRIBUTION OF σ_1 THROUGH 1/4 INCH THICK PLATE AFTER 40 SECONDS OF HEATING

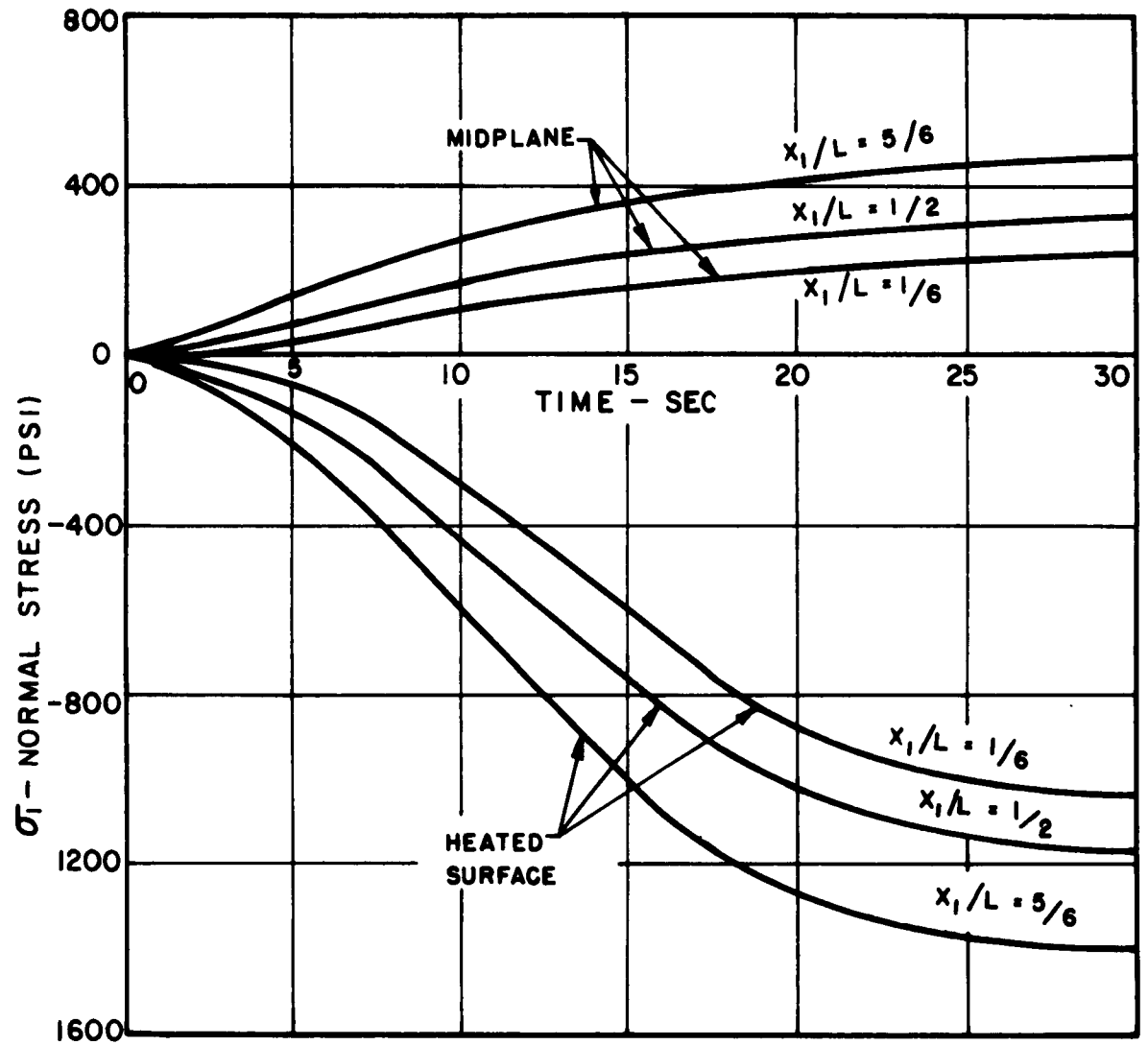


FIG. 18 VARIATION OF σ_1 AT HEATED SURFACE AND MIDPLANE OF 1/8 INCH THICK PLATE

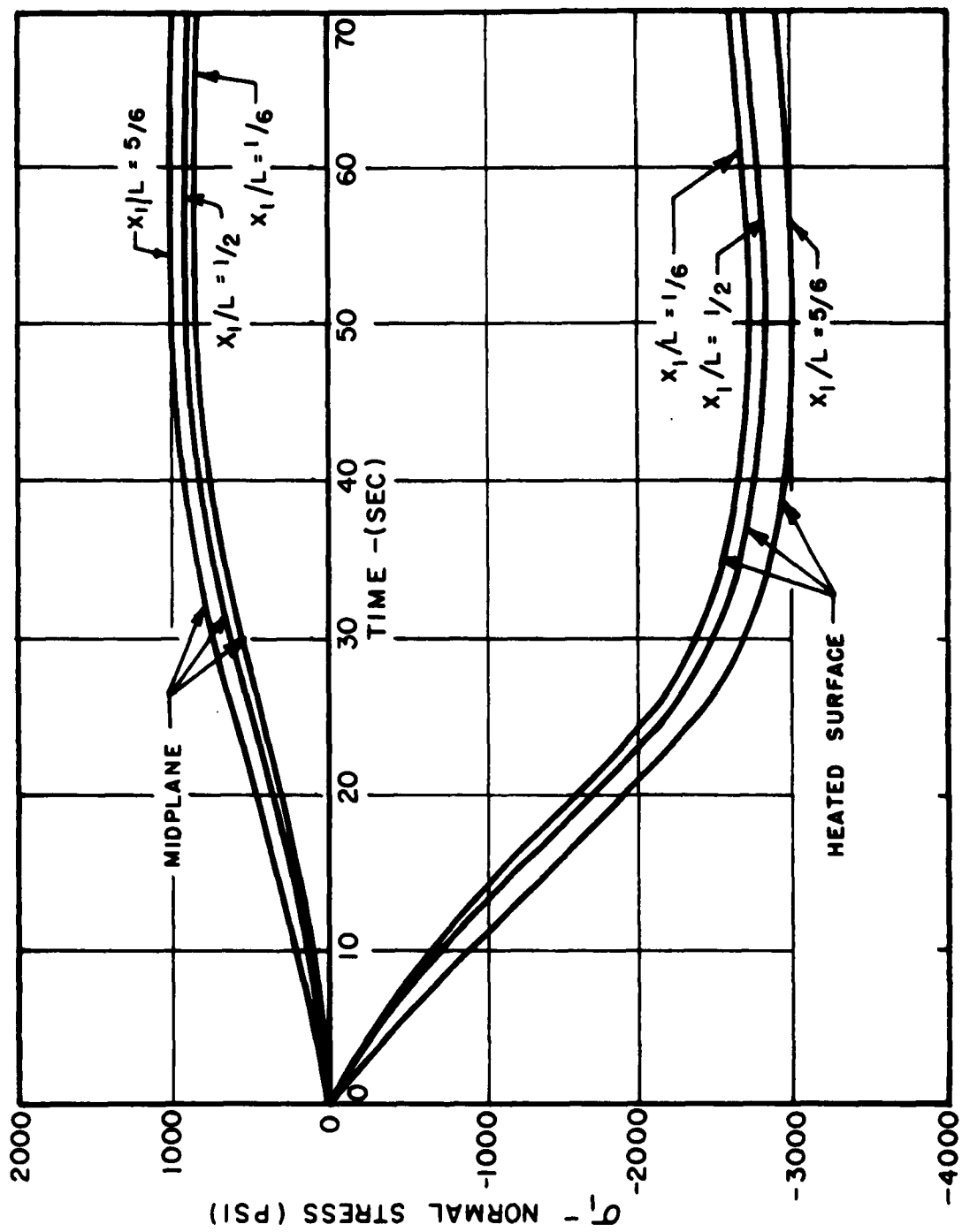


FIG. 19 VARIATION OF σ_1 AT HEATED SURFACE AND MID PLANE OF $\frac{1}{4}$ INCH THICK PLATE

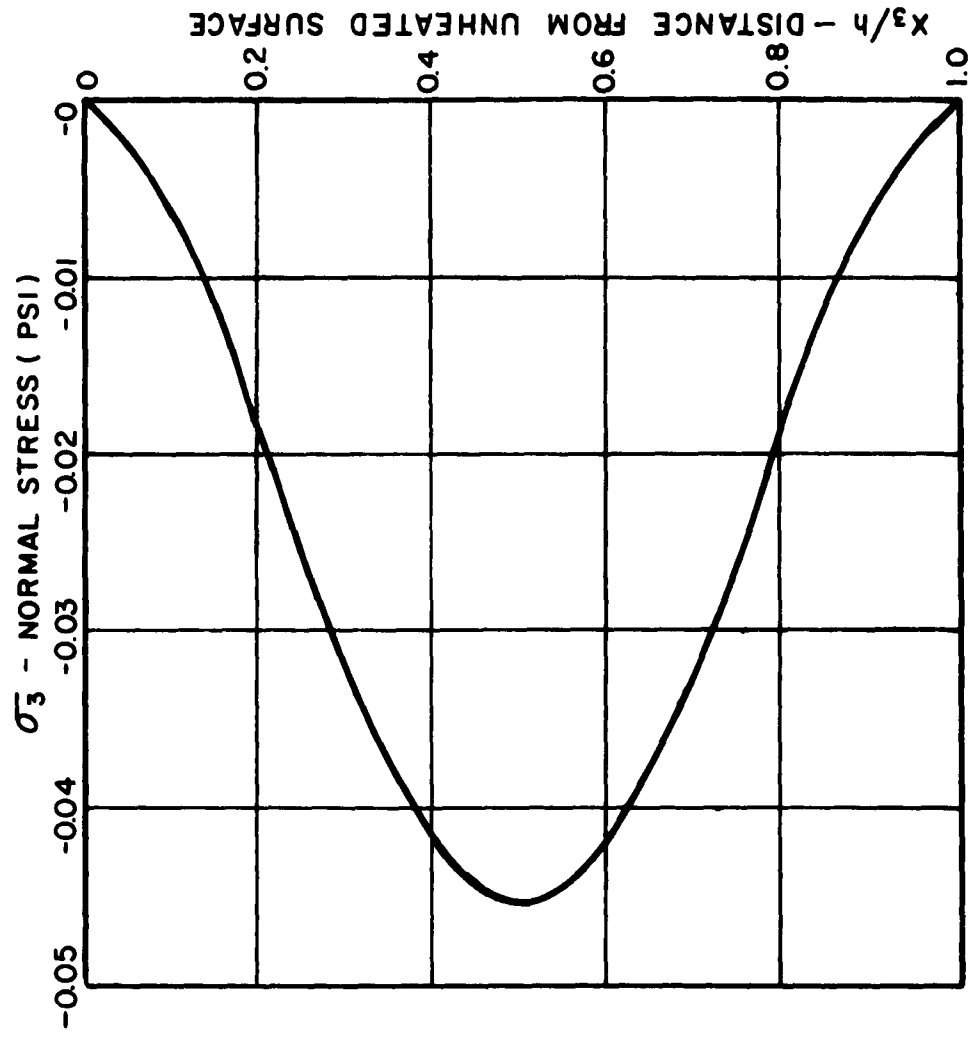


FIG. 20 DISTRIBUTION OF σ_3 THROUGH 1/4 INCH THICK PLATE AFTER 40 SECONDS OF HEATING

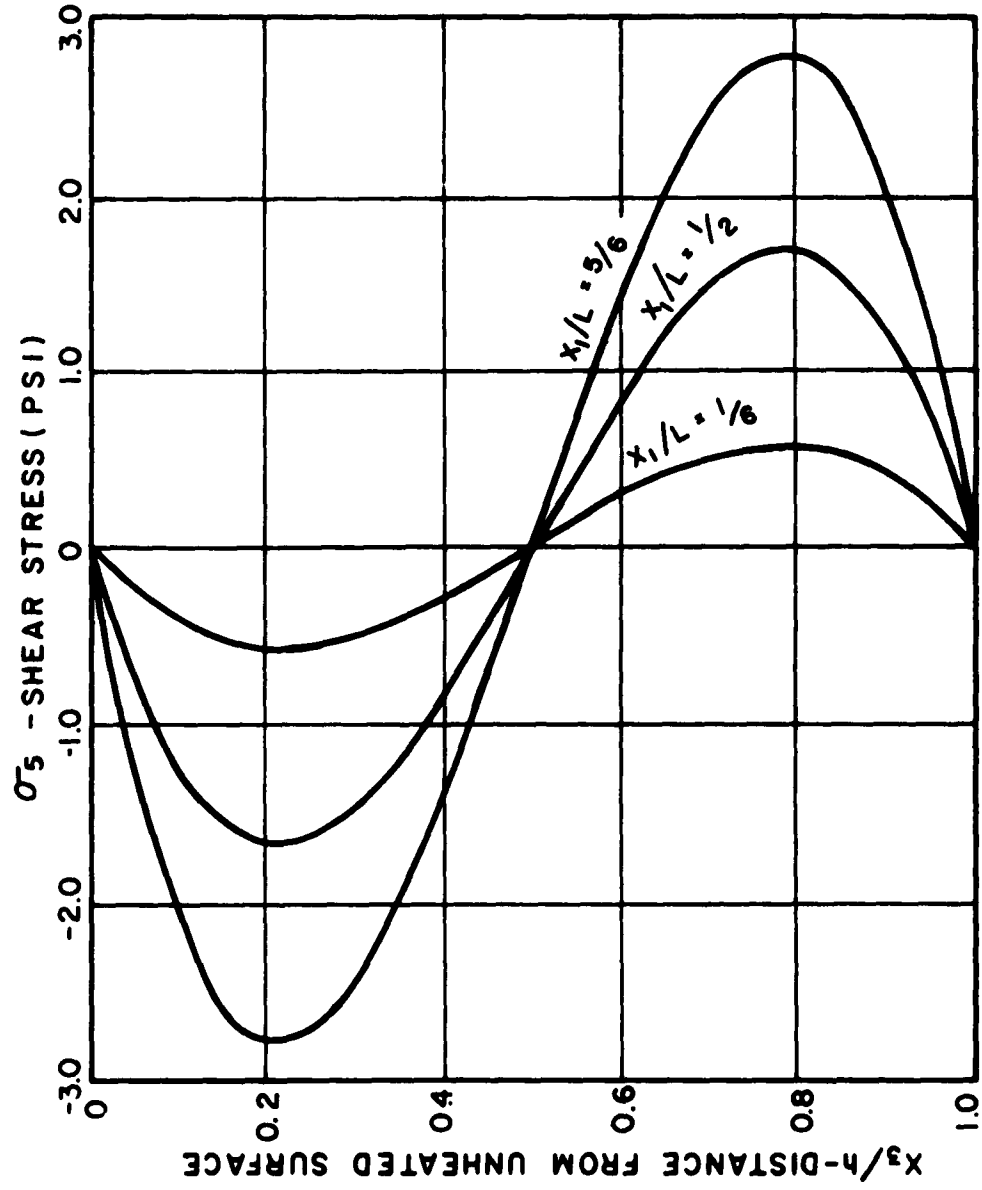


FIG. 2.1 DISTRIBUTION OF σ_x THROUGH 1/4 INCH THICK PLATE AFTER 40 SECONDS OF HEATING

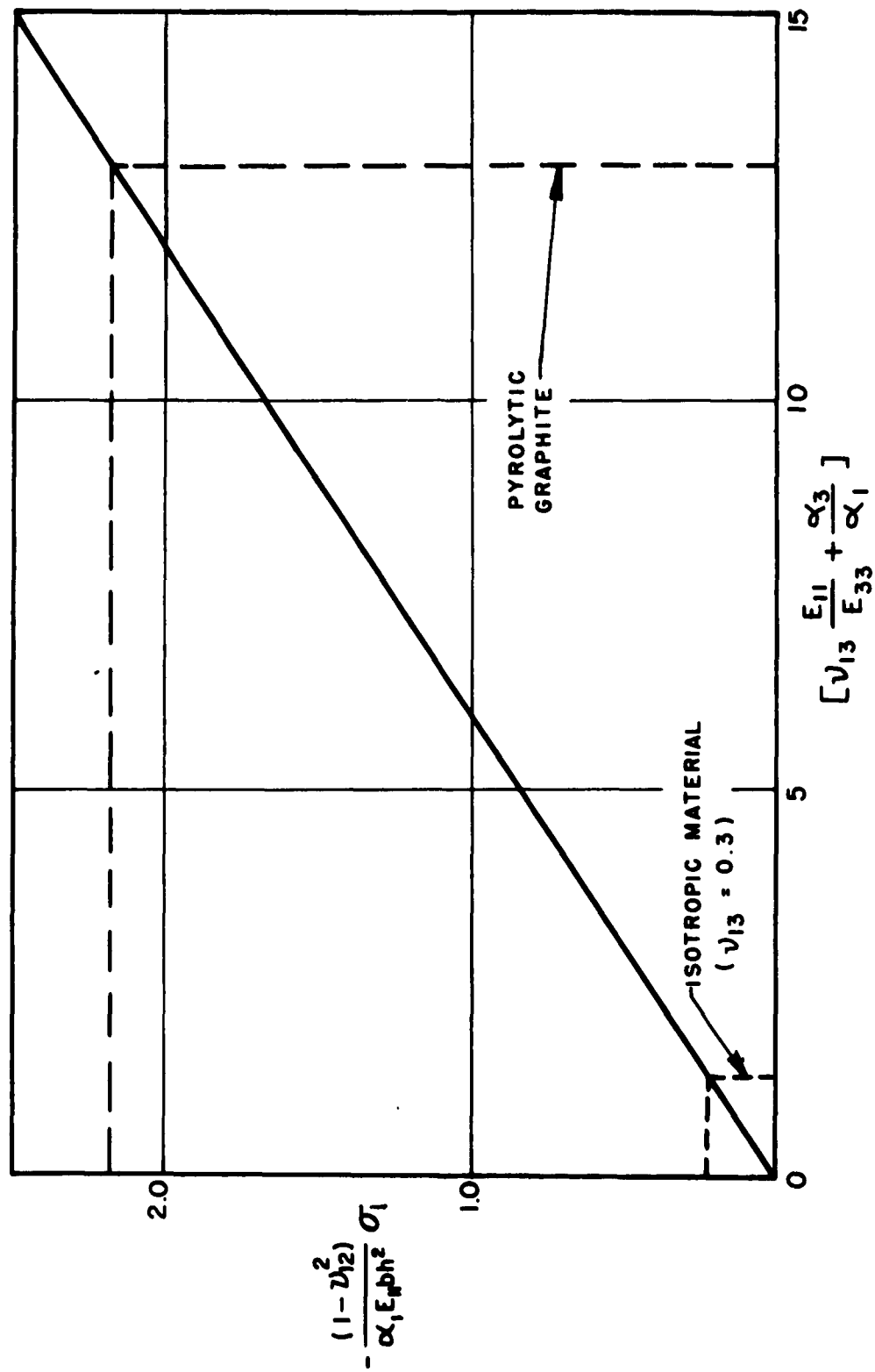


FIG. 22 VARIATION OF THERMAL STRESS WITH DEGREE OF ANISOTROPY

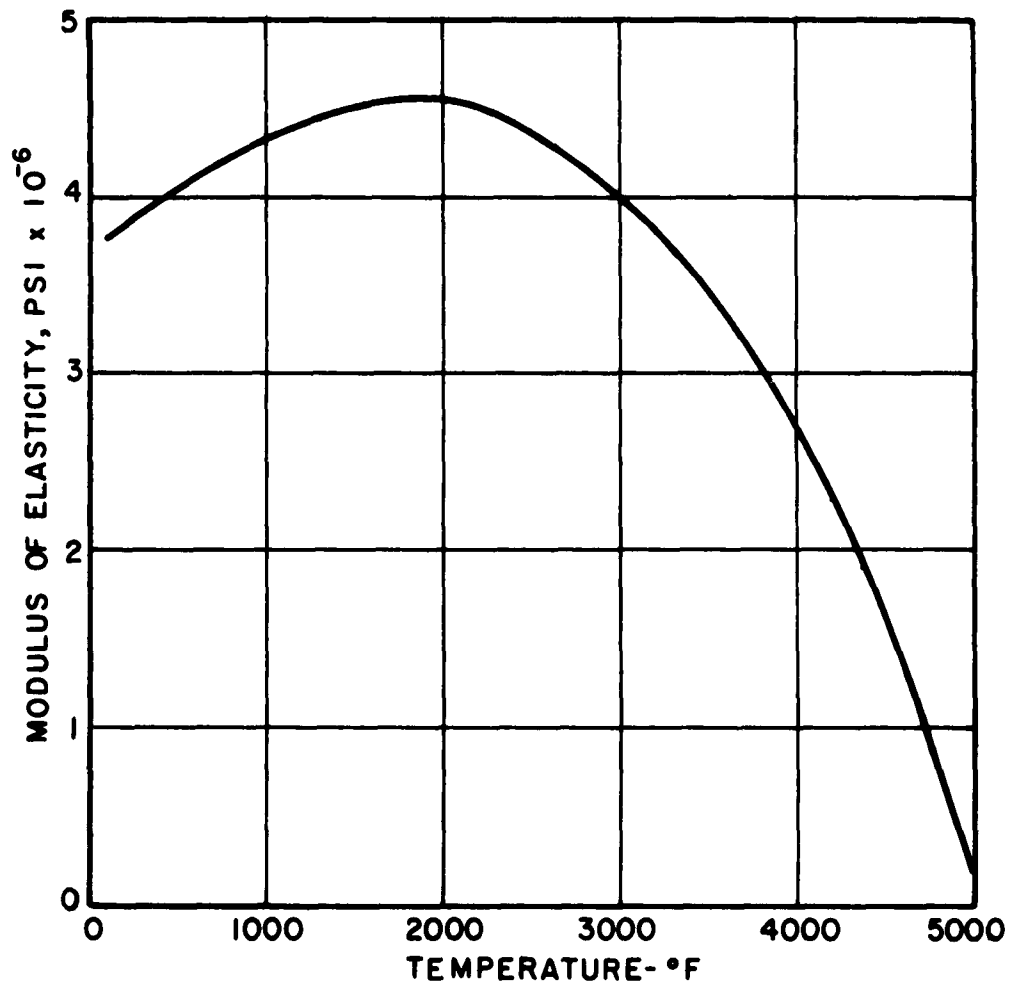


FIG. 23 MODULUS OF ELASTICITY OF PYROLYTIC GRAPHITE
IN THE "a" DIRECTION vs TEMPERATURE

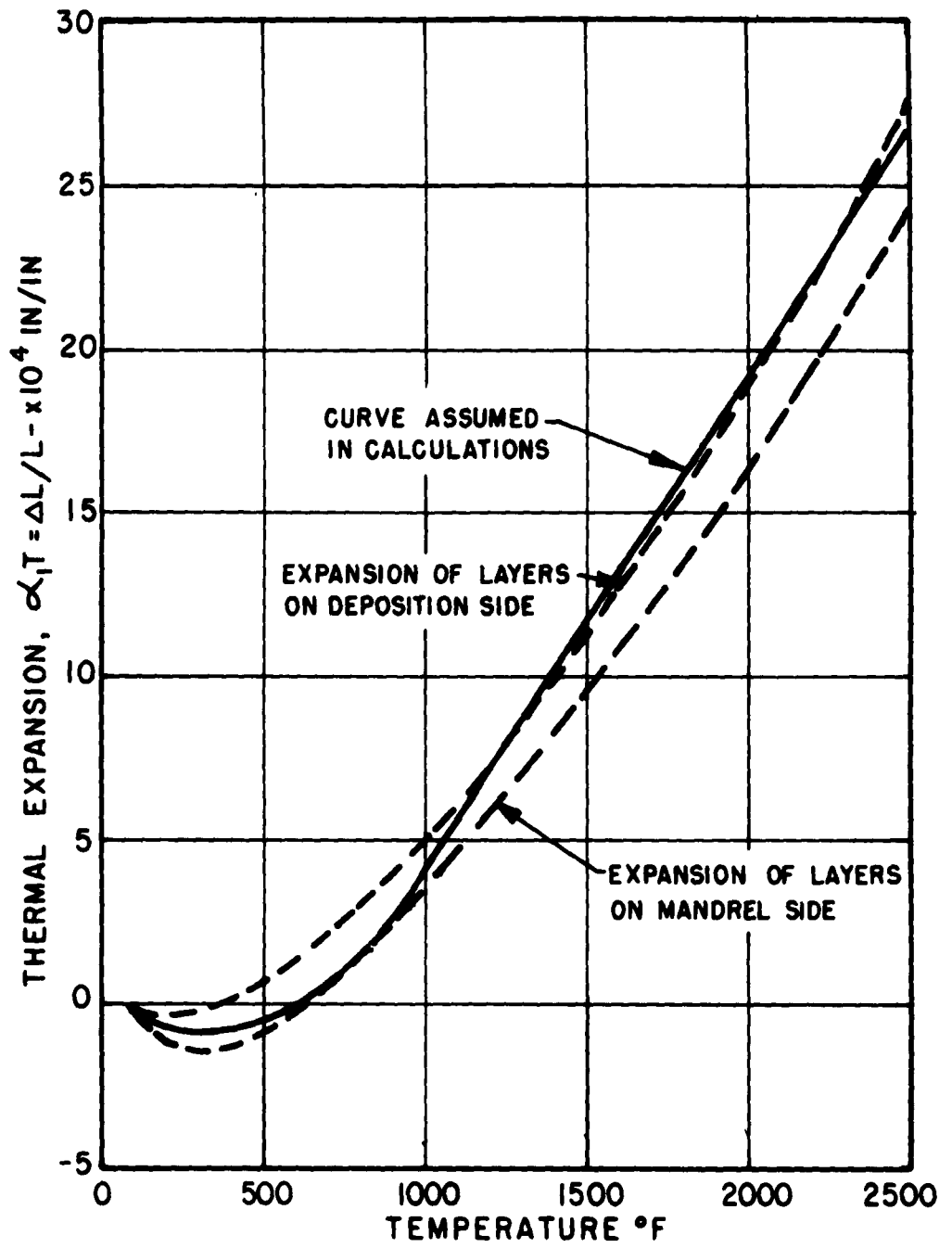


FIG. 24 THERMAL EXPANSION OF PYROLITIC GRAPHITE IN THE "a" DIRECTION

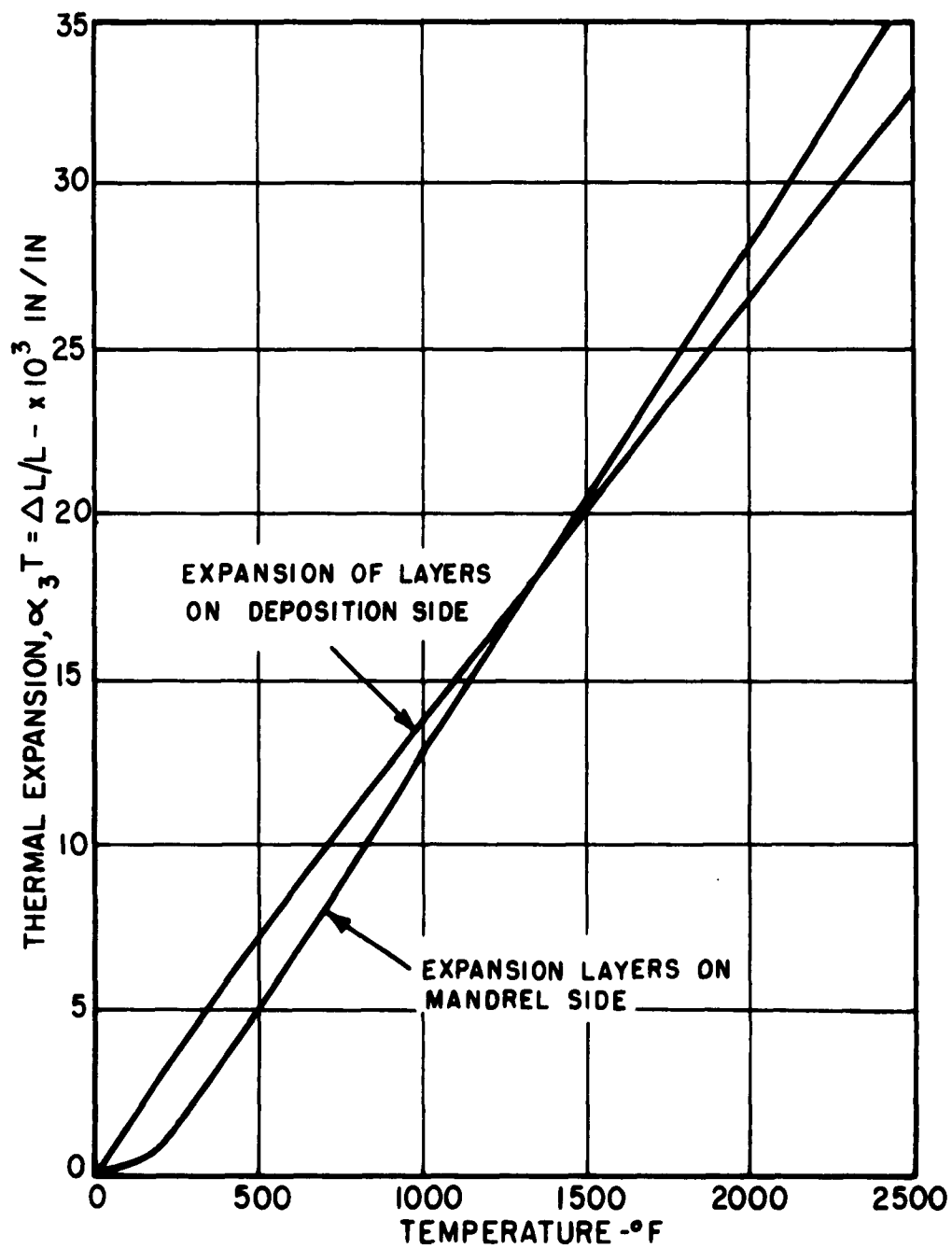


FIG. 25 THERMAL EXPANSION OF PYROLYTIC GRAPHITE IN THE "C" DIRECTION

APPENDIX I

REDUCTION OF INDEPENDENT ELASTIC CONSTANTS FOR VARIOUS TYPES OF SYMMETRY

For the general anisotropic solid, the generalized Hooke's law including thermal strain is expressed by¹¹

$$\left. \begin{aligned}
 \epsilon_{11} &= \frac{\partial u}{\partial x_1} = a_{11}\sigma_{11} + a_{12}\sigma_{22} + a_{13}\sigma_{33} + a_{14}\sigma_{23} + a_{15}\sigma_{13} + a_{16}\sigma_{12} + \alpha_1 T \\
 \epsilon_{22} &= \frac{\partial v}{\partial x_2} = a_{12}\sigma_{11} + a_{22}\sigma_{22} + a_{23}\sigma_{33} + a_{24}\sigma_{23} + a_{25}\sigma_{13} + a_{26}\sigma_{12} + \alpha_2 T \\
 \epsilon_{33} &= \frac{\partial w}{\partial x_3} = a_{13}\sigma_{11} + a_{23}\sigma_{22} + a_{33}\sigma_{33} + a_{34}\sigma_{23} + a_{35}\sigma_{13} + a_{36}\sigma_{12} + \alpha_3 T \\
 \epsilon_{23} &= \frac{\partial w}{\partial x_2} + \frac{\partial v}{\partial x_3} = a_{14}\sigma_{11} + a_{24}\sigma_{22} + a_{34}\sigma_{33} + a_{44}\sigma_{23} + a_{45}\sigma_{13} + a_{46}\sigma_{12} + \alpha_4 T \\
 \epsilon_{13} &= \frac{\partial w}{\partial x_1} + \frac{\partial u}{\partial x_3} = a_{15}\sigma_{11} + a_{25}\sigma_{22} + a_{35}\sigma_{33} + a_{45}\sigma_{23} + a_{55}\sigma_{13} + a_{56}\sigma_{12} + \alpha_5 T \\
 \epsilon_{12} &= \frac{\partial v}{\partial x_1} + \frac{\partial u}{\partial x_2} = a_{16}\sigma_{11} + a_{26}\sigma_{22} + a_{36}\sigma_{33} + a_{46}\sigma_{23} + a_{56}\sigma_{13} + a_{66}\sigma_{12} + \alpha_6 T
 \end{aligned} \right\} (A.1)$$

It is convenient to introduce the following notation:

$$\begin{aligned}
 \epsilon_{11} &= \epsilon_1 & \sigma_{11} &= \sigma_1 \\
 \epsilon_{22} &= \epsilon_2 & \sigma_{22} &= \sigma_2 \\
 \epsilon_{33} &= \epsilon_3 & \sigma_{33} &= \sigma_3 \\
 \epsilon_{23} &= \epsilon_4 & \sigma_{23} &= \sigma_4 \\
 \epsilon_{13} &= \epsilon_5 & \sigma_{13} &= \sigma_5 \\
 \epsilon_{12} &= \epsilon_6 & \sigma_{12} &= \sigma_6
 \end{aligned}$$

Then equations (A.1) may be abridged as:

$$\epsilon_i = a_{ik}\sigma_k + \alpha_i T \quad (i = 1, 2, \dots, 6)$$

The isothermal elastic coefficients, a_{ik} , are defined as¹²

$$a_{ik} = \left(\frac{\partial \epsilon_i}{\partial \sigma_k} \right)_{T, \{\sigma\}} \quad (i = 1, 2, \dots, 6)$$

where the subscript T denotes constancy of temperature and subscript $\{\sigma\}$ denotes constancy of all σ_i other than σ_k . Since the indices of a_{ik} can take six values, it comprises a 6 x 6 matrix. However, the symmetry condition, $a_{ik} = a_{ki}$, reduces the number of independent coefficients to twenty-one. Then the general matrix can be written as

$$a_{ik} = \begin{bmatrix} a_{11} & a_{12} & a_{13} & a_{14} & a_{15} & a_{16} \\ \dots & a_{22} & a_{23} & a_{24} & a_{25} & a_{26} \\ \dots & \dots & a_{33} & a_{34} & a_{35} & a_{36} \\ \dots & \dots & \dots & a_{44} & a_{45} & a_{46} \\ \dots & \dots & \dots & \dots & a_{55} & a_{56} \\ \dots & \dots & \dots & \dots & \dots & a_{66} \end{bmatrix}$$

The a_{ik} are symmetric about the diagonal.

The coefficients of thermal strain, α_i are defined by¹²

$$\alpha_i = \left(\frac{\partial \epsilon_i}{\partial T} \right)_{\{\sigma\}} \quad (i = 1, 2, \dots, 6)$$

where the subscript $\{\sigma\}$ denotes constancy of stresses.

The number of independent elastic constants, a_{ik} , of a solid reduce considerably when the solid exhibits elastic symmetry with respect to a plane or about an axis. A solid is said to exhibit elastic symmetry

with respect to a transformation if the elastic constants are invariant in this transformation. Consider the transformation of one system of axes x_1, x_2, x_3 to another system of axes x'_1, x'_2, x'_3 . Suppose this transformation is connected by the orthogonal scheme

	x_1	x_2	x_3
x'_1	l_1	m_1	n_1
x'_2	l_2	m_2	n_2
x'_3	l_3	m_3	n_3

where l, m, n denote direction cosines. It can be shown that the corresponding transformation of stresses and strains are given by¹¹

$$\sigma'_1 = l_1^2 \sigma_1 + m_1^2 \sigma_2 + n_1^2 \sigma_3 + 2m_1 n_1 \sigma_4 + 2n_1 l_1 \sigma_5 + 2l_1 m_1 \sigma_6$$

.

$$\sigma'_6 = l_1 l_2 \sigma_1 + m_1 m_2 \sigma_2 + n_1 n_2 \sigma_3 + (m_1 n_1 + m_2 n_1) \sigma_4$$

$$+ (n_1 l_2 + n_2 l_1) \sigma_5 + (l_1 m_2 + l_2 m_1) \sigma_6$$

.

$$\epsilon'_1 = l_1^2 \epsilon_1 + m_1^2 \epsilon_2 + n_1^2 \epsilon_3 + m_1 n_1 \epsilon_4 + n_1 l_1 \epsilon_5 + l_1 m_1 \epsilon_6$$

.

$$\epsilon'_4 = 2l_2 l_3 \epsilon_1 + 2m_2 m_3 \epsilon_2 + 2n_2 n_3 \epsilon_3 + (m_2 m_3 + m_3 n_2) \epsilon_4$$

$$+ (n_2 l_3 + n_3 l_2) \epsilon_5 + (l_2 m_3 + l_3 m_2) \epsilon_6$$

.

As a specific example, consider the case of one-plane symmetry with respect to the $x_1 x_2$ -plane such that

$$x_1 = x'_1, \quad x_2 = x'_2, \quad x_3 = -x'_3$$

The direction cosines of this transformation are as follows

	x_1	x_2	x_3
x'_1	1	0	0
x'_2	0	1	0
x'_3	0	0	-1

Transformations of stresses and strains give

$$\sigma'_i = \sigma_i, \quad \epsilon'_i = \epsilon_i \quad (i = 1, 2, 3, 6)$$

$$\sigma'_4 = -\sigma_4, \quad \epsilon'_4 = -\epsilon_4, \quad \sigma'_5 = -\sigma_5, \quad \epsilon'_5 = -\epsilon_5$$

For the x'_1, x'_2, x'_3 system, the Hooke's law relation for the strain ϵ'_1 is

$$\epsilon'_1 = a_{11}\sigma'_1 + a_{12}\sigma'_2 + a_{13}\sigma'_3 + a_{14}\sigma'_4 + a_{15}\sigma'_5 + a_{16}\sigma'_6 + \alpha_1 T$$

Transforming to the x_1, x_2, x_3 system, the strain becomes

$$\epsilon_1 = a_{11}\sigma_1 + a_{12}\sigma_2 + a_{13}\sigma_3 - a_{14}\sigma_4 - a_{15}\sigma_5 + a_{16}\sigma_6 + \alpha_1 T$$

However, since the a_{ik} are invariant, the strain can be written without reference to the x'_1, x'_2, x'_3 system as

$$\epsilon_1 = a_{11}\sigma_1 + a_{12}\sigma_2 + a_{13}\sigma_3 + a_{14}\sigma_4 + a_{15}\sigma_5 + a_{16}\sigma_6 + \alpha_1 T$$

Comparison of the two equations yields

$$a_{14} = a_{15} = 0$$

Examining $\epsilon_2, \epsilon_3, \dots$ in turn, the following must also hold:

$$a_{24} = a_{25} = a_{34} = a_{35} = a_{46} = a_{56} = 0$$

Thus the elastic matrix for one-plane symmetry with respect to the plane can be written as

$$a_{ik} = \begin{bmatrix} a_{11} & a_{12} & a_{13} & 0 & 0 & a_{16} \\ & a_{22} & a_{23} & 0 & 0 & a_{26} \\ & & a_{33} & 0 & 0 & a_{36} \\ & & & a_{45} & a_{46} & 0 \\ & & & & a_{55} & 0 \\ & & & & & a_{66} \end{bmatrix} \quad \begin{array}{l} 13 \text{ independent} \\ \text{constants} \end{array}$$

By following the same procedures, it can be shown that for three-plane (orthotropic) symmetry the matrix reduces to

$$a_{ik} = \begin{bmatrix} a_{11} & a_{12} & a_{13} & 0 & 0 & 0 \\ & a_{22} & a_{23} & 0 & 0 & 0 \\ & & a_{33} & 0 & 0 & 0 \\ & & & a_{44} & 0 & 0 \\ & & & & a_{55} & 0 \\ & & & & & a_{66} \end{bmatrix} \quad \begin{array}{l} 9 \text{ independent} \\ \text{constants} \end{array}$$

And for the solid which is transversely isotropic in the x_1x_2 -plane such that the x_3 -axis is an axis of symmetry, the matrix reduces to

$$a_{ik} = \begin{bmatrix} a_{11} & a_{12} & a_{13} & 0 & 0 & 0 \\ & a_{11} & a_{13} & 0 & 0 & 0 \\ & & a_{13} & 0 & 0 & 0 \\ & & & a_{44} & 0 & 0 \\ & & & & a_{44} & 0 \\ & & & & & a_{66} \end{bmatrix} \quad \begin{array}{l} \text{5 independent} \\ \text{constants} \end{array}$$

APPENDIX II

CALCULATIONS

II.A Properties of Pyrolytic Graphite

Although extensive work has been done on evaluating the properties of pyrolytic graphite, much of the available data is only preliminary and some of the properties, such as the shearing modulus G_{44} , have not been measured. In some cases the properties can only be estimated; while in other cases a reasonable choice must be made between conflicting data.

The modulus of elasticity in the "a" direction is plotted as a function of temperature in Figure 23. These data were taken from Reference 21. More recent data²² indicate that the "a" direction modulus may be as large as 10×10^6 psi in compression. It is also indicated that the "c" direction modulus may exhibit the same type of behavior. The "c" direction modulus in tension has been measured to be 1.5×10^6 psi, and in compression it has been measured to be 16×10^6 psi.

The thermal expansion in the "a" direction and in the "c" direction is plotted against temperature in Figures 24 and 25, respectively. These data were also taken from Reference 21. The difference in the thermal expansions of the top and bottom layers is attributed to the presence of residual stress. The solid curve in Figure 24 is the average curve used in the numerical calculations.

A value of 0.24 was reported²¹ to have been measured for the Poisson's ratio in the basal plane (ν_{12}). This ratio in the lateral direction (ν_{13}) has not been measured yet.

The value of the shear modulus G_{44} is unknown, but judging from the laminate-type structure of pyrolytic graphite, it seems reasonable

to assume that greater rigidity will be exhibited to shearing forces normal to the basal plane than to shearing forces parallel to this plane. Then the following inequality is noted:

$$G_{44} > G_{11} = \frac{E_{11}}{2(1 + \nu_{12})}$$

For calculation purposes, the following approximation was made:

$$G_{44} = 2G_{11} = \frac{E_{11}}{(1 + \nu_{12})}$$

II.B Calculation of Stresses and Strains

The stresses and strains are given by equations (8) and (9) which account for property variations, and by equations (31) and (32) which are based on constant properties. Numerical calculations were carried out for the strain, ϵ_1 , at the unheated surface ($Z = 0$) and for the stresses, σ_1 , σ_3 , and σ_5 .

In evaluating equations (8) and (9) for ϵ_1 and σ_1 (σ_3 and σ_5 are zero) the elastic modulus was taken as a constant, along with the Poisson's ratio, since it does not vary much from room temperature to 3000° F (cf., Figure 23). The following values were assumed:

$$E_{11} = 5.0 \times 10^6 \text{ psi}$$

$$\nu_{12} = 0.24$$

The integrals N_T and M_T were evaluated numerically by dividing the thickness of each plate into 20 equal increments, Δx_3 . The numerical

expressions for ϵ_1 and σ_1 appear as follows:

$$\epsilon_1(x_3=0) = \frac{1}{20} \sum_{i=1}^{20} \alpha_1 \bar{T} - \frac{3}{10h} \sum_{i=1}^{20} \alpha_1 \bar{T} (\bar{x}_{3_i} - \frac{1}{2} h) \quad (\text{in/in})$$

$$\sigma_1(x_3) = \frac{5.0 \times 10^6}{1 - 0.24} \left\{ -\alpha_1 T(x_3) + \frac{1}{20} \sum_{i=1}^{20} \alpha_1 \bar{T} + \frac{3(x_3 - \frac{1}{2} h)}{5h^2} \sum_{i=1}^{20} \alpha_1 \bar{T} (\bar{x}_{3_i} - \frac{1}{2} h) \right\} \quad (\text{psi})$$

where:

\bar{x}_{3_i} = average distance of i^{th} increment from x_1 -axis

$\alpha_1 \bar{T}$ = thermal expansion at average temperature \bar{T} of i^{th} increment

$T(x_3)$ = temperature at x_3 .

The temperature curves used in these calculations are shown in Figures 10 and 11. The thermal expansion, $\alpha_1 \bar{T}$, was obtained from the solid curve of Figure 24.

In evaluating equations (31) and (32) for ϵ_1 , σ_1 , σ_3 , and σ_5 , the following average values of the properties were assumed:

$$E_{11} = 5.0 \times 10^6 \text{ psi}$$

$$E_{33} = 15.0 \times 10^6 \text{ psi}$$

$$\nu_{12} = 0.24$$

$$\nu_{13} = 0.30$$

$$G_{44} = 4.0 \times 10^6 \text{ psi}$$

$$\alpha_1 = \begin{cases} 1.00 \times 10^{-6} \text{ } ^\circ\text{F}^{-1} & \text{for the 1/8" thick plate} \\ 0.75 \times 10^{-6} \text{ } ^\circ\text{F}^{-1} & \text{for the 1/4" thick plate} \end{cases}$$

$$\alpha_3 = 13.0 \times 10^{-6} \text{ } ^\circ\text{F}^{-1}$$

The larger compressive value of E_{33} was chosen because σ_3 is always in compression (See Figure 20). The larger value of α_1 was assumed for the 1/8 inch thick plate because of the slightly higher temperatures.

The parameters defined by equation (17) were then calculated to have the following values:

$$\beta = 1.063$$

$$\eta = \begin{cases} 6.58 \text{ psi/}^\circ\text{F} & \text{1/8" plate} \\ 4.93 \text{ psi/}^\circ\text{F} & \text{1/4" plate} \end{cases}$$

$$\zeta = \begin{cases} 69.5 \text{ psi/}^\circ\text{F} & \text{1/8" plate} \\ 69.4 \text{ psi/}^\circ\text{F} & \text{1/4" plate} \end{cases}$$

γ was not calculated since it does not appear in the final equations.

Substitution of these parameter values in equations (31) and (32) yielded the following numerical expressions for ϵ_1 , σ_1 , σ_3 , and σ_5 :

For the 1/8" thick plate:

$$\epsilon_1 \Big|_{\substack{x_3=0 \\ x_1=1''}} = [2.245 c \times 10^{-2} + 1240 b + a] \times 10^{-6} \text{ in/in}$$

$$\epsilon_1 \Big|_{\substack{x_3=0 \\ x_1=3.5''}} = \epsilon_1 \Big|_{\substack{x_3=0 \\ x_1=1''}} + [-5.50 c \times 10^{-2} + 10.35 b + 2.5 a] \times 10^{-6} \text{ (in/in)}$$

$$\sigma_1 = 3.70 c X^2 \left(-\frac{1}{6} + z - z^2 \right) + 1.086 b \left(-\frac{1}{6} + z - z^2 \right) \\ + 1.696 \times 10^{-2} c \left(-\frac{1}{30} + \frac{2}{15} z - \frac{1}{6} z^4 \right) + \text{negligible term (psi)}$$

For the 1/4" thick plate:

$$\epsilon_1 \Big|_{\substack{x_3=0 \\ x_1=3.5''}} = [-10.91 c \times 10^{-2} + 2.63 a] \times 10^{-6} \text{ (in/in)}$$

$$\sigma_1 = 11.09 c X^2 \left(-\frac{1}{6} + z - z^2 \right) + 4.34 b \left(-\frac{1}{6} + z - z^2 \right) \\ + 0.271 c \left(-\frac{1}{30} + \frac{2}{15} z - \frac{1}{6} z^4 \right) + \text{negligible term (psi)}$$

$$\sigma_3 \Big|_{\tau=40\text{sec}} = 4.34 \left(-\frac{1}{6} z^2 + \frac{1}{3} z^3 - \frac{1}{6} z^4 \right) \text{ (psi)}$$

$$\sigma_5 \Big|_{\tau=40\text{sec}} = -17.3 X \left(-\frac{1}{3} z + z^2 - \frac{2}{3} z^3 \right) \text{ (psi)}$$

The constants a, b, and c are the coefficients of the temperature curves in Figures 12.A through 13.G. The total strain ϵ_1 and the total stresses, σ_1 , σ_3 , and σ_5 were found by adding the results of the separate calculations.